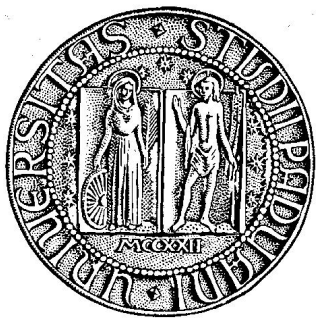

UNIVERSITÀ DEGLI STUDI DI PADOVA

FACOLTÀ DI SCIENZE MM. FF. NN.

Dipartimento di Geoscienze

Direttore Prof.sa Cristina Stefani

TESI DI LAUREA SPECIALISTICA
IN
GEOLOGIA E GEOLOGIA TECNICA

THE EFFECT OF Vshale 3D DISTRIBUTION ON THE SECONDARY MIGRATION OF HYDROCARBONS

Relatore: Prof. Massimiliano Zattin

Correlatori: Dott.ssa Livia Bazzana

Dott. Paolo Ruffo

Laureando: Davide Mencaroni

ANNO ACCADEMICO 2013 / 2014

ABSTRACT

Questo lavoro di tesi si colloca nell'ambito del Petroleum System Modeling, cioè di quel campo della geologia che si occupa di modellare il sistema petrolifero usando diversi software finalizzati a valutare la quantità ed il tipo di idrocarburi potenzialmente accumulatisi in una trappola. In particolare, questo studio si è occupato di Migri, un software che simula percorsi e accumuli conseguenti ai processi di migrazione secondaria. Nonostante questo tipo di studi vengano già condotti attraverso altri software, il senso di questo lavoro è stato quello di approcciarsi a una metodologia innovativa, attraverso dei dati che, all'interno di Eni, non erano mai stati correlati con le problematiche riguardanti i processi di migrazione secondaria: per la prima volta infatti i flussi vengono considerati all'interno di un modello 3D caratterizzabile litologicamente.

Come primo approccio, i test effettuati in questo studio miravano a comprendere come il volume di argille (Vsh) all'interno delle formazioni possa influenzare i flussi degli idrocarburi, e di conseguenza gli accumuli. La metodologia utilizzata per questo scopo si è basata sull'acquisizione del valore di Vsh attraverso l'analisi di log gamma ray, effettuata in corrispondenza di 32 pozzi, e questi valori sono poi stati interpolati attraverso dei criteri geostatistici, al fine di costruire delle mappe di distribuzione di Vsh per ogni *layer* interessato dal processo di migrazione secondaria. In particolare, i test sono stati eseguiti sulla base di quattro diversi scenari di distribuzioni di Vsh. I risultati ottenuti rappresentano un buon punto di partenza nella comprensione del software; oltre all'influenza diretta del valore di Vsh, infatti, è risultato chiaro che la qualità dei risultati sia strettamente connessa con la qualità del modello di partenza. Inoltre, questi test hanno permesso di comprendere meglio il funzionamento stesso del software, e quali siano i naturali sviluppi di questo tipo di studio, al fine di ottenere dei risultati il più possibili rappresentativi della situazione reale.

ABSTRACT

This thesis discusses some topics related to the Petroleum System Modeling, a geology field of study that deals with simulation of various petroleum system elements in order to evaluate amount and type of potential hydrocarbons accumulations. In particular, this study is based on Migri, a software which aims to simulate hydrocarbons paths and accumulations linked with secondary migration process.

In spite of this kind of studies have already been performed with other software, the aim of this work has been to approach a new methodology, using data that have never been considered in Eni for secondary migration simulation: in fact, this is the first time in which the flow has been considered into a 3D model lithologically defined.

As a first approach, tests have been performed in order to understand how the formation shale volume (Vsh) could influence the hydrocarbon flow, and consequently the accumulations. This information started with Vsh values acquisition from gamma ray logs, carried out in correspondence of 32 wells. These values have been interpolated thanks to geostatistic methods, in order to build Vsh distribution maps for each layer interested by secondary migration processes. In particular, tests were performed on the basis of four different Vsh distribution scenarios.

Obtained results represent a good starting point in the study of this software. In fact, in addition to information about the direct influence of Vsh in the model, it has been possible to understand that the results accuracy is strongly linked with the starting GeoModel quality.

TABLE OF CONTENTS

1. INTRODUCTION

Within the oil exploration, current techniques allow to have an acceptable knowledge of the structures and parameters that characterize the GeoModel in which we have one or more petroleum systems. However, modeling of the Petroleum System processes is still in the development phase; in particular, the hydrocarbon flow in the rock porosity from the source rock to the reservoirs (secondary migration) is still not modeled with sufficient detail.

In general, in order to reduce the uncertainties in the exploration phases, a critical contribution is given by the Petroleum System Modeling (PSM) techniques, a geology field of study recently developed, that aims to model numerically the behavior of various geological processes. The processes studied by the PSM concern heat flow variations, burial histories, temperature and pressure evolution, hydrocarbons generation and expulsion and hydrocarbon flow. This last one, that is the modeling of secondary migration paths, is the goal of this study.

The software tools used to perform this kind of studies are quite complex and they have been internally developed by oil companies (only a few, included Eni) or by software vendors. All the components of the PSM are subjected to continuous development, as both the technology and the requirement of management of more complex cases increases. Furthermore hydrocarbon migration is still under development as the current technologies (simple ray tracing, Darcy, percolation) at the moment are able to produce only inaccurate and approximate results due to different technical limitations.

The thesis work described in these pages is the result of an internship project, made possible by a collaboration between Università degli Studi di Padova and Eni - Upstream and Technical Services. This activity is part of a larger project aimed to test and introduce a new approach to secondary migration proposed by a recently developed software called Migri, developed by the Norwegian company Migris A.S.

The goals of these software are ambitious in terms of Petroleum System Modeling innovation, and the innovative elements respect to the current software are visible.

The software used so far in Eni to model all the processes of Petroleum System Modeling is a package called e-simba™ (SIMBA). The package uses mainly internal developed technologies but also external ones, like the software performing secondary migration calculation that is called SEMI, developed by SINTEF and that is based on a simple ray-tracing approach.

SIMBA is a "4D" software, i.e. the GeoModel is described geometrically in the four dimensions where the fourth variable is the geological time. The limitation of Semi is that, for each time step, it is a "2D and a half" modeling: in fact, simulations are performed on a 2D map at a time of the 3D GeoModel, following its temporal evolution during the simulation of the migration. In this way it is not possible to take automaitically into account the 3D (evolving) GeoModel and more important the 3D properties of the layers of the GeoModel. In particular, using SEMI is not possible to consider the real volume loss of hydrocarbons flowing in the layers between the source and the carrier, and in fact the user currently have to set arbitrarily a loss factor of the expelled hydrocarbons.

Migri approach to migration is based on a combination of migration travel-path search (in 3D) and Darcy flow along the found travel-paths. It is therefore a full 3D approach where the GeoModel represents a real 3D cell based model, in which it is possible to insert all the necessary variables that describe the real lithological properties. The software is able to compute permeability and entry pressure (in order to model hydrocarbons flow) starting from these assigned properties, as it will be explained in the following chapters.

The research project is therefore aimed to better understand which is the influence of these input parameters, based on a real lithological case study, on the secondary migration processes, in order to validate the innovation introduced by Migri.

During the stage it was investigated in particular the influence of the shale volume fraction (Vshale) in the hydrocarbon flow dynamic. Vshale values were derived from the analysis of log data, as it will be explained : in the following pages. This

has been one of the first times in which in Eni a simulation of secondary hydrocarbons migration was performed on a regional scale in a full 3D model filled with lithological properties derived from well data (where the other case studies were based in the use of percolation.)

In order to understand the reliability of the results, it has been necessary to test this new software on a mature area in terms of exploration, as in this case the position of the pools was known for calibration and comparison. The chosen area is the Western Desert (North Egypt), with a decades-long exploratory and productive history.

Moreover, on this area various PSM GeoModels constructed with SIMBA were already available, and one of these has been uploaded in Migri and used as reference model, filled with the Vsh data derived from well logs analysis. Thanks to it, we avoided to build a new GeoModel from scratch, operation that would have implied a too long time for the period available to conclude this study.

2. GEOLOGY OF WESTERN DESERT

2.1 GEOGRAPHICAL OVERVIEW

The Western Desert cover a total surface of 681.000 km², equal to two-thirds of the entire Egypt (Younes, 2012), from the Nile's Valley to the east, to its delta to the west, and from the Mediterranean coast to the Sudan. This area lies between the latitude 22°00'-26°30'N and longitude 28°30'-33°00'E (Zaher, 2009), and its medium altitude is 500 m.s.l. (**Fig. 2.1**).

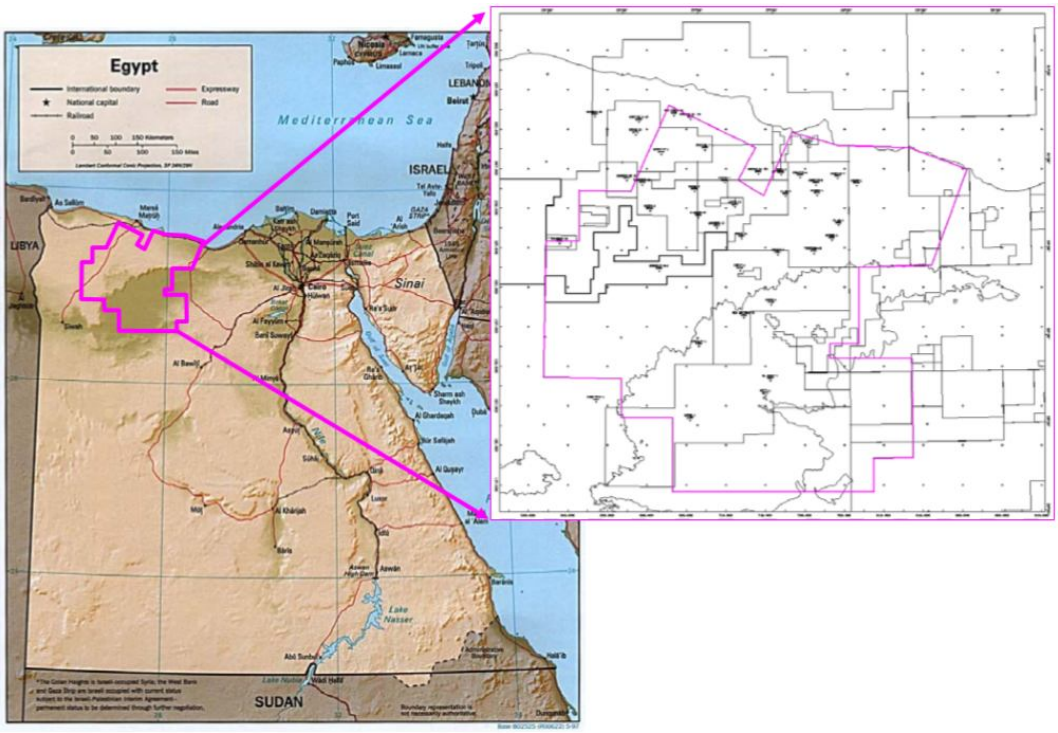

Fig. 2.1: *location of Western Desert and area of study*

Petroleum system of the zone is strongly linked with tectonic history of its sedimentary basins, that creates a series of seal-reservoir combinations, in particular starting from Upper Cretaceous to the Eocene.

The most productive source rocks are instead from Jurassic, and they provide almost half of the Western Desert oil amount (43%) and most of the gas (84%) while the rest of the reserves are generated from Lower Cretaceous source rocks (Ahmed, 2008).

2.2 GEOLOGICAL OVERVIEW

The geological settings of Egypt is characterized by a sedimentary cover that become thicker going towards north, from a maximum thickness of 3 km in the southern part, to more than 6.5 km of sediments near the Mediterranean Sea, even if this increasing thickness is not uniform. In fact, a lot of thickness anomalies are present in correspondence with the basinal areas (El-sadec et al, 2007). For example, the Abu Gharadig Basin is a sedimentary basin where sediment thickness reach 13 km in its depocenter, while in its northern margin, constituted by the Ras Qattara Ridge, sediments are less than 3 km thick.

Leaving out these local anomalies, the general trend is however a general thickening toward north, and for this reason a progressive formations rejuvenation is visible from south (where some parts of pre-Cambrian basement are locally visible) to the north, where Quaternary Nile's deposits are present (**Fig. 2.2**). Considering this progressive rejuvenation of the formations toward north, an exception is represented by oasis, typically imposed over anticline folds that have been eroded and now show older formations, as it is visible in the oasis of Siwa, Farafra, Bahariya and into the Qattara depression (El Sizi et al., 2002, Gindi et al., 1969).

In literature, in particular after R. Said studies (1962, 1990), Egypt is usually divided in two macroareas, based on the thickness and the type of sedimentary cover:

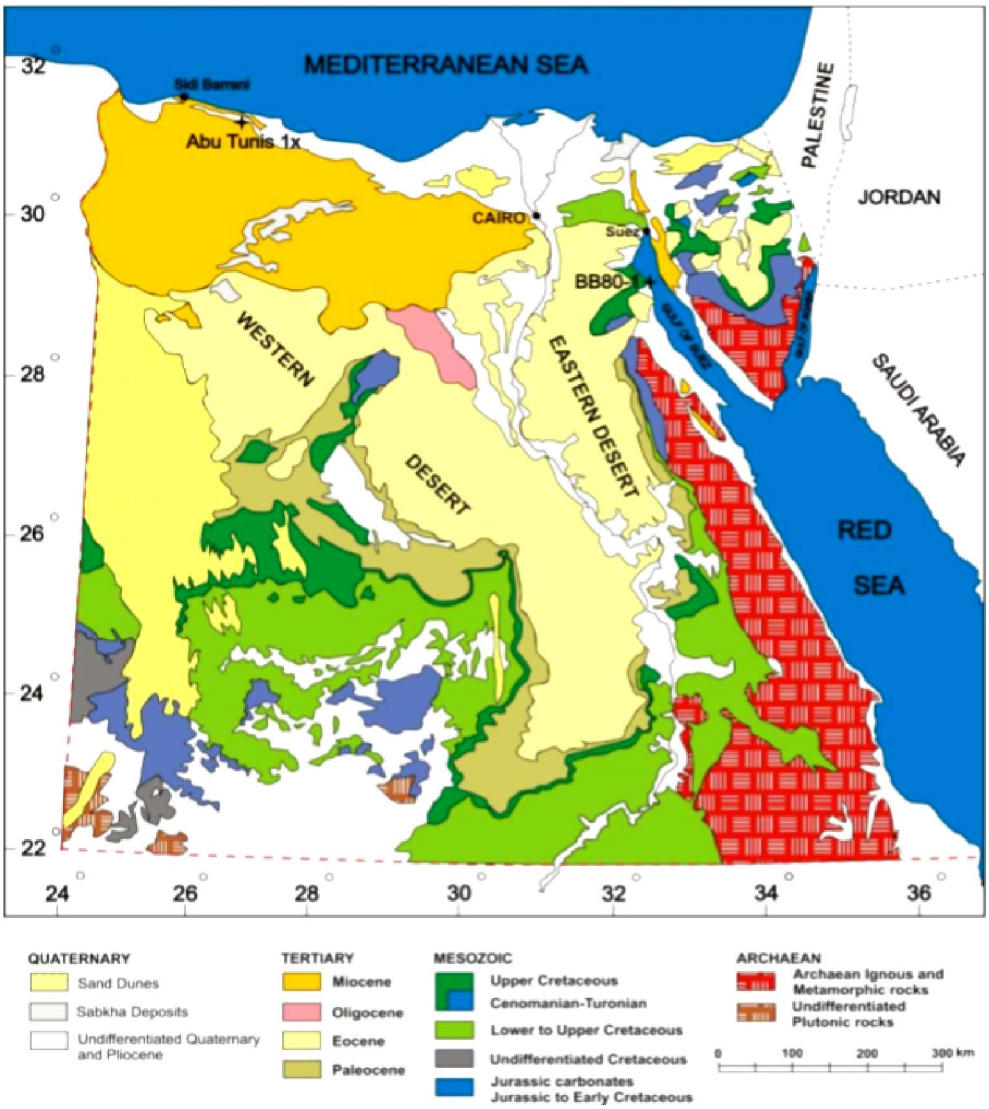

***Fig. 2.2**: Geological map of Egyp: it's visible how exposed formations are progressively younger going from south to north. After Deaf, 2009.*

- The Arabic-African craton, that forms a stable tectonic unit, in which the basement rocks are exposed; it appears in the Eastern Desert, in the southern part of the Sinai peninsula and in some isolated outcrops in the southern part of the Western Desert;
- The Shelf Areas, which are in turn divided in three sub-units (**Fig. 2.3**) (Said, 1990; Ahmed, 2008):

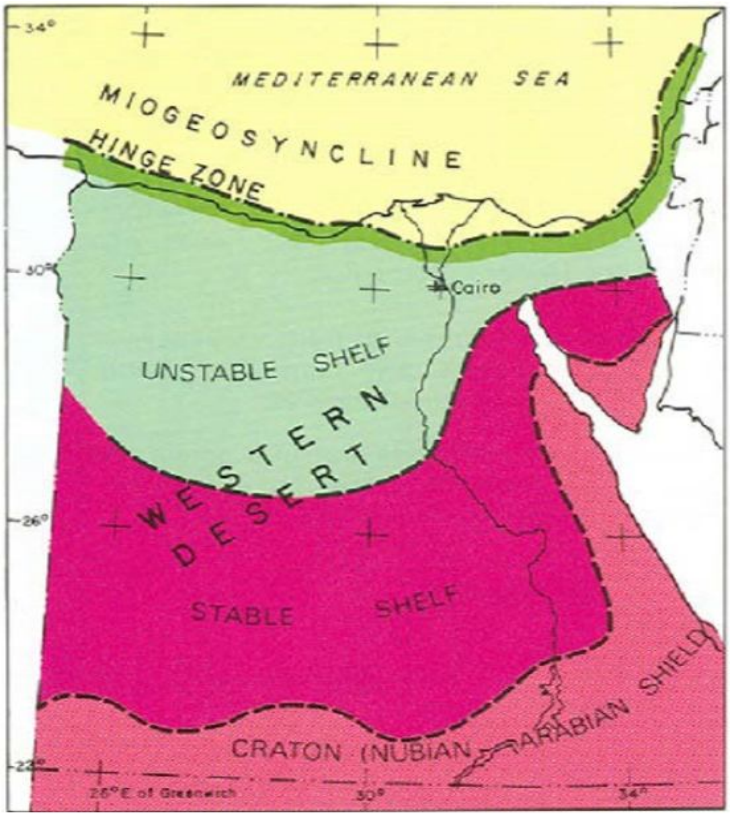

Fig. 2.3: *Subdivision of Egypt area in the four principal units. After Said, 1962.*

1. *Stable Shelf*: it extends from the southern part of the Egypt to the northern limit of Sinai; it is characterized by smooth and low relief, with a discontinue and rich of unconformity sedimentary cover, that ranges between 400 m and 2500 m, deformed by a series of regional belts.
2. *Unstable Shelf*: it is the northern part of Western Desert, and it represents the main target area of this study. It is characterized by a gentle thickness increasing of the sedimentary cover toward north, from 2500 m to 8000 m (Younes, 2012). Morphology is marked by relief due to an intense faulting phase that interested the basement, generating horst and graben structural setting. It is in contact with the Stable Shelf.
3. *Hinge zone*: it's located on the Mediterranean coasts and separates

the Unstable Shelf with the so-called *Miogeosynclinal* basinal area. In this portion, a sudden sediment thickening is visible toward the sea, and presently that sediments are covered by the Pliocene - Pleistocene Nile's sediments, with a total thickness that exceed 13 km (Said, 1990).

2.2.1 STRUCTURAL SETTING

Structurally, Egypt can be described by 5 units (**Fig. 2.5**):

1. Mediterranean faults zone: it extends along all along the Mediterranean coast, and it displaces for some thousands of metres the carbonates developed from the Mesozoic to Eocene. According to some authors, this faults zone represents the facies limit between platform and slope limestones (Harms and Wray, 1990).
2. Horst and Graben zone: it represents the main structural style of Western Desert; a deep series of horsts with limited height and grabens, further divided in smaller tilted blocks, that form the main structural depressions of the zone with a main NE-SW direction (**Fig. 2.4**).

   This alternation of highs and depressions from Paleozoic, is on the base of any sedimentary basins present both in the central part of the Western Desert (as Abu Gharadig and Shoushan basins) and in the western part (Faghur-Siwa and Matruh basin) and eastward (Natrun and Guindi basins).

   Starting from Upper Cretaceous, a compressive movement began, reactivating older normal faults as reverse and forming flower structures and folds.

   Another main event in the geodynamic evolution of the zone was the beginning of the Red Sea rifting phase, started from Cenozoic. This new tectonic event gave rise to a series of structures reflecting various stages of extension and compression (Giraud, 1999), as will be better explained in the next pages.

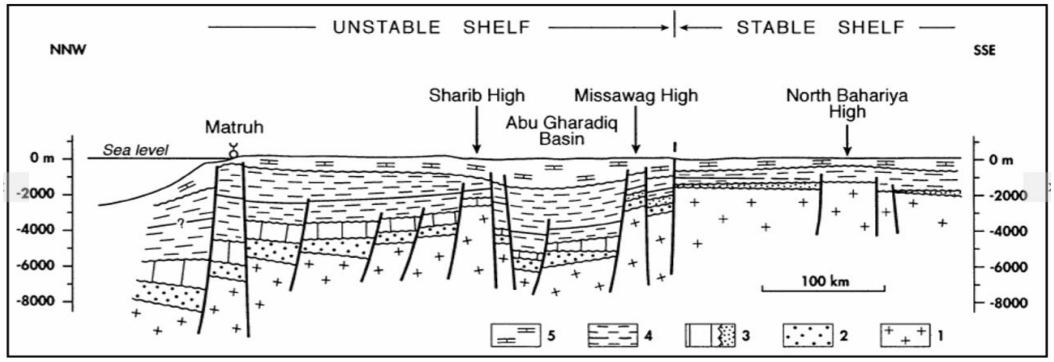

Fig. 2.4*: schematic section along the Unstable Shelf and the Stable Shelf. Legend: 1, Pan-African basement; 2, Paleozoic; 3, Continental (dots) and marine (vertical lines) Jurassic sediments; 4, Cretaceous; 5, Cenozoic.*

Specifically in the North Western Desert, five mega-structures affecting the basement have been identified. They have a strong influence on localization and orientation of the main sedimentary basins in the area, and on their tectonic and sedimentary evolution (Said, 1990):

- *Bahariya-Diyur High*: it is located in the south, where the sediments cover above the basement is thick no more than 3 km (except the Guindi basin, 5 km).
- *Gib-Afia High*: oriented with a SW-NE direction, from the western part of the Shiwa's oasis, it constitutes the NW boundary of the Qattara Depression, that is one of the main sedimentary basin of Egypt. Discordant opinions about its origin are existing: even if it is bounded by the Gif-Alfia High and 150 km northward respect to the Bahariya-Diyur Hight and it follows the direction of the others basins, according to some authors its origin would be not due to tectonics, but to fluvial erosion and karstic processes (Albritton et al. 1990). According to other authors (Gindy et al., 1991), instead, the position of Qattara Depression, 50 km west to the Siwa Depression, and in orientation continuity with it, would be the proof that the two basins are part of the same tectonic

structure.

- *Sharib-Sheiba High*: it extends with a E-W direction, from the western part of the Gib-Afia high to the intersection with the Kattaniya High eastward.
- *Kattaniya High*:, it's a raised block bounded by faults with NE-SW direction.
- *Abu Gharadig Basin*: the oldest and deepest basin in the area. Its sedimentary sequence reaches up to 13 km of thickness in its depocentre (Deaf, 2009).

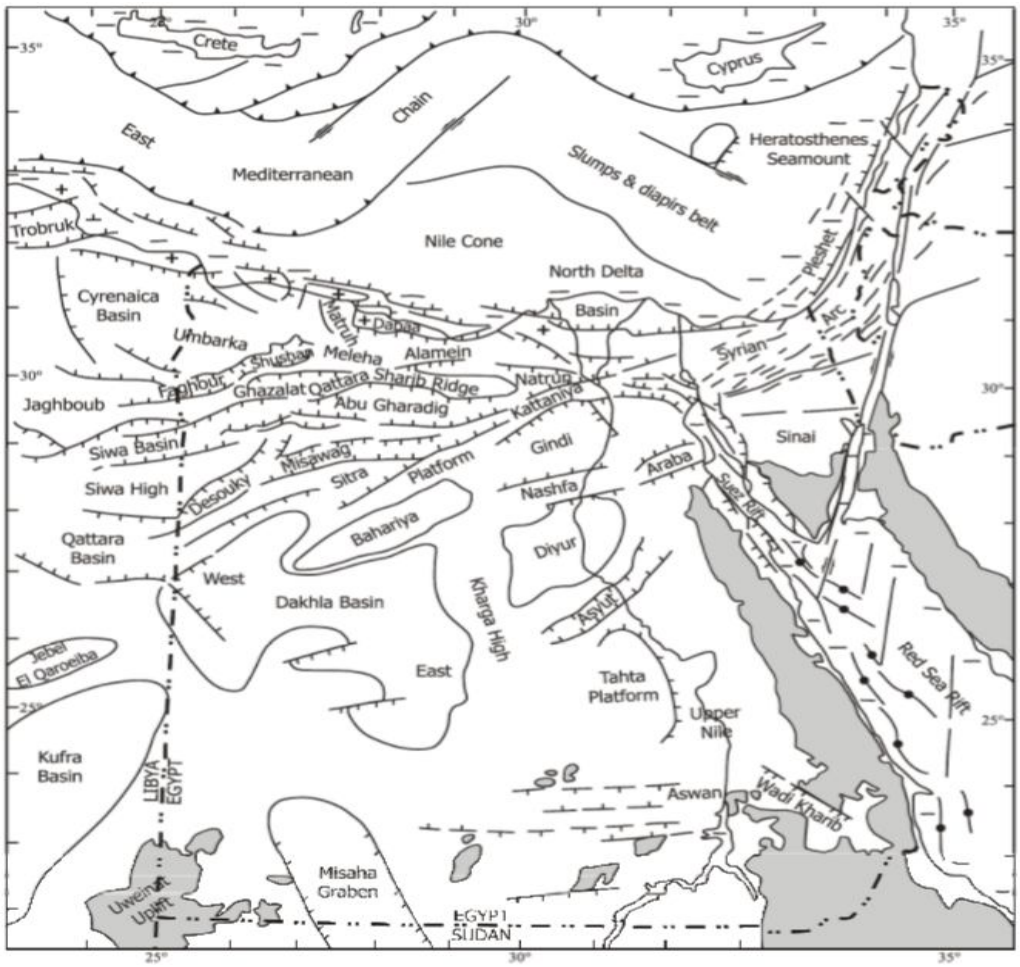

Fig. 2.5: *Map of structural elements and sedimentary basins.*

3. The graben of Suez and Red Sea: the rifting event that is still evolving in the Red Sea zone developed a structural low into the Mesozoic-Paleogenic structures in the N-E part of Egypt. The rift doesn't involve the Mediterranean Sea, but it finishes in the northern part of Suez.
   Pre-rift sequences are visible just in the north of the zone interested, and they are composed by tilted blocks, salt domes and superficial folds from pre-Miocene (Said, 1990).

4. Souther Egypt intracratonic basin: the pre-Cambrian basement principally outcrops in the southern part of Sinai, and just locally in the Red Sea mountains (Sestini, 1995, Ahmed, 2008). Into the northern zone of Western Desert, the depth of the basement is between 1500 and 4000 m under the sea level (El-sadec et al, 2007).

2.2.2 GEOLOGICAL EVOLUTION

The geological evolution of Africa starts from Panafrican event, which developed during Proterozoic and that formed the Gondwana super-continent from 720 to 580 My (**Fig. 2.7**) (Guiraud et al., 2005).
After that, during the Phanerozoic, the development of sedimentary basins was linked to multiple phases of break-up, caused by movements that developed principally through existing faults and fracture surfaces formed during the pan-African event.
The geodynamic setting that characterized Africa from the Paleozoic onwards is principally extensional, although some important exceptions are present, like the compressive movement related to the Paleotethys subduction and the Alpin-Himalayan orogeny (Bumby et al., 2005). Different phases of basin filling which formed during that time have been also influenced by climatic changes, that reflected in the alternation of transgressive and regressive see level cycles.
In this paragraph a more detailed description about the tectonic and eustatic events

is reported (**Fig. 2.6**).

1. ***PALEOZOIC:***

- CAMBRIAN-ORDOVICIAN: Starting from Paleozoic, the actual African continent was located at the centre of the Gondwana super-continent (Bumby et al., 2005). With the beginning of the Cambrian, a short transgressive phase took place, but it finished at the end of that period, due to sea-level falling and regional uplift (Guiraud et al., 1999).

  For this reason, sedimentary facies at the Cambrian-Ordovician limit are mainly continental, given bymolasse and fluvial sediments resulting from structural high that interested the basement (Ahmed, 2008, Guiraud et al., 1999).

  These terrigenous facies dominated the sedimentation also during the Lower Ordovician, when marine regression was caused by a strong glacial event, which protracted until the end of that period (Guiraud et al., 1999; Bumby et al., 2005). The current Western Desert, at the end of Ordovician was located close to the Paleo-South Pole (Guiraud et al., 1999; Lüning, 2000), and so sediments from Middle and Upper Ordovician were continental in the study area.

- SILURIAN: From the Lower Silurian, the Gondwana super-continent started to move northward and this motion continued for the entire Paleozoic (Bumby et al., 2005). This period was characterized by a sea rising phase, due to melting of the icecap (Bumby et al., 2005; Lüning, 2000). In the Western Desert, as well as in the eastern part of Egypt, shallow sea conditions were established, allowing the deposition of sandstones and shales (Guiraud et al., 1999).

  In the upper part of the period, a new tectonic instability phase is recorded

by many depositional hiatus and unconformities. The origin of this phase could be associated, according to some authors, to an orogenic phase given by collision between Gondwana and Laurentia (Bumby et al., 2005). According to other Authors, uncorfomities formed after the uplift of rift shoulders related to the Paleotethys rifting early stage, the newly-formed ocean that started the Gondwana break up (Guiraud et al., 1999; Ahmed, 2008).

- DEVONIAN: at the beginning of the period, a generalized sea-level falling took place; despite this event, the northern African margin was submerged (Guiraud et al., 1999). North-east successions related to this period are composed by fine-marine and fluvio-deltaic sediments, carbonates and sandstones (Ahmed, 2008). Locally some volcanic effusions happened, as in the Sheiba Hight zone.

- CARBONFIEROUS: in the Lower Carboniferous, the Arabic-African margin was interested by a deep see environment (Guiraud et al., 1999; Ahmed, 2008; Bumby et al., 2005), but new regression stage started from the middle part of the period, when a shallow-water sea environment characterized the northern Egypt (Guiraud et al., 1999). Transition from Carboniferous to Permian was marked by a regional unconformity, due to a deformation event developed after the Hercynian orogeny (Guiraud et al., 1999; Ahmed, 2008; Bumby et al., 2005).

- PERMIAN: Permian sediments in Western Desert are rare, due to the great tectonic instability that characterized this zone during this period, because of the Hercynian orogeny movements, that led to the collsion between Laurussia and Gondwana and to the Palaeotethys closure. This event can be considered as the last unification phase of all world's lands in

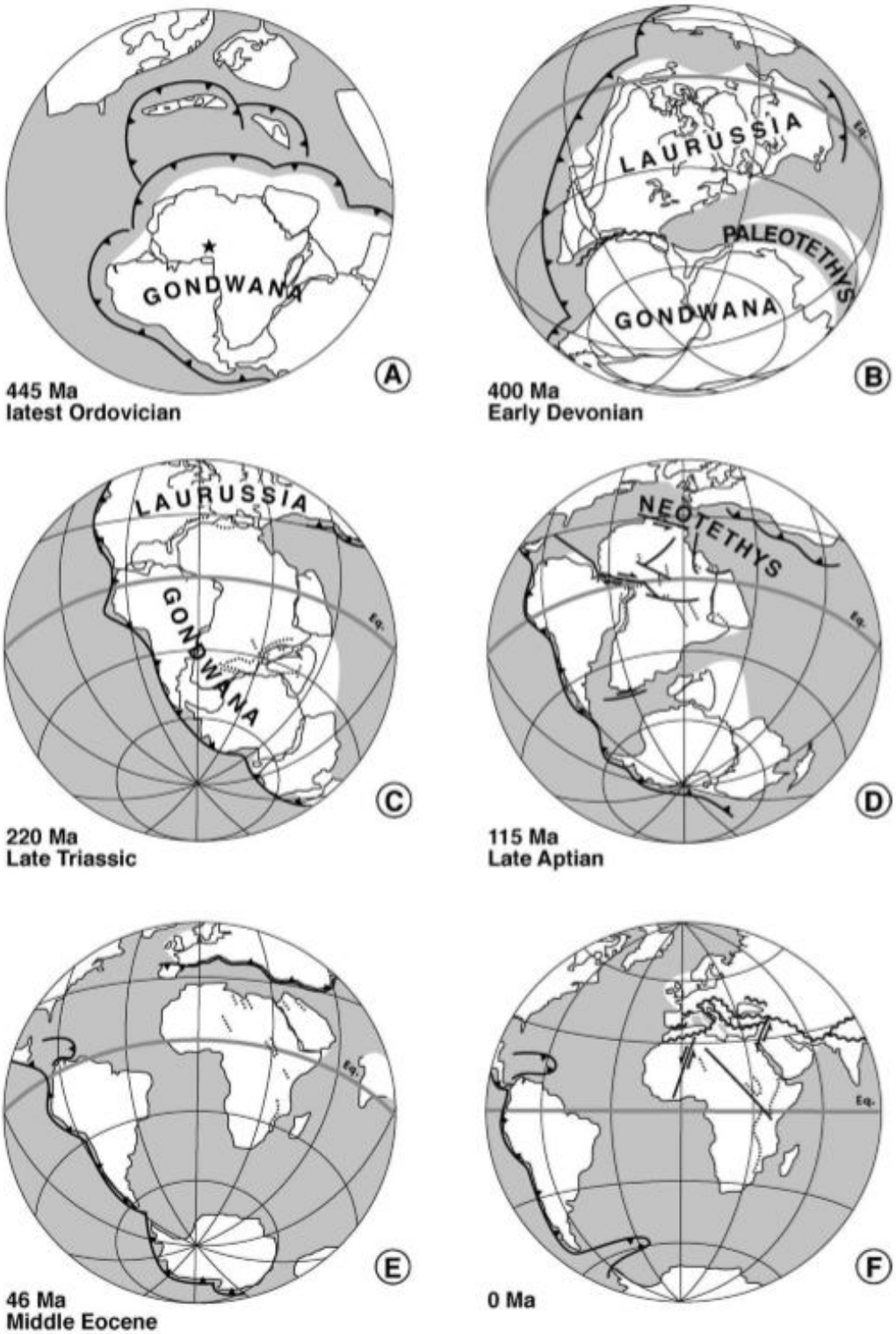

Fig. 2.6*: Paleo-geographic reconstruction of the evolution of Gondwana super-continent. A: 440 Ma, Upper Ordovician; B: 400 Ma, Lower Devonian; C: 220 Ma, Upper Triassic; D: 115 Ma, Upper Aptian; E: 46 Ma, Middle Eocene; F: current situation. After Guiraud et al., 1999.*

a unique super-continent, Pangea (Guiraud et al., 2005), that in the later tectonic stages experienced break-up events (Guiraud et al., 1999; Bumby et al., 2005).

Carboniferous-Permian and Permian-Triassic limits can be recognized by their erosion surfaces, depositional hiatus and unconformities, with local shallow water sediments.

2. MESOZOIC:

- TRIASSIC: from the Permo-Trias limit until the end of Lower Triassic, Western Desert experienced an uplift period (Carminati et al., 2012), with sediment deposition allowed only in the low-structural areas. There were overall *red-beds* and sandstone deposits.

  Starting from Triassic, the area was subjected to a generalized extensional period, with associated basaltic effusions (Guiraud et al., 1999) that continued for the entire Jurassic, resulting in the Neotethys formation (Deaf, 2009). During the Triassic, North Africa underwent a big change in the tectonic regime, from convergence started with the Paleotethys closure, to a passive margin and generalized extension situation, when the Neotethys began to open (Bumby et al., 2005).

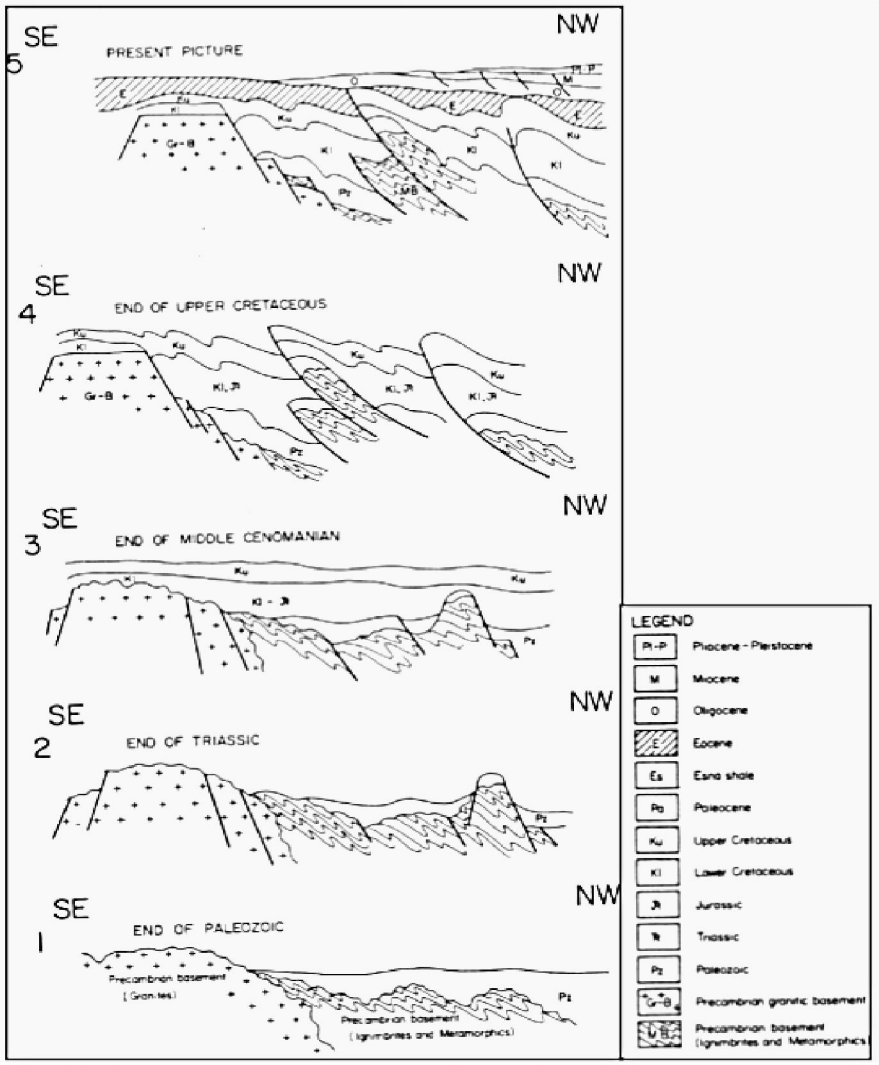

Fig. 2.7: *Schematic section representing the evolution of basins in northern part of Western Desert during the time. After Ahmed, 2008.*

- JURASSIC: during Lower Jurassic, Western Desert was in a shallow water environment that until the Middle Jurassic experienced a deepening tendency, interrupted only by some minor regressive events (Guiraud et al., 1999). The deepening was caused by the break-up of the Turkish micro-plate from the Gondwana super-continent due to the Neotethys development (Deaf, 2009; Bumby et al., 2005). From the Lower Jurassic onwards, both the basement and the Paleozoic sediments were strongly faulted, and this phase created new sedimentary basins principally developed in NE-SW

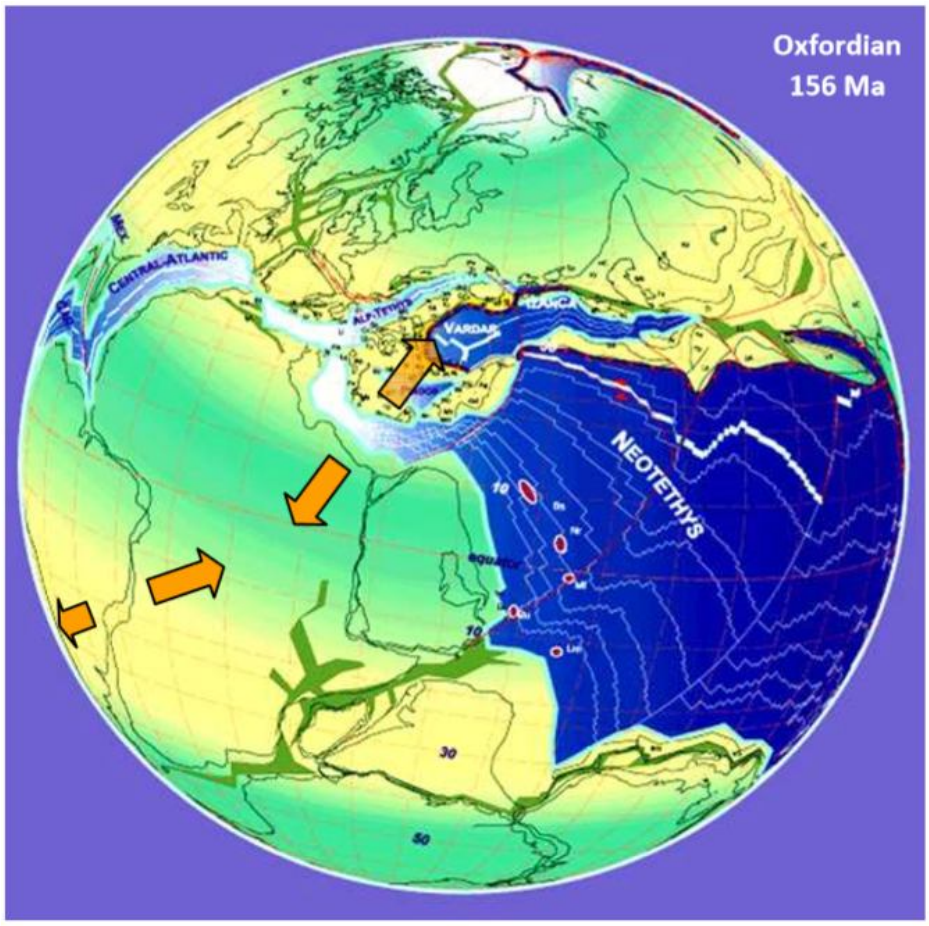

***Fig. 2.8**: Reconstruction of the Turkish micro-plate break-up from Gondwana, with the consequent formation of the Neotethys, Upper Jurassic. After Stampfli et al., 2002*

direction (**Fig. 2.8**) (Ahmed, 2008).

This environment developed a strong sedimentation, overall in some basin as in the Abu Gharadig (Ahmed, 2008).

The Jurassic-Cretaceous limit coincided with a new period of strong tectonic activity, starting from the Kimmeridgian orogeny, mainly in the south-eastern Europe. This tectonic phase generated a generalized uplift of this zone, and this is recorded in the Western Desert sediments as a series of unconformities and depositional hiatus (Guiraud et al., 1999).

- CRETACEOUS: starting from Cretaceous, the Arabic-African plate was subjected to important rifting events, principally developed along an E-W direction. New accommodation space allowed deposition of fluvial and lacustrine sediments deposited(Guiraud et al., 1999). In the upper part of the

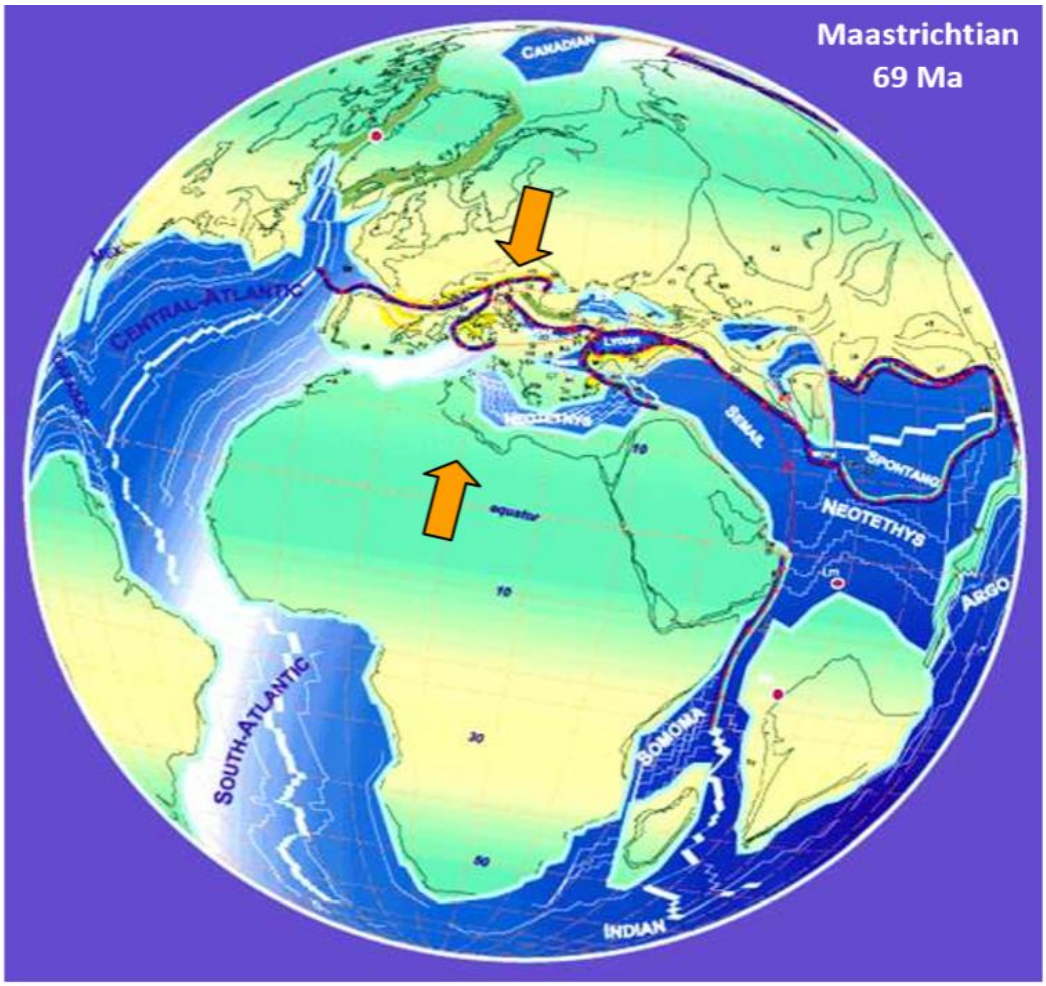

***Fig. 2.9**: Schematic reconstruction of the Gondwana break-up, Upper Cretaceous: Paleotethys closed and the Neotethys opened. After Stampfli et al., 2002.*

period, the zone was subjected to a very important compressive event, started from the Alpine orogeny. The Atlantic Ocean opened in its southern part, and this generated an important compressive phase, which involved uplift and new faults system development, with strong displacements rates (Ahmed, 2006; Bumby et al., 2005). Tectonic movements related to this period are essential in the Western Desert petroleum system development, because the main traps are associated with the Upper Cretaceous movements (**Fig. 2.9**).

3. CENOZOIC:

- PALEOCENE-EOCENE: Until the end of the Paleocene, this zone recorded another strong tectonic period, which was manifested principally with the subduction of the main sedimentary basins (Said, 1990). Anyway, the most important Ceneozoic tectonic event developed starting from Medium-Upper Eocene, and it was still due to the Alpine orogeny. In the Western Desert, this period is called “Eocene Inversion Phase”: this compressive movement reactivated normal faults previously developed as inverse faults (Ahmed, 2008; Guiraud et al., 1999), generating a period of strong uplift in the Western Desert, and placing horsts and grabens in their current position.
  During this period, lots of Cretaceous sediments were eroded, and Eocene units are very fine grained or absent.

- UPPER EOCENE-PLIOCENE: After the inversion phase, a new transgressive phase took place starting from Upper Eocene. This phase continued until the end of the Lower Oligocene. Deltaic deposits were deposited, supplied by rivers from the blocks previously uplifted (Ahmed, 2008).
  Starting from Late Oligocene, transgressive phase linked with the Red Sea

rifting started; at the beginning of Miocene the rift shoulders lifted, with a generic uplift in the Eastern Desert that allows the rivers flowing in this zone to unload their sediment charge into the Western Desert (Guiraud et al., 1999; Bumby et al., 2005).

The Mediterranean crisis, occurred during Messinian, caused a radical sea level lowering,deposited with formation of evaporites in the external parts of Egypt (for this reason, these formations are not visible into the Western Desert9.

2.3 CHRONO - STRATIGRAPHY AND PETROLEUM SYSTEM

The Western Desert succession is characterized by an alternation of carbonatic and clastic sediments, coming from the repetition of transgressive and regressive cycles as previously described.

This is one of the keys of the Mesozoic-Cenozoic petroleum system, as alternations of different sediments allows potential source rocks formation (already starting from Carboniferous), reservoirs and seals.

Studies focused on the hydrocarbon generation potential of the Western Desert showed that there are multiple levels of source rocks, with different thermal maturation degrees (De Poli et al., 2009; Younes, 2012).

Other important events in the formation of petroleum system in this zone are subsidence phases developed from the Upper Jurassic to the Upper Cretaceous, that created the main sedimentary basins, and the Upper Cretaceous-Paleocene movements that allowed traps formation (Sestini, 1995).

In the following part of this chapter, the chrono-stratigraphy of Western Desert will be explained in detail, with particular attention to the main elements which constitute this petroleum system.

2.3.1 PRE-CAMBRIAN BASEMENT:

Egypt's crystalline basement is pre-Cambrian (Said, 1990), and it is composed by granites and granitoids with a low-grade metamorphism (Ahmed, 2008). Isotopic studies have shown that two different intrusive events occurred: the firs took place between 1000 and 850 Mya, with calc-alkaline diorites and granitoids; the second more recent and about 650 to 500 Mya old, with K-feldspar rich granites (Ahmed, 2008).

2.3.2 PALEOZOIC:

Depocenters of Paleozoic show an approximate NNW-SSE trend, controlled by the major faults developed during pre-Cambrian;, , the sedimentary cover increases from SE to NW (**Fig. 2.10**).

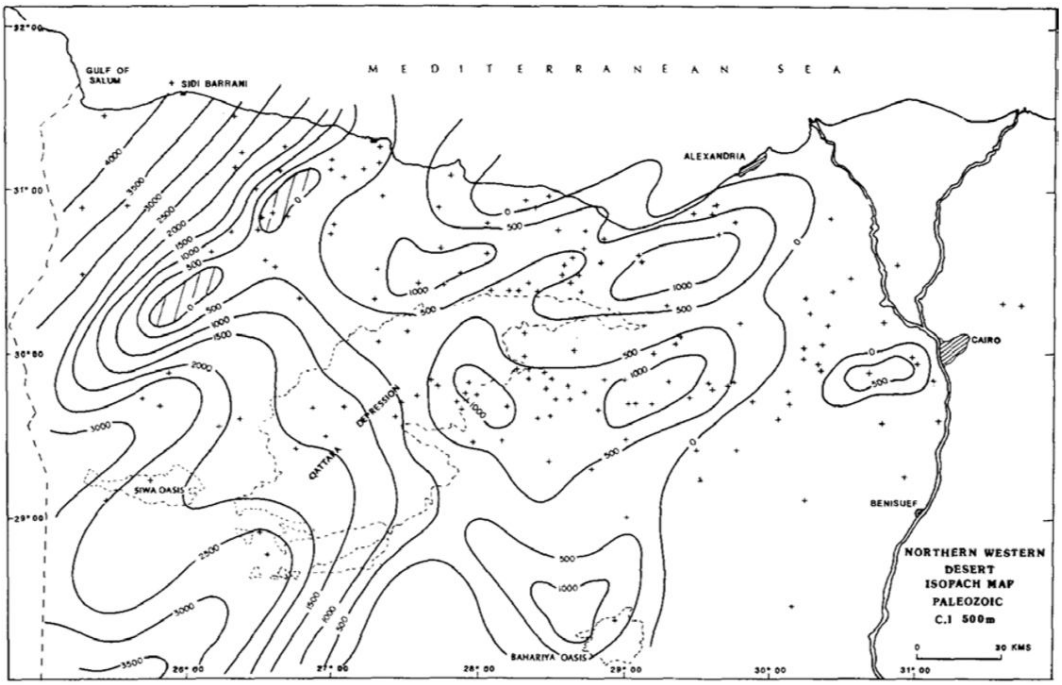

***Fig. 2.10**: isopach map of the Paleozoic*

Therefore, the thickest deposits are close to Libya, with sedimentary successions greater than 4000 m in the northern zone (Ahmed, 2008).
Vice versa, southward there are some places where Paleozoic is not visible, and where Mesozoic association directly lie on the basement.
Because of the intensive tectonic activity recorded during the Paleozoic, limits between one formation and the other are often hardly visible or incomplete in the southern part, while moving toward Libya, stratigraphy is clear and complete, and formations are clearly distinguishable (Ahmed, 2008; Said, 1990).
With regard to the lithologies, Paleozoic rocks are principally arenaceous, deposited in continental or shallow water environment, with shaly interlayers and in some case, overall in the upper part, limestones.
These formations can be distinguished into two macro-groups: the Siwa group (Cambrian-Silurian) and the Faghur group (Deovonian-Carboniferous). (Paleoservice, 1986). More specifically:

- CAMBRIAN-ORDOVICIAN: the low transgressive period that characterized the Early Cambrian, ending in the upper part of that period, is visible in the **Shifah Fm** sediments (Cambrian-Ordovician), belonging to the Siwa macro-group. Within this formation it is possible to see thin calcareous layers (Ahmed, 2008), even if the main lithologies deposited at this time were mostly terrigenous; the Shifah Fm in fact consists of fluvial sandy sediments, fine to coarse, deposited in tidal or beach environment, interbedded with shaly sub-layers and many depositional hiatuses.
  The glacial period, occurred in the final part of Ordovician (Guiraud et al., 1999) resulted in a strong marine regression, marked by quartz fluvio-glacial sandstone.

- SILURIAN: Formations from this period have been deposited in

unconformity over the **Shifah Fm**, because the glacial erosion developed until the Ordovician-Silurian limit.

The subsequent transgressive phase allowed the deposition of the Khola Fm which, mainly consists of clean marine sandstone (Paleoservice, 1986). Another formation deposited in this period is the **Basur Fm**: sandstone beds alternate with thin limestone sheets that, even if they were very rich in organic matter, doesn't represent important source rocks because of their limited thickness (Lüning, 2000).

- DEVONIAN: Formations belonging to Faghur Group started to deposit during Devonian. Even in this case, the base of succession is on unconformity respect to Silurian top. The main formation which deposited in this period was the **Zeitoun Fm** (Devonian), marked by a continuous sediment supply, mainly consist of schists, siltstone and marine sandstone (Sestini, 1995), testifying a marine environment (Ahmed, 2008); thanks to its high organic content, Zeitun Fm is considered a Paleozoic source rock (Ahmed, 2008).

- CARBONIFEROUS: the transition that occurred in Carboniferous from a shallow water to continental environment is clearly visible into the Western Desert rocks. The first Carboniferous formation is made by sands and shales belonging to **Disoqy Fm** (Lower Carboniferous), over which the **Diffah Fm** (Muscovian) deposited in stratigraphic continuity: these are shaly-interbedded limestones, replaced at the top by fluvial sandstones (Ahmed, 2008). Above the Dhiffah Fm, the **Safi Fm** (Muscovian-Gzhelian) is present; it is composed by fluvial sandstones, which indicate a return to a continental environment.

- PERMIAN: the base of Permian is characterized by a regional unconformity, due to a continuous compressive movement that lifted up this area and involved a sea level falling. Deposits from the Early Permian are lacustrine, while the Guadalupian transgressive phase, that affects just few portions of Egypt coast, is evidenced by the presence of shallow-water sea and platform limestones. These deposits are not always easily observable and recognizable; because of this, and the absence of biostratigraphic markers, it's not simple to distinguish the Paleozoic-Mesozoic limit (Sestini, 1995).

2.3.3 MESOZOIC:

- TRIASSIC: Triassic sediments are nearly absent in Western Desert; local sedimentation led to the deposition of the **Eghei Fm**, a sandstone interbedded with *red-beds* type deposits. The only areas in which it is possible to recognize this formation are some parts of the Abu Gharadig Basin and, some other low-structural areas.

- LOWER JURASSIC: a new transgressive event occurred in Lower-Medium Jurassic, and it led to a new shallow-water deposition stage. Jurassic formations are easy recognizable everywhere in Western Desert, with a bathimetry deepening towards North, where also deep sea deposits are present, somewhere thicker than 2500 m.

  The first visible Jurassic formation is the **Bahrein Fm** (Millde-Upper Jurassic), made by a fine-grained quartz sandstone, with shaly and anhydritic intercalations. This formation deposited in continuity with the **Wadi Natrun Fm** sediments (Middle Jurassic) in the North-East; it is made by lagoon marly limestones, interbedded with anhydrite levels.

  Westward, Bahrein Fm is located above Paleozoic structural highs.

- MIDDLE JURASSIC: at this time, deposition of **Khatatba Fm** occurred. This formation has a great importance on this study, because it has the double role of reservoir and most important source rock of Western Desert (Younes, 2012).

  The high petroleum potential of this formation is due in particular to some levels that show an high organic carbon content. The highest TOCs are recorded where the source rock levels reach 100-200 m of thickness in its upper member and 150-220 m in the lower, while the minimum values are found in correspondence of the areas where the source rock is too much shallow or thicker than the reported thickness.

  An explanation about the relationships between high TOC values, formation thickness and depth could be found in the excessive organic matter dilution by sediments where they are too thick, and the low preservation degree where they are too shallow, due to oxidation processes.

  Khatatba Fm is characterized by a great lateral and vertical heterogeneity, both in terms of lithology and sedimentology. For this reason, it is usually divided into 3 members (SGEG-SPES, 2012).

  The two lowest members are characterized by an alternation of sandstone and mudstone, constituting the source rocks:

    - Khatatba2 Lower (175-169 Mya): typical arenaceous and shaly transgressive facies, deposited in a marginal marine environment.

    - Khatatba2 Upper (169-167 Ma): mainly represented by continental fluvio-deltaic cycles. It shows a great lateral variability, due to the presence of deltaic channels.

- Khatatba 1. (167-164 Ma): it is the shallowest member, composed by carbonates interbedded with thin sandy and shaly intervals. The carbonates decrease moving upward, when terrigenous sediments appear (Ahmed, 2008). In particular, the upward increase of sandstone component makes this part of the Khatatba Fm an important reservoir rock, and one of the carrier levels that will be carefully investigated in the next chapters.

- UPPER JURASSIC: **Masajid Fm** (Oxfordian-Kimmeridgian) lies over the Khatatba Fm, and it consists of a massive limestone deposited after a sea-level rise period that occurred until the Jurassic-Cretaceous limit. It represents an important regional seal for the underlying Katatba1 member (Ahmed, 2008).

  Going toward North-West, the Upper Jurassic is instead represented by the **Sidi Barrani Fm** (Medium Jurassic-Lowe Aptian), deposited in a low energy environment and with a limited accommodation space. Unlike Masajid, Sidi Barrani continued to deposit even for the entire Lower Cretaceous.

- LOWER CRETACEOUS: after a strong tectonic activity period during the Jurassic-Cretaceous limit, that caused a diffused uplift (with consequent unconformities and depositional hiatuses), an extensional phase affected the Western Desert and it caused subsidence and a succession deepening along the whole period. This sedimentary condition is represented by **Alam el Bueib Fm** (Berriasian-Aptian). This formation is composed by fine to coarse sands, which have a great importance in the Western Desert petroleum system. In fact, it is the thickest formation of the entire succession, with thicknesses also greater than 4000 m (Sestini, 1995).

  Its extreme internal variability, both lithological and in terms of organic

matter content, allows to identifying three main source rocks intervals: a lower member, consisting of continental sandstone, followed by an intermediate member and by an higher one, even composed by sandstone, but intercalated by marly limestones, that represent the first fluvio-deltaic deposit after Upper Jurassic regional uplift event (Ahmed, 2008). Based on further analysis, it seems that only the intermediate source rock levels have been able to contribute significantly to the petroleum potential of the Western Desert, and only in the southern part of Abu Gharadiq Basin, because of its insufficient values of temperature and vitrinite reflectance in other areas (De Poli et al., 2009; SGES-SPES, 2012).

In some parts of Western Desert it is also present, , a different formation, coeval to the Alam el Bueib Fm, called **Matruh Fm** (Berriasian-Barremian).

During the Aptian, the transgressive phase reached its apex (Ahmed, 2008), and this event important event is well represented in the stratigraphic record by the **Alemein Fm** (Upper Aptian), This succession is given by dolostone characterized by facies heteropy: laterally an alternation of shales and dolostone is visible, while upwards it passes from dolostone to limestone or marly-limestone (SGEG-SPES, 2012).

This formation is easily recognizable through seismic section, because it cause a strong acoustic impedance contrast (Ahmed, 2008) (**Fig. 2.11**).

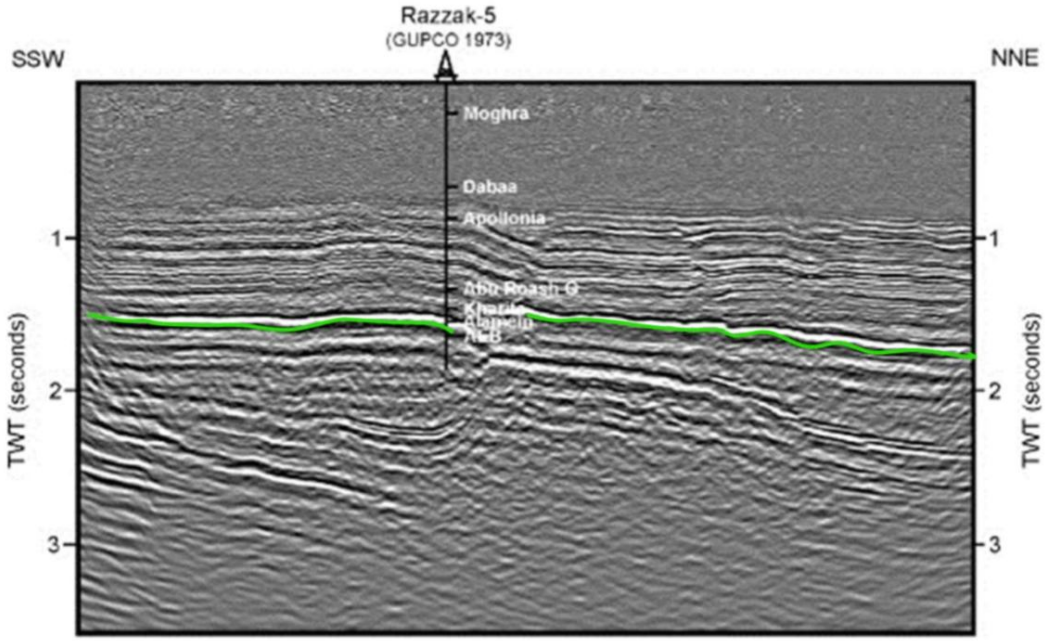

***Fig. 2.11**: seismic section in which the Alemein Fm dolostone level is showed. After Bevan et al., 2012*

Some authors (Neftex, 2013) argue that between Aptian and Albian a new sea level fall occurred, and this regressive stage would have eroded part of Alemein Fm, leading to mudstones deposition with some siltstone intervals and thin sandstone layers, corresponding to **Dahab Fm** (Upper Aptian). This formation is very important in Western Desert petroleum system because it represents a very good seal, even if not so extended and without a perfect lateral continuity. According with other authors (Said, 1990), instead, the sea level fall did not occurr, and they considering the Dahab Fm in stratigraphic continuity with the underlying formations.

Starting from Middle Aptian to the end of the Lower Cretaceous, deposition of quartz sandstone occurred, with subordinate shale limestone levels which constitute the **Kharita Fm** (Albian). This succession is in stratigraphic continuity with the Dahab Fm only in few areas, while in others it is on unconformities or, in the souther parts, in contact with the oldest formation, or even with the basement (Sestini, 1995).

- UPPER CRETACEOUS: starting with the Upper Cretaceous, deposition of **Bahariya Fm** (Cenomanian) began. It developed in stratigraphic continuity with the underlying Kharita Fm (Gadallah et al., 2010). At their base, clean coarse grading fluvial sandstones are present, with a typical festoon stratification and high porosity, These properties made this formation the main reservoir rock in the whole Western Desert. (Sestini, 1995; Ahmed, 2008; El-sadec et al, 2007; Gadallah et al., 2010). In its intermediate levels, formation changes to an estuary environment with finest sandstone, fossils rich, while at the formation top dolostones and lagoon limestones are present (Sestini, 1995, Gadallah et al., 2010), characterized by a strong organic content that make this formation also a potential source rock (Ahmed, 2008). We can therefore assume that during deposition of this formation, the northern part of the Western Desert was slightly submerged (no more p than 50 m), while the southern areas were interested by meandering channels (Ahmed, 2008).

  After that, the **Abu Roash Fm** deposited (Upper Cenomanian-Santonian). Even this formation is divided in many members, diversified according to eustatic variations occurred in this period (Ahmed, 2008).

  In particular, seven different layers (A-G) can be distinguished, four of which consist of limestone and dolostone, while the other three are an alternation of sandstone and shales rich in organic matter, that constitute a potential source rock. Petroleum potential is important in particular within F anf G members of Abu Roash Fm, even if their general immaturity in the depocenter areas, visible in their low Ro%, makes this rock not efficient to contribute to the hydrocarbon generation, except in the deeper zone of Abu Gharadiq Basin, where depths more than 11 km are reach (Sestini, 1995).

  In the middle part of Upper Cretaceous, in particular during Santonian, along the African-Arabian margin, an important uplift occurred, due to the

tectonic events previously described. This event generated large unconfomities and thickness variations. Rocks deposited in this period are fine-grained or absent, or shows multiple levels of onlap or unconformities, testifying this tectonic instability (Ahmed, 2008).

2.3.4 CENOZOIC:

- PALEOCENE-EOCENE: A new compressive phase occurred along all the Mediterranean region starting from the end of Cretaceous (Giraud, 1999), causing a strong erosion of the sediments previously raised. Sedimentation continued just in the low structural areas, and was characterized by limestone and fossiliferous muds, as the **Esna Fm** (Paleocene).

  In the areas close to the Mediterranean it was possible the deposition of **Apollonia Fm** (Paleocene – Middle Eocene),.Different depositional environment it shows differences based on its depositional environment: in correspondence of the horsts, nummulites limestones formed, while in the low structural parts (as the Abu Gharadic, Gindi and Natrun Basins) micritic limestones deposited (**Fig. 2.12**) (Sestini, 1995; Mohammed, 2012).

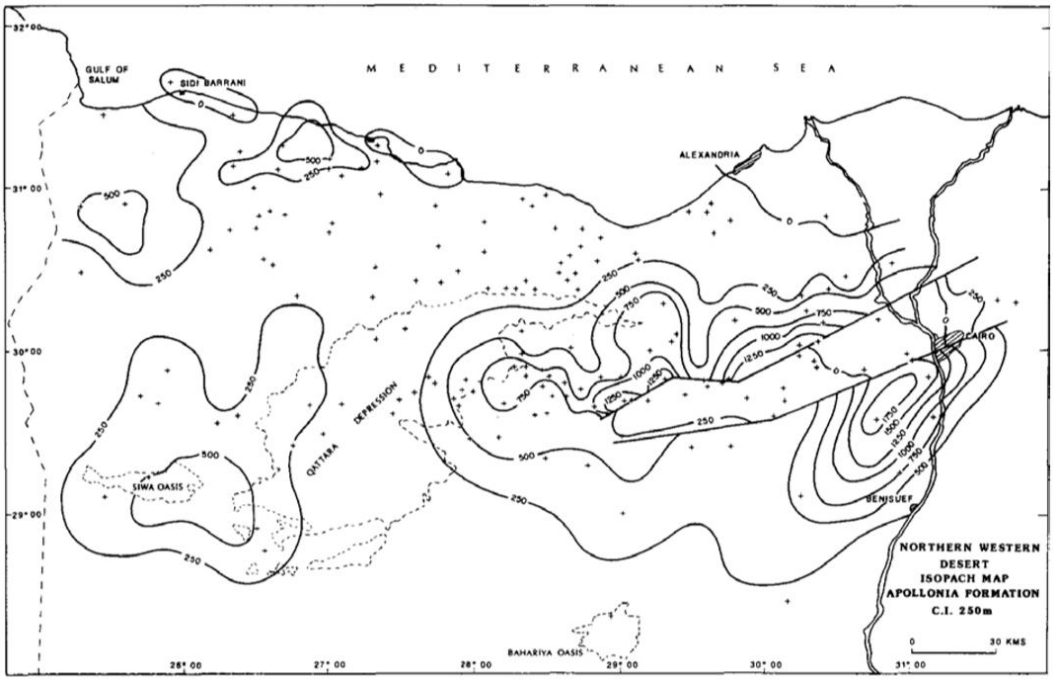

***Fig. 2.12**: Isopach map of Apollonia Fm. After Said, 1990.*

- UPPER EOCENE: starting from the end of Eocene, a new transgressive phase interested the Western Desert and it allowed the deltaic deposits to form, fed by big rivers that flowed from the southern raised parts, with terrigenous sedimentation in the northern areas. Under this setting, the **Dabaa Fm** deposited (Upper Eocene – Oligocene), composed by brown to green deltaic mudstone (Sestini, 1995).

- LOWER MIOCENE: During the Lower Miocene, the uplift of the shoulders linked to the Red Sea rifting has made possible the development of big rivers flowing toward West, with deposition of fluvial sandstone and deltaic siltstone, that pass to limestone in the external parts (Sestini, 1995).

  First deposits have formed the **Moghra Fm** (Lower-Medium Miocene), while the second ones are shown into the **Marmarica Fm** (Medium-Upper Miocene), just visible in the northern part of the Western Desert (Said, 1990).

- UPPER MIOCENE: starting from Serravallian, the so-called "Mediterranean crisis", due to the closure of the Strait of Gibraltar, induced to a diffused subaerial exposure of the zone. The classical evaporites often referred to this period are not visible in Western Desert, but just in the closer parts, as the Red Sea or the Nile Delta, or in the current Egypt offshore zones.

- QUATERNARY: the most recent deposits in the North-West part of Egypt are dominated by continental facies, and they recorded a series of pluvial phases through the formation of alluvial fans, braided deposits and *sabkha* (Said, 1990). This area has continued to be exposed, as we can see it until the present days.

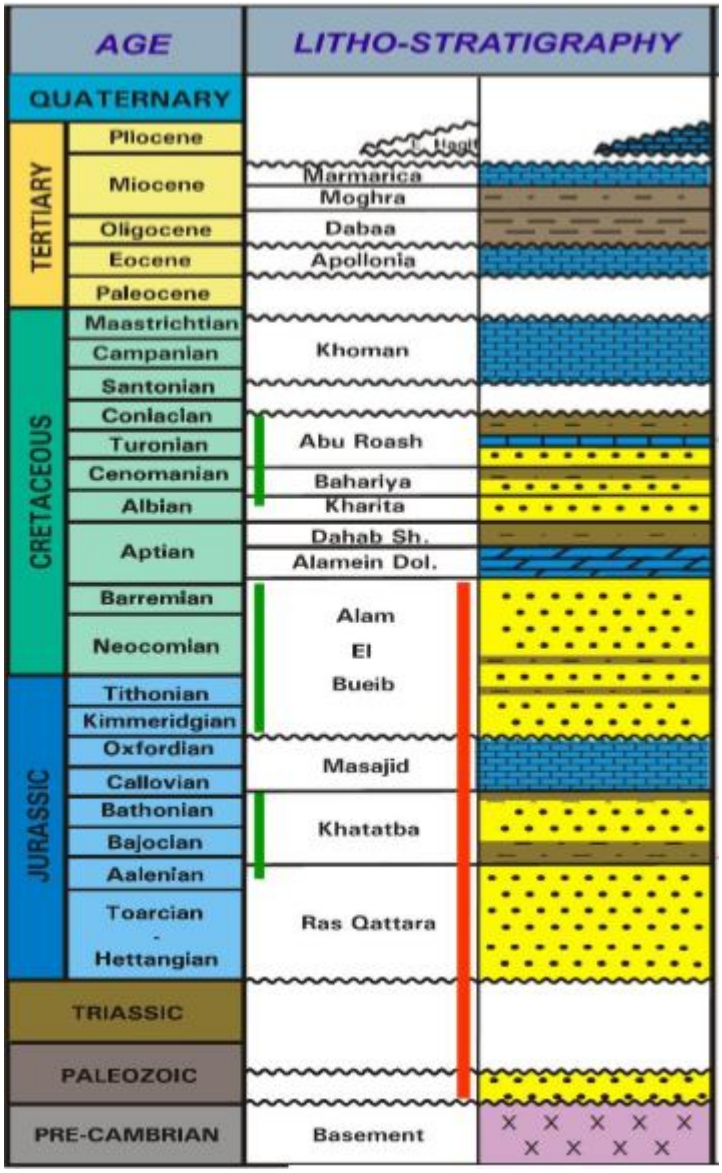

***Fig. 2.13**: Stratigraphy of the Western Desert*

3. FORMATIONS TOP DATA

The Egypt Western Desert experienced a long exploration history, starting from the end of the nineteen century until our days (Ahmed, 2008). This is the reason why in this area there are many exploration and production wells, both in the North and in the South side. However, sometimes it's not so easy to obtain data about these wells, because of different data sources whit incomplete or contrasting data.

In this study, as the objective is to model secondary migration using the software Migri, by Migris A.S., we need to obtain the Vshale information form available wells as the volume of shale in the different layers has a strong impact on hydrocarbons migration.

In order to find the Vshale values for the different formations in each well, we needed:

- wells coordinates;
- formations top in the wells;
- logs data for the whole well's depth, in particular gamma-ray logs.

In this chapter it will be explain how the formation tops in the wells were obtained.

In addition, since the model used for the validation of Migri technologies was referred to the 3D GeoModel used in the Petroleum System Modelling study of 2009 (Baiocco et al., 2009), we also needed to calculate the formations depths at wells location for the 3D GeoModel, in order to compare them with the wells top depths. In this way it could be possible to have a confirm of the coherency of the 3D GeoModel with well data.

3.1 PSM 3D GEOLOGICAL MODEL

The aim of the PSM was to evaluate the presence and hydrocarbon generation potential of four main modeled source rocks intervals (2 sequences inside Khatatba Fm., Alam el Bueib and Abu Roash F-G members) and to produce preliminary results about the regional hydrocarbons migration.

The geological model consists in 10 grid maps, coming from seismic interpretation. Other maps have been created in order to better define horizons not interpreted or not identified; in particular, the Khatatba Fm was subdivided in 3 sublayers and the Alam el Bueib Fm has been divided in 6 sublayer (**Fig. 3.1**) (Baiocco et al., 2009).

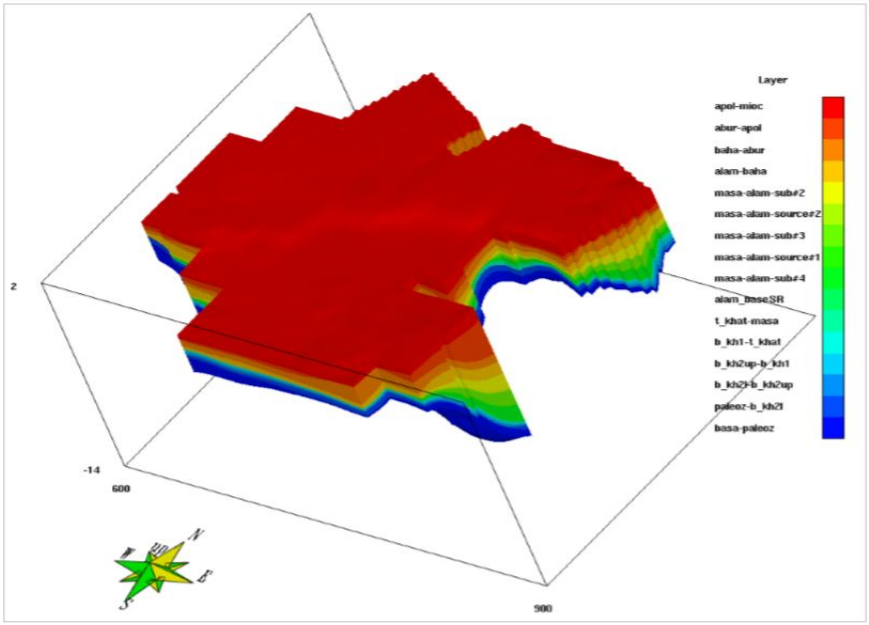

***Fig. 3.1**: 3D GeoModel resulting from PSM study*

The maps used to build the PSM 3D model have been uploaded in Migri, in order to build a new 3D GeoModel in which it could be possible to perform hydrocarbon migration tests (**Fig. 3.2**). However, because it was impossible to obtain all the maps necessary to define each layer it was not possible to divide the Alam el Bueib Fm in sublayers.

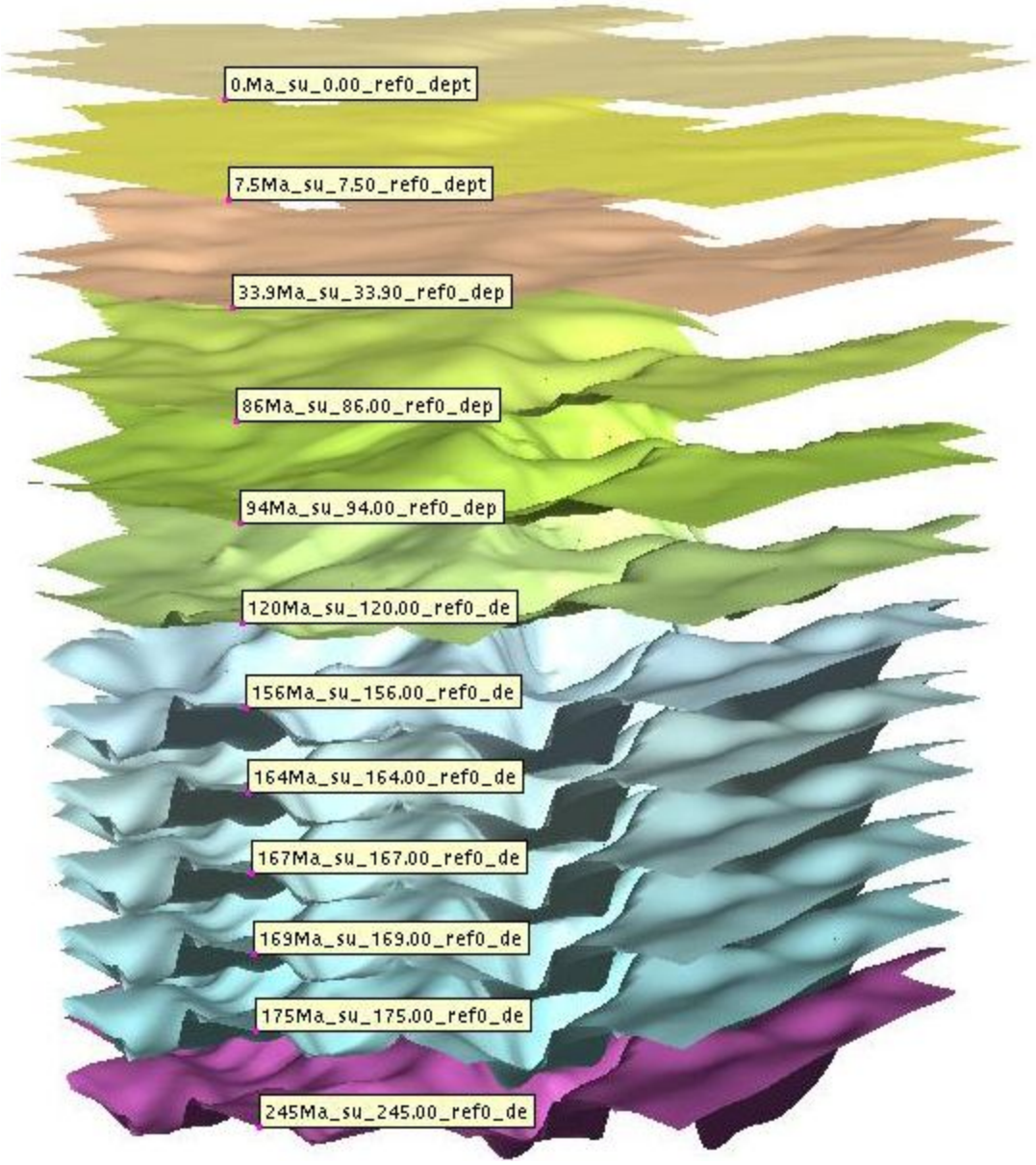

***Fig. 3.2**: 3D GeoModel used for this hydrocarbon migration test*

The final Migri 3D GeoModel is made up of 12 layers, instead of the original 17 layers used for the PSM (**Tab. 3.1**).

Layer Number	***Event***	***Initial time of deposition (My)***	***Final time of deposition (My)***
1	Basament - top Paleozoic	590	245
2	Top Paleozoic - base Khatatba	245	175
3	Base Khatatba2Lower - base Khatatba2Upper	175	169
4	Base Khatatba2Up - Base Khatatba1	169	167
5	Base Khatatba1 – top Khatatba	167	164
6	Masajid	164	156
7	Alam el Bueib	156	120
8	Top Alam el Bueib - top Bahariya	120	94
9	Top Bahariya - top Abu Roash	94	86
10	Top Abu Roash - top Apollonia	89	33.9
11	Top Apollonia - top Miocene	33.9	7.5
12	Top Miocene - topography	7.5	0

Tab.3.1: *3D GeoModel used for this hydrocarbon migration test*

3.2 DEFINITION OF WELL DEPTHS

Once the layers in the GeoModel were defined, an analysis of the percentage of shale volume was conducted. For this aim the stratigraphic tops in the wells were considered in order to define the Vsh for each layer. Through the Eni's Wells

database, it has been possible to recover the tops of considered layers in each well with their (X, Y, Z) coordinates (**Tab. 3.2**).

BASE KHATATBA 1	**167.00 My**		
WELL NUMBER	**X-COORDINATE (m)**	**Y-COORDINATE (m)**	**DEPTH (m)**
1	717309	298028	3987,57
2	703209	293345	3780,22
3	800832,06	296163,05	4175,44
4	700386	289777	3633,13
5	712301,9	269342	3204,72
6	673169,53	304662,63	3900,53
7	747319,12	210527,16	2822,12
8	778445	203870	
9	828709,56	255047,08	2873,2
10	733603,8	277402,5	
11	833210	269058	
12	769700,2	321310,2	4190,75
13	711012	302262	4085,89
14	717937	286388	3547,06
15	746736	220849	
16	775105,3	296525,6	4138,21
17	767684	305634	
18	723837	282776	3594,55
19	707497	283672	3497,94
20	785180,46	261831,05	3570,73
21	828663,38	296973,41	3596,4
22	702905,64	280777,73	3422,46
23	822493,67	250607,57	2697,63
24	729333	212827,4	2094,91
25	718700	282100	3410,21
26	697570.71	278805,95	
27	628867,7	250546,3	4013,2
28	681165	321790	3956,23
29	786271,85	147490,7	3134,46
30	740141	287605	4055,13
31	751008,81	252601,76	2797,28
32	700747	271552	3440,17

Tab. 3.2: *definition of wells coordinate and Base Khatatba1 depths for any available wells*

In order to test the coherency of the 3D GeoModel built for the Migri validation test, with the GeoModel used for mentioned PSM, the next step has been to obtain the Z depth of each layer of the 3D PSM GeoModel at the wells coordinates.

As this operation may introduce some interpolation error (from the available top layers' grids) in order to be guarantee the maximum of accuracy a geostatistical interpolation has been used, implemented in the Eni proprietary software KrigTree **(Fig. 3.3)**. With this approach a "back-interpolated" Z value of each top layer of the PSM GeoModel, for each well, has been obtained.

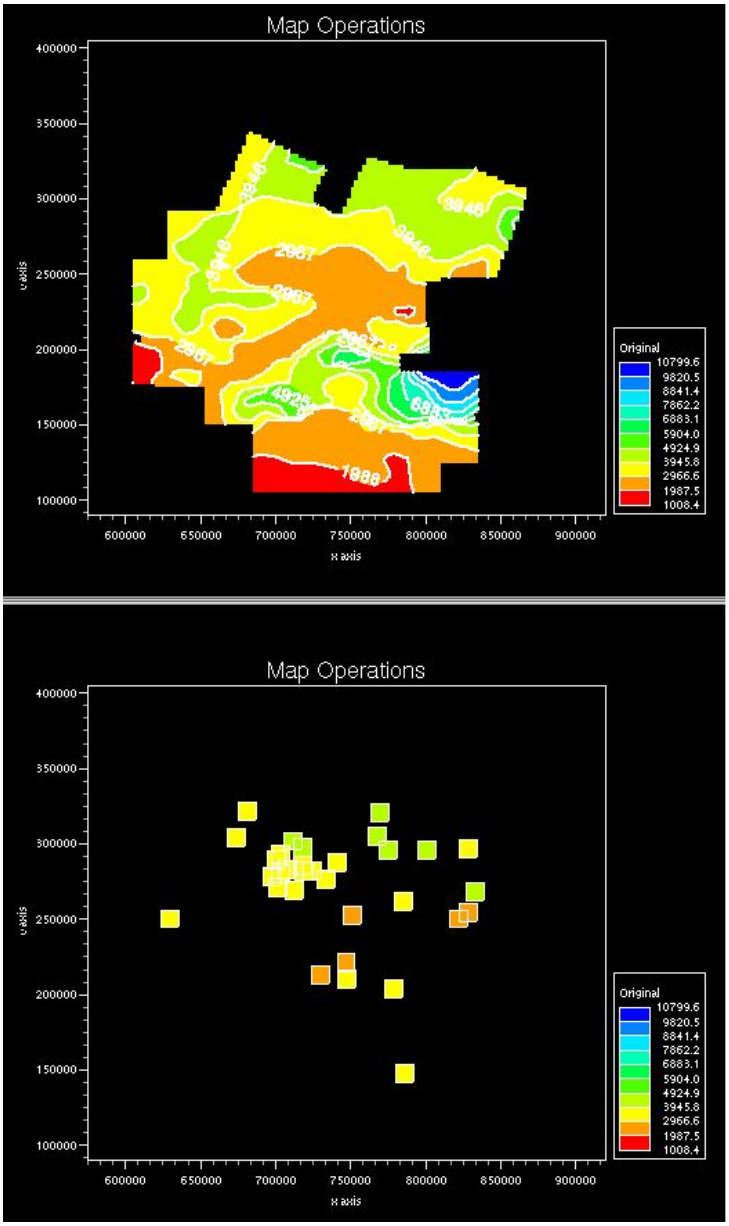

Fig. 3.3: *KrigTree screenshot after wells coordinates plotting*

3.3 FORMATIONS DEPTHS COMPARISON

As previously explained, while the stratigraphic well tops obtained from Eni's Wells database are referring to interpreted measurements in each well, the 3D PSM GeoModel was built starting from seismic interpretation. Assuming that the wells data are the “true values”, in the case of a perfect coherency between the 3D PSM GeoModel and Wells Tops we would expect almost the same depth Z values for both the wells tops and the back-interpolated depths of the GeoModel, except for approximation errors. But indeed, the results coming from this comparison show a number of marked discrepancies (**Tab. 3.3 - 3.4**):

TOP ABU ROASH	86 My		
WELL NUMBER	WELL DEPTH (m)	3D MODEL DEPTH (m)	WELL-MODEL COMPARISON (m)
1	888	888,517	0,517
2	986,8	989,516	2,716
3	1086	1073,222	-12,778
4	990	990,449	0,449
5	892	892,162	0,162
6	935	934,391	-0,609
7		861,151	
8		848,391	
9	785	894,523	109,523
10		1022,143	
11	929	1023,259	94,259
12	1208	1207,364	-0,636
13	904	1012,506	108,506
14		1032,438	
15		922,25	
16		983,412	
17	963	962,732	-0,268
18	1067,5	1068,296	0,796
19		922,6	
20	912	911,881	-0,119
21		980,743	
22		960,116	
23		962,742	
24		655,02	
25	1191,6	1042,961	-148,639
26		953,922	
27		967,771	
28		1016,859	
29		937,753	
30	1287	1291,903	4,903
31	756	755,813	-0,187
32	1025	1009,435	-15,565

Tab. 3.3: Comparison between wells and 3D GeoModel dephts refers in layer9 (Top Abu Roash); the red numbers indicate differences greater than 50 m.

BASE KHATATBA 1	167 My		
WELL NUMBER	WELL DEPTH (m)	3D MODEL DEPTH (m)	WELL-MODEL COMPARISON (m)
1	3774.57	4022.51	247.94
2	3541.22	3515.44	-25.78
3	3183.29	3184.12	0.82
4	4060.44	4113.06	52.62
5	3399.13	3432.05	32.92
6	2982.72	3003.79	21.07
7	3648.53	3717.31	68.78
8	2750.12	3656.44	906.32
9		2739.33	
10	2642.2	2617.17	-25.03
11		3456.42	
12		4239.71	
13	4073.75	4259.48	185.73
14	3867.89	4211.27	343.38
15	3322.06	3354.08	32.02
16	3966.21	4049.83	83.62
17		4319.35	
18	3372.05	3451.16	79.11
19	3325.94	3270.34	-55.6
20	3357.73	3441.01	83.28
21	3510.4	3606.64	96.24
22	3422.46	3267.4	-155.06
23	2445.63	2514.84	69.21
24	2021.91	2219.45	197.54
25	4394.99	4368.87	-26.12
26	3387.21	3199.86	-187.35
27	3803.2	3422.54	-380.66
28	3842.13	3930.37	88.24
29	3739.23	3723	-16.23
30	3102.46	3416.86	314.4
31	2555.28	2582.38	27.1
32	3232.17	3167.35	-64.82

Tab. 3.4: Comparison between wells and 3D model dephts refers in layer 4 (base Khatatba1); the red numbers indicate differences greater than 50 m.

In the examples reported it's possible to see that the differences between depths in Wells and the PSM GeoModel are higher in Layer4 than in Layer9; in general, it can be noticed that these differences increase going from the upper part of the succession to the lower. In particular, starting from Alam el Bueib Fm these differences become much higher, and they reach also hundreds meters (as it's possible to see in Table 3B). This problem could be due to a different seismic interpretation of the Layer7 (Alam el Bueib Fm), referring to current well tops interpretation, that consequently influences all deeper data.

Due to these important discrepancies, it has been decided to avoid to apply a

correction of the GeoModel so make it fit to assigned wells tops as this would have introduced surely false structural features. Also the reinterpretation of the GeoModel was considered not feasible in the available timeframe, as it also usually happens in the real practice of a PSM study.

The conclusion was the decision to proceed in parallel with two scenarios:

- Scenario A: the Vsh values are computed as a function of assigned wells tops and then they are “inserted” in the Migri's GeoModel for each corresponding layer;
- Scenario B: the Vsh values have been re-computed from well measurement, using the depths back-interpolated from the 3D PSM GeoModel.

These two scenarios are the ones that a petroleum system modeler would have to face, given the mentioned time constraints: in the first case use the correct well data transferred to the given GeoModel, in the second case to use the GeoModel as the reference also for deriving well’s information, disregarding the available information about wells tops.

4. Vshale VALUES: DATA ACQUISITION AND PROCESSING

The volume of shale in a formation influences in particular two important petrophysical parameters, critical in the evaluation of petroleum potential in an area: water saturation and porosity.

The aim of this study is to focus our attention on the second parameter: in fact porosity influences in turn rocks permeability, thorough a non-linear relationships; for this reason, Vsh values have a strong influence in the migration paths as well as on hydrocarbon migrated amounts.

4.1. THE ROLE OF SHALE IN MIGRATION PROCESSES

One of the most controversial problems in formation evaluation is the shale effect on the permeability of rocks; the evaluation of shale volume from different shale indicator tools allows us to determine the effective porosity, that affects the permeability (Hammada, 1996).

4.1.1 SEAL CAPACITY OF A ROCK

There are two principal pressures that determine a seal capacity: buoyancy pressure and capillary pressure.

The buoyancy pressure is related to the contrast in density between water and petroleum, and to its height above the free-water level, depth at which both are in equilibrium. When petroleum is present under a cap rock seal, there is always this pressure pumping up.

The maximum petroleum column is also controlled by the capillary entry pressure

of the petroleum into the largest pores of the seal. The capillary entry pressure of a water-wet rock is given by the equation:

$$Pd = \frac{2\gamma\cos\vartheta}{R}$$

where Pd is the capillary entry pressure, γ is the interfacial tension between the water and the petroleum, ϑ is the contact angle due to the wettability and R is the radius of the largest pores. The petroleum in a reservoir displays at first in the bigger pores, because the capillary pressure is minor.

These properties are routinely established from laboratory experiments on rocks, and the procedure involves injecting the pores with mercury and converting it to a petroleum-water system at in situ conditions, using standard equations. The seal capacity now determines the height of a petroleum column that can be trapped below it, and the seal will be breached when the buoyancy pressure (Ph) exceeds the seal capillary entry pressure (Pd) (Gluyas et al, 2004).

After this definitions, it is easy to understand that if Vsh value in a formation is high, the medium size of pores will be smaller and then capillary pressure higher. For this reason, oil and gas will penetrate with difficultly into the rock, therefore Vsh has a big influence in the migrations paths, both stopping the flow and deviating it from the natural vertical direction due to buoyancy only.

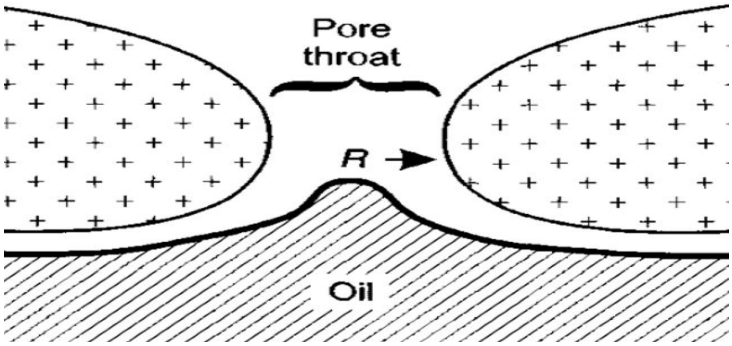

***Fig. 4.1**: schematic representation about the influence of pore space on permeability.*

The evaluation of the Vsh effect in the secondary migrations processes mainly means to understand what is the shale amount over which the rock assumes a seal behaviour, becoming impermeable and preventing the passage of hydrocarbon fluids.

Considering that we are working on regional scale, it is also important to consider not only impermeable barriers extended to the whole area of interest, but also local less permeable bodies. These are defined with the help of well data and mapped thanks to geostatistical techniques, so to define in space the way in which these heterogeneities will induce a change in hydrocarbons path direction.

4.1.2 SHALE DISTRIBUTION

By definition, the clay material can be distributed in sand formations in three different forms **(Fig. 4.2)**:

- *Dispersed*: dispersed clays come from the precipitation of clay crystals contained in pore fluids. This process occurs when there is a change in water chemistry due to filtration processes or by pressure or/and temperature changes. Dispersed clays can occur in pores as discrete particles, that form a relatively thin and continuous coating that reduces the pores volume, and hence the permeability of the formation (Ahmed, 2008).
- *Laminates*: within a sand body, thin lamina of clay are of detrital origin and they are formed outside the sandstone framework: these are called "*laminated shales*", and if they have a lateral continuity they could act as vertical permeability barriers.
- *Structural*: clay can be of diagenetic origin, formed simultaneously with the sand framework. One source of diagenetic clay is the in-situ alteration of non-quartz particles by reaction with formation water. The most common of this type of alteration are those in which there is a transformation from feldspar to kaolinite and from hornblende to chlorite. This leads "*structural*

clays”.

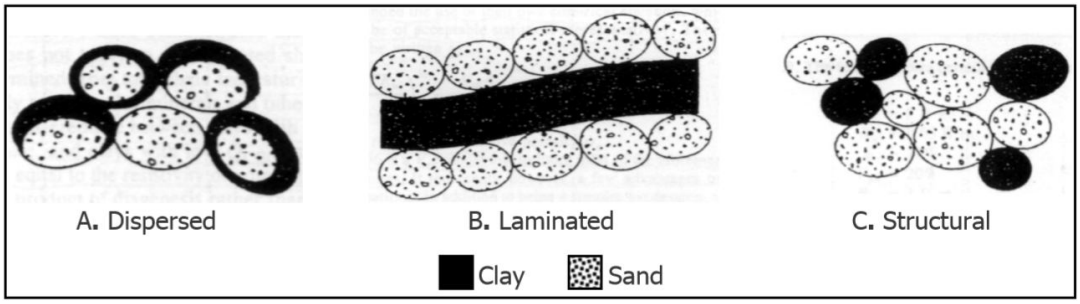

***Fig. 4.2**: Shale distribution mode (Ahmed, 2008)*

Each of these type of distributions will reduce the porosity of rocks and consequently their permeability. The discrimination of the different types of clay distributions into rocks is possible by specific core tests on formation samples. However, to perform such detailed study at basin scale would require not only an enormous amount of time, but also a useless level of detail; in fact as characterization of hydrocarbon migration is made at regional scale, we are required to assign a Vsh value for each layer, whose scale dimension is much greater than that of the cores, where the different types of clay distributions are meaningful.

A greater accuracy in this kind of work will not be obtained by specifying in detail the distribution type of shale, but by creating the highest possible numbers of thin “sublayers” in order to approach as much as possible at the hydraulic behaviour of the real geological model. Consequently, we may assume that the type of shale distribution that can be considered for hydrocarbon migrations is the “laminated type”. For example, in the extreme case of an infinitesimal layer, the Vsh value will tend to 1 in correspondence of a completely shaly lamina. If this hypothetical infinitesimal layer will have a good lateral continuity and a sufficient thickness, this influences the secondary migration acting as a seal. On the contrary a dispersal or structural distribution, would have been recorded by a rise in layer Vsh values.

4.2 Vshale VALUES FROM GAMMA RAY LOGS

In order to calculate the Vshale values it is necessary to apply petrophysical technologies and know-how.

Vsh is a value estimated from well logs data with different approaches using all available information in order to obtain a result as accurate as possible.

In this study, only the gamma ray logs have been used, mainly due to the extra time needed to find other types of log (that needed also to be pre-processed to clean them from noisy information). However, an explanation of all different methods to estimate Vsh are reported in the following chapter.

4.2.1 Vsh DETERMINATION METHODS

The radioactive components originally occurred in the igneous rocks are subsequently distributed unequally throughout sedimentary formations during erosions, transport and deposition. Radioactive elements tend to accumulate in clay minerals, which can absorb them (Ahmed, 2008).

Gamma ray log is a continuous recording of the total intensity of natural gamma radiation emanating from the formation. It reflects the total radioactivity of the different formations surrounding the well, and this information is used to delineate shale beds and their correlation (**Fig. 4.3**).

Shale is usually more radioactive than sand or carbonate, so gamma ray log can be used to calculate volume of shale into the rocks.

The way in which shale affects a log response is controlled by type of shale, its volume and mode of distribution.

Gamma ray log can be described using several non-linear empirical responses and a linear responses:

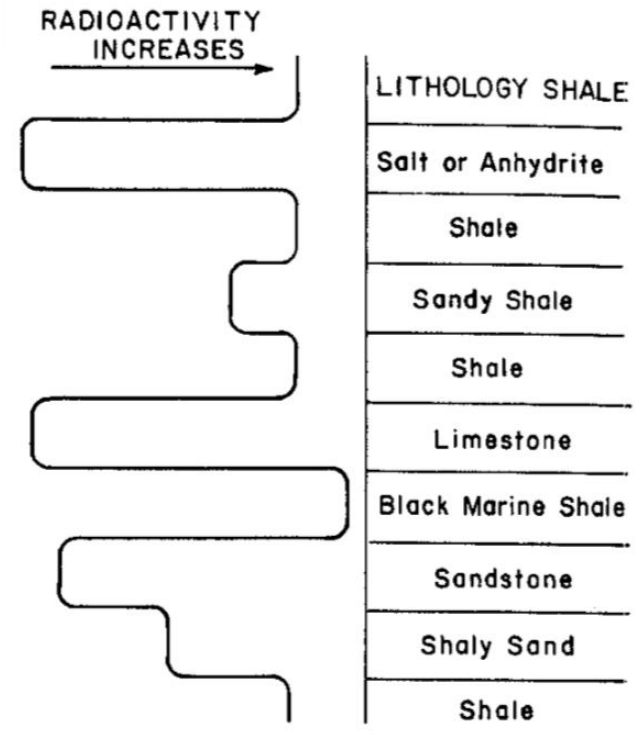

***Fig.4.3**: relative degrees of radioactivity of the most common sedimentary rocks*

- Linear Response:

$$Vsh = I_{GR} = \frac{GR_{\log} - GR_{min}}{GR_{max} - GR_{min}}$$

where:

GR : gamma ray log reading in zone of interest;

Gr_{min} : gamma ray log reading in 100% clean zone;

Gr_{max} : gamma ray log reading in 100% shale;

I_{GR} : gamma ray index.

- Non-linear responses:

a) Larionov (1969) for Tertiary rocks:

$$Vsh = 0.083(2^{3.7 I_{GR}} - 1)$$

b) Steiber (1970): it is used in unconsolidated rocks because they tend to be more chemically immature and they may contain radioactive minerals such as feldspars that could contribute to gamma ray, but they are unrelated to shale volume.

$$Vsh = \frac{I_{GR}}{3 - 2\,x\,I_{GR}}$$

c) Clavier (1971) it is a compromise between Tertiary rocks and olders:

$$Vsh = 1.7 - [3.38 - (I_{GR} + 0.7)^2]^{(1/2)}$$

d) Larionov (1969) for older rocks:

$$Vsh = 0.33\,x\,(2^{(2I_{GR})} - 1)$$

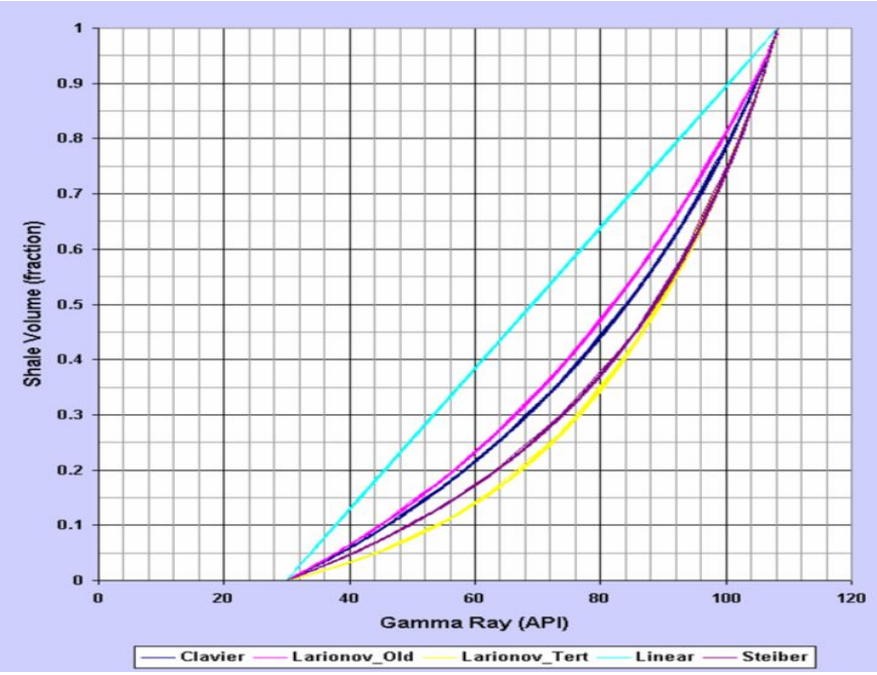

***Fig.4.4**: Comparison between linear and emphirical methods (Saputra, 2008)*

The assumption that $Vsh=I_{GR}$, used in the linear relation, tends to exaggerate the shale volume; empirical relationships coming from non-linear responses and based

on the geographic area or formation age were found to be more reliable (Bassiouni, 1994). However, current experience has shown that the gamma ray index approach provides a reasonable estimate for Vsh (**Fig. 4.4**) (Saputra, 2008).

Determination of shale content with the total gamma ray log responses assumes that all the radioactive minerals are contained in shale. This assumption could lead to a serious misinterpretation, because a high level of radioactivity is not always associated whit the presence of clay minerals (Asquith et al., 1984). In fact, clean sandstone may also produce an high gamma ray response if it contains potassium feldspar, micas, glauconite or radioactive contaminants which are present in the analysed formation. Formation water cold also contain dissolved radioactive salts (Bassiouni, 1994).

Another problem could be the possible existence of passive shale, like kaolonite and chlorite, with essentially zero cation exchange capacity (in contrast with the so-called "effective shale", like motmorillonite e bentonite), that do not record any gamma ray anomaly. The lowest value of shale volume has to be used in the calculation, in order to minimize errors due to the possible existence of passive shale and radioactive sands (Hammada, 1996).

Other methods used to compare the result with gamma ray log methods are (Adeoti et al., 2009):

e) Neutron-density combination:

$$\frac{\emptyset_N - \emptyset_D}{\emptyset_{NSH} - \emptyset_{DSH}}$$

$\emptyset_N$: neutron porosity in the sand;

$\emptyset_D$: density porosity in the sand;

$\emptyset_{NSH}$: neutron porosity in adjacent shale.

$\emptyset_{DSH}$: density porosity in adjacent shale;

f) Resistivity:

$$\frac{\log(RESD) - \log(RESTD_{CLN})}{\log(RESD_{SHL}) - \log(RESD_{CLN})}$$

$RESD$: resistivity log reading from zone of interest;

$RESD_{CLN}$: resistivity log reading from clean sand;

$RESD_{SHL}$: resistivity log reading from shale;

g) Combinations of different methods

Another tool used in the past to determine the shale percentage into the rocks was the spontaneous potential log, but today this technique is no more used in Eni, because of its low accuracy.

4.3 GAMMA RAY LOG ANALYSIS

Once retrieved the information about wells formation top , these were provided to the petrophysical team and processed in order to achieve a Vsh value for every layer, in correspondence with each available well. This operation was possible thanks to the availability of the Western Desert's gamma ray logs in their databases (**Fig. 4.5**).

At first, we could observe a good match between well formation tops coming from database, referred to core measurement and previous log interpretation, and the lithologies changes visible in the logs in which we were working on. Moreover, these changes showed lothologies matching with the formations that were considered in the GeoModel, and confirmed by the trend of density and neutron logs.

This correspondence showed that the formation tops data coming from the database were reliable, and confirmed us the differences with the depths of the PSM GeoModel **(Tab. 4.6)**.

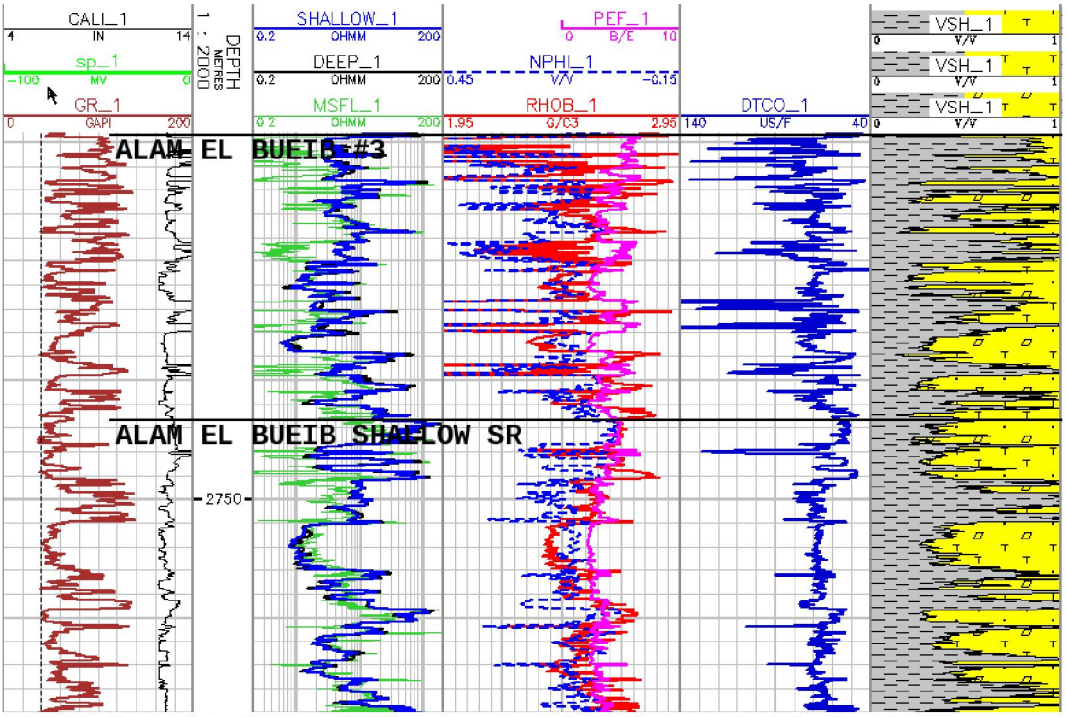

Fig. 4.5: *Screenshot about Geolog log viewer; the first column on the left referred on gamma ray and caliper log; in the secon d column resisitivity logs are reported; in the third colum a comparison between neutron and density log is showed. In the last column (on the right) a Vsh calculated viewer is showed.*

BASE KHATATBA 1	167 My			
WELL NUMBER	WELL DEPTH (m)	MEASURED LOG DEPTH	3D MODEL DEPTH (m)	WELL-MODEL COMPARISON (m)
1	3774.57	3774	4022.514	247.944
2	3541.22	3540	3515.439	-25.781
3	3183.29		3184.115	
4	4060.44	4060	4113.062	52.622
5	3399.13	3399	3432.05	32.92
6	2982.72	2982	3003.792	21.072
7	3648.53	3648	3717.309	68.779
8	2750.12		3656.436	906.316
9			2739.326	
10	2642.2	2642	2617.166	-25.034
11			3456.417	
12			4239.711	
13	4073.75	4065	4259.483	185.733
14	3867.89	3867	4211.273	343.383
15	3322.06	3321	3354.08	32.02
16	3966.21	3966	4049.828	83.618
17			4319.35	
18	3372.05		3451.157	79.107
19	3325.94		3270.342	-55.598
20	3357.73	3357	3441.012	83.282
21	3510.4	3510	3606.641	96.241
22	3422.46	3422	3267.4	-155.06
23	2445.63	2445	2514.843	69.213
24	2021.91		2219.453	197.543
25	4394.99		4368.873	-26.117
26	3387.21	3179	3199.864	-187.346
27	3803.2	3803	3422.539	-380.661
28	3842.13		3930.374	88.244
29	3739.23	3738	3723.002	-16.228
30	3102.46	3102	3416.858	314.398
31	2555.28	2555	2582.378	27.098
32	3232.17	3220	3167.346	-64.824

Tab. 4.6*: the table shows a comparison between formations tops measured observing the logs, the database formation tops and the depths calculated from the PSM GeoModel. This comparison confermed the godness of the well depths (first column) and the serious differences between them and the PSM cuttings.*

4.3.1 "SCENARIO A": Vsh DETERMINATION

In Scenario A, definition of the formation tops is given by the well interpretation and the Vsh values are associated to the corresponding layer in the PSM GeoModel, even if they could be at different depths.

In order to calculate Vsh values, we analysed gamma ray logs using the linear

method, assuming as minimum and maximum values 5 and 95 percentile (**Fig. 4.6**), and so the used formula can be written as:

$$Vsh = I_{GR} = \frac{GR_{\log} - GR_5}{GR_{95} - GR_5}$$

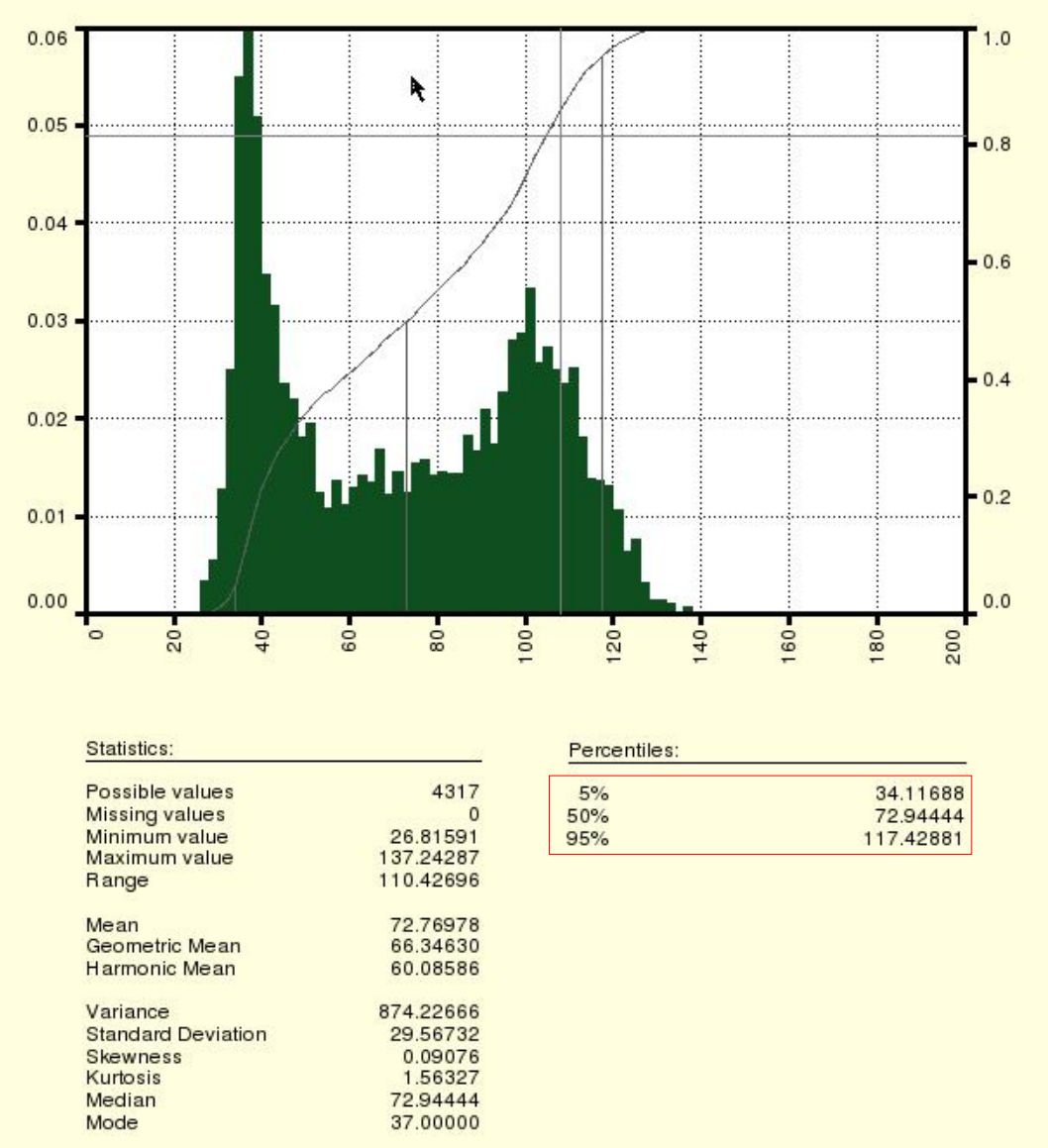

***Fig. 4.6**: Geolog screenshot representing gamma ray values distribution; with the red rectangle the percentile values used in the Vsh calculation formula are showed.*

4.3.2 "SCENARIO B": Vsh DETERMINATION

In Scenario B, formation tops are derived from the PSM GeoModel and their depths are used to re-compute the Vsh values, disregarding well formation tops interpretation.

Besides the values of Vsh referred to all the layers, the petrophysical team has provided also complete datasets, calculated for the entire depth of each well, reporting the Vsh values calculated approximately every 10 cm, coming from the software *Geolog*® (by Paradigm).

Through these datasets it was possible to obtain representative values of Vsh for the formation tops coming from PSM GeoModel. In order to do this, it was first necessary to extract from these datasets the values of Vsh in the depths range corresponding to the PSM model formations top in each well. Then it was possible to build frequency curves, with the values of Vsh on x-axes and their frequency on the y-axis (**Fig. 4.7**).

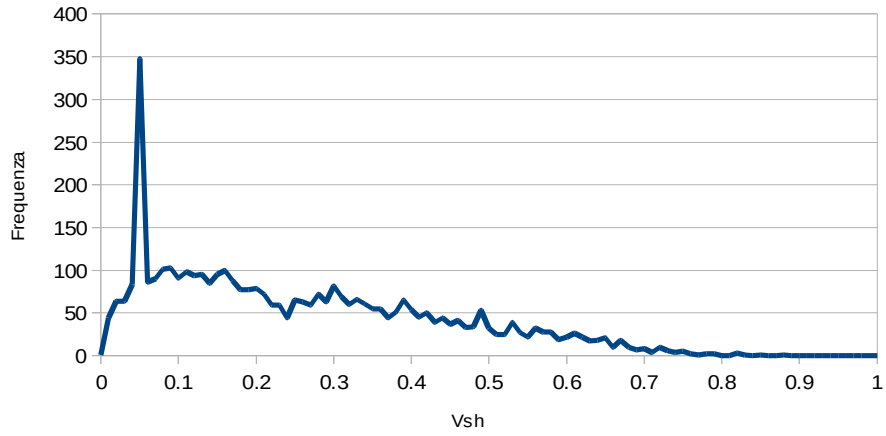

AVARAGE	0.25
MEDIAN:	0.21
STDV:	0.18

***Fig. 4.7**: Distribution curve used to calculate avarage, median and standard deviation, in order to understand what was the best representative value referred to Bahariya Fm in well n.6.*

Also in this case it was calculated the median of these curves, and the resulting value of Vsh was assumed as representative of the whole layer, referred to the PSM GeoModel formation tops. In order to avoid problems in the use of *Migri*, it was decided to change the end members of the Vsh values (0 and 1) with the values 0.05 and 0.95; this choice doesn't induce visible differences on the results, but it will preserve from the possibility of numerical instabilities in the software computations, due to min-max bounds surmounting.

The last processing on the Vsh data was the reproduction, using a simple spreadsheet, of a vertical Vsh profile. The values of Vsh were related to their corresponding depth, producing graphs of Vsh vs depth (**Fig. 4.8).**

The aim of this operation was to identifying possible sub-layers of shales, showing a considerable thickness and a good lateral continuity, in order to insert potential new layers in the GeoModel previously built to be used in *Migri*.

As shown if **Fig 4.9**, the creation of additional layers, showing a significant shale content and a good lateral continuity, could have been done improving the GeoModel for the hydrocarbon migration modelling, but unfortunately this operation was practically difficult to run as it would have required also an interpretation of the new added layers far from the wells, which was not possible in the short time available for this study.

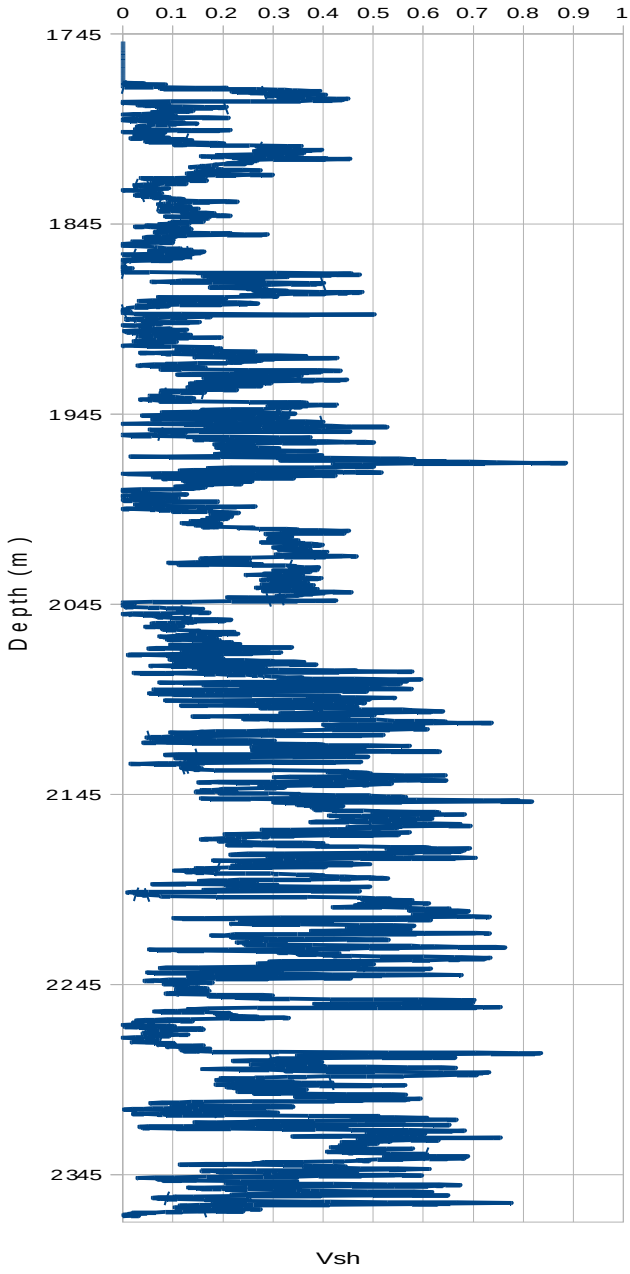

***Fig. 4.8**: Vertical Vsh profile of the preavious example.*

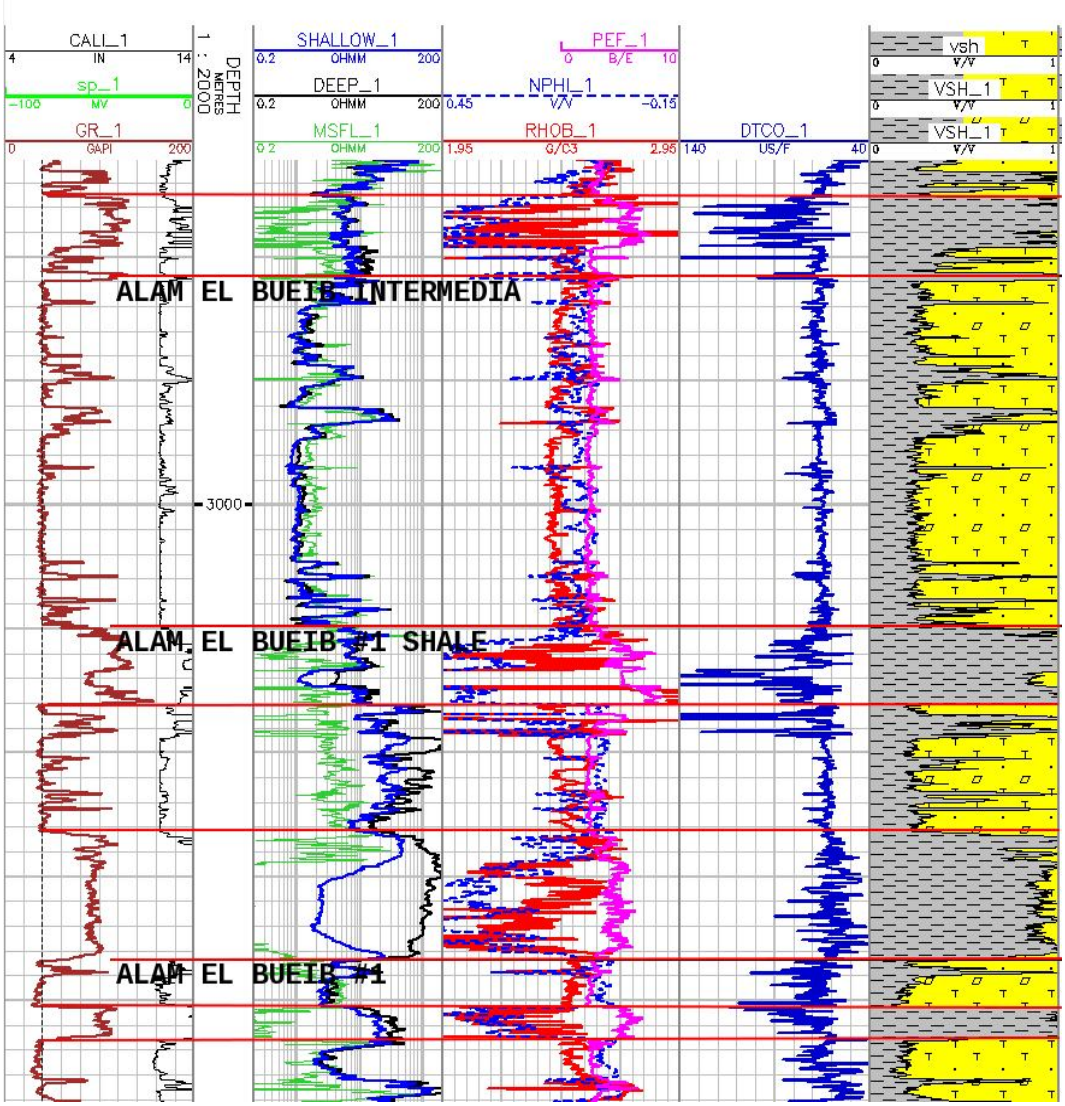

Fig. 4.9*: Logs examples; looking at the Vsh log (on the right) the presence of important shaily level alternated with sandy level is clearly visible into the same formation.*

5. GEOSTATISTICAL METHODS TO CONTSTRUCT PROBABILISTIC Vsh MAPS

The computation of Vsh values from gamma ray logs, described in the previous chapter, is aimed to the construction of maps showing Vsh distribution in the whole Western Desert area, using computed values at well points. This operation is performed using geostatistical methodologies.

In order to better understand how this goal has been reached, a short introduction about geostatistical methods is needed.

The information about geostatistics that is shown in this introduction has been taken from the book “Practical Geostatistics” by Isobel Clark, that represents a standard reference in introductory courses.

5.1 INTRODUCTION TO GEOSTATISTICS

The main purpose of geostatistics is to obtain, starting from data of various quality a map that will fit by construction in the best possible way the experimental data. This allows to interpolate, without the introduction of any bias, the values in areas in which we do not have any information. Therefore, in this study geostatistical methods has been used to estimate Vsh values where a direct measurement was not available, namely in all the points far from wells.

As for each estimation method, the accuracy of the results will increase with the data available and their spatial coverage. In our case available data values were few and they were not homogeneously distributed.

5.1.1 SEMI-VARIOGRAM AND KRIGING

Let's assume a sampling along a N-S line direction in an area *A*, at a regular interval h of 10 m, so that *h* is the distance between a sample and another along that direction. We may then consider all the couples that are spaced 2*h* (20 m), 3*h* (30 m), and so on, as long as the sampling will allow it.

We can describe the *variance of the mean difference* between all the values of the couples of sample points, as a function of their distance *h* :

$$2\gamma^{*}(h)=\frac{1}{n(h)}\sum\left[g(x)-g(x+h)\right]^{2}$$

Υ^{*} is called the semi-variogram and it is a base element in the geostatistics analysis. In the above equation, *g* represent the variable of interest, *x* is the position of the first sample, *(x+h)* is the location of a second sample which is at a distance *h* from the previous one and *n(h)* is the number of pairs that have a distance *h* between them. The symbol * indicate that the semi-variogram is computed from experimental data, and it distinguish it from the theoretical semi-variogram chosen to fit the experimental one.

In the theoretical case, the semi-variogram Υ have its origin at *h*=0, that is

$$\Upsilon(0)=0$$

this is because theoretically two samples in the same location must have the same value. In the real case instead we may have measurement errors in case of repeated measurements so that

$$\Upsilon^{*}(0)=c$$

with $c \neq 0$. To avoid an inconsistency it is assumed that these repeated measurements are at a very small distance ε between them :

$$\Upsilon(\varepsilon)=c$$

The semi-variogram will increase progressively with the distance, until it usually reaches a limit for distances greater than a threshold value called the *range,*. This

is because beyond the *range* the two samples are independent among them and the difference between their values will became a constant equal to the statistical variance of the data. In **Fig. 5.1** it is shown theoretical γ model called the *spherical model*:

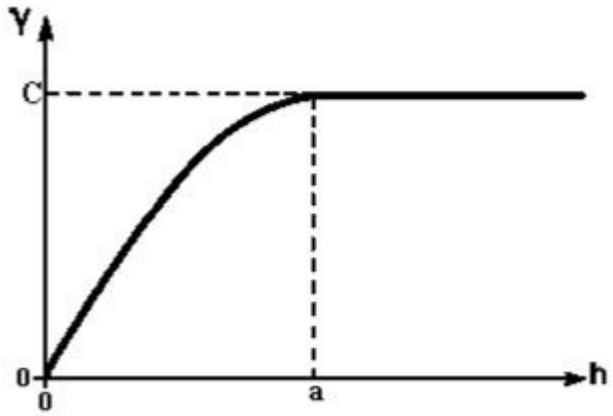

Fig. 5.1*: The spheric curve of a variogram, after I. Clarck, Pratical Geostatistic, 2001*

In **Fig. 5.1** the distance corresponding to *a* is the above mentioned "range of

$$\gamma(h) = C * (\frac{3h}{2a} - \frac{h^3}{2a^3}) ; where\ h \leq a$$

influence", or simply the *range*. The maximum value C of γ reached beyond this distance is called the *sill*.

In the theoretical *spherical model* equation we have :

$$\gamma(h) = C ; where\ h \geq a$$

Another theoretical model of semi-variogram used frequently is the *exponential model*, described by the equation:

$$\gamma(h) = C[1 - \exp(-h/a)]$$

The *exponential model* shows a slower increasing of γ, compared to the *spherical model*, and it reaches the sill *C* at an infinite distance (**Fig. 5.2**), that is an asymptote of γ.

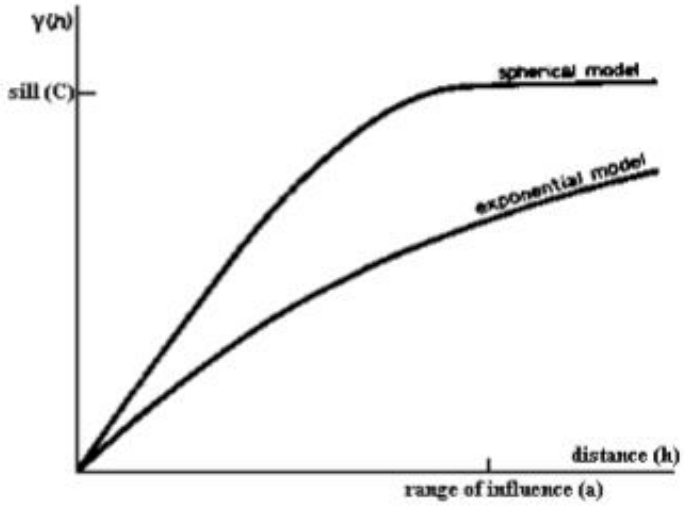

Fig.5.2: *Comparison between spheric and exponential models, after I. Clarck, Pratical Geostatistic, 2001*

We have introduced the semi-variogram as a graph (or a formula) that describes the dissimilarity of the values that we may expect between pair of samples, as a function of their distance, along a specific orientation.

$$\gamma^{*}(h)=\frac{1}{2n(h)}\sum\left[g(x)-g(x+h)\right]^{2}$$

The fitting of the experimental semi-variogram with a theoretical one is done usually visually by trial and error as it is necessary to judge the quality of the experimental ΄Υ* points to be fitted as a function both of the number of pairs that contributed to compute it and also to the distance (at far distances the statistical reliability of experimental ΄Υ* points decreases).

Considering the semi-variogram definition, it is possible to evaluate the dissimilarity (or the correlation) of the points along different directions. Each experimental curve will correspond to a single direction. In order to compute the main directions of an elliptic anisotropy, we need at least to compute the semi-

variogram along two different directions.

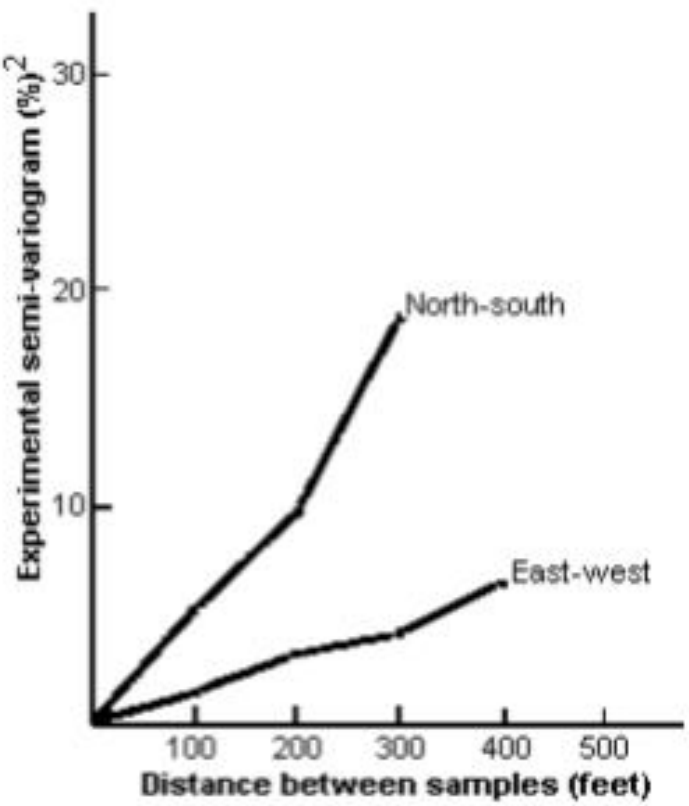

***Fig.5.3**: Experimental semi-variogram in N-S and E-W direction, after I. Clarck, Pratical Geostatistic, 2001*

In the example reported in **Fig.5.3**, the minor inclination of the E-W semi-variogram indicate a minor sample variability compared with the N-S direction; this kind of behaviour shows the presence of an anisotropy, whose direction can be derived computing the experimental semi-variogram also in other directions.

The choice of the best theoretical semi-variogram model to be used to fit the experimental one is a choice of the modeller as it is related to the analysis of the type of data under examination, mainly to their spatial continuity.

In fact, once that a theoretical semi-variogram model has been chosen and fitted to the experimental one, it is used in the process of the geostatistical estimation, the so called *kriging*.

Kriging is a linear interpolation technique able to interpolate the value of a "random field" (in our case the Vsh value of a layer as a function of the sedimentological settings) at an unobserved location from observations of its value at nearby locations. Kriging is by construction an optimal, unbiased, exact interpolator, which means that it is able to produce not only the estimated map but also its uncertainty, in average there is no bias in the estimation and it reproduces input data exactly.

Knowing the value of Vsh in the well points, the values of Vsh in the whole area of interest can be estimated. The unknown value in one point is calculated by a weighted mean of known values, and the weight has to be assigned based on the fitted semi-variogram.

Kriging allows also to manage the situation, like in this case, in which not all the samples have the same importance and it is necessary to take this into account. In general, the assumption is that a magnitude of the variable of interest varies continuously in space, i.e. "nearer points have best spatial relationships than farther points" (De Poli et al., 2009).

5.2 KrigTree AND SEMI-VARIOGRAM MODELS

The software that it was used to elaborate the available data is KrigTree; it was already mentioned in this work because it was used to produce a basemap with the wells locations in the Western Desert Area of Interest.

Krig-tree was used to identify a theoretical trend for each experimental semi-variogram, obtained from the Vsh data available for each layer (**Fig. 5.4**).

The knowledge of the theoretical semi-variogram model to be used in the fitting of the experimental data is necessary to the next step of this work. In particular to build the Vsh distribution maps with the software FlowMap.

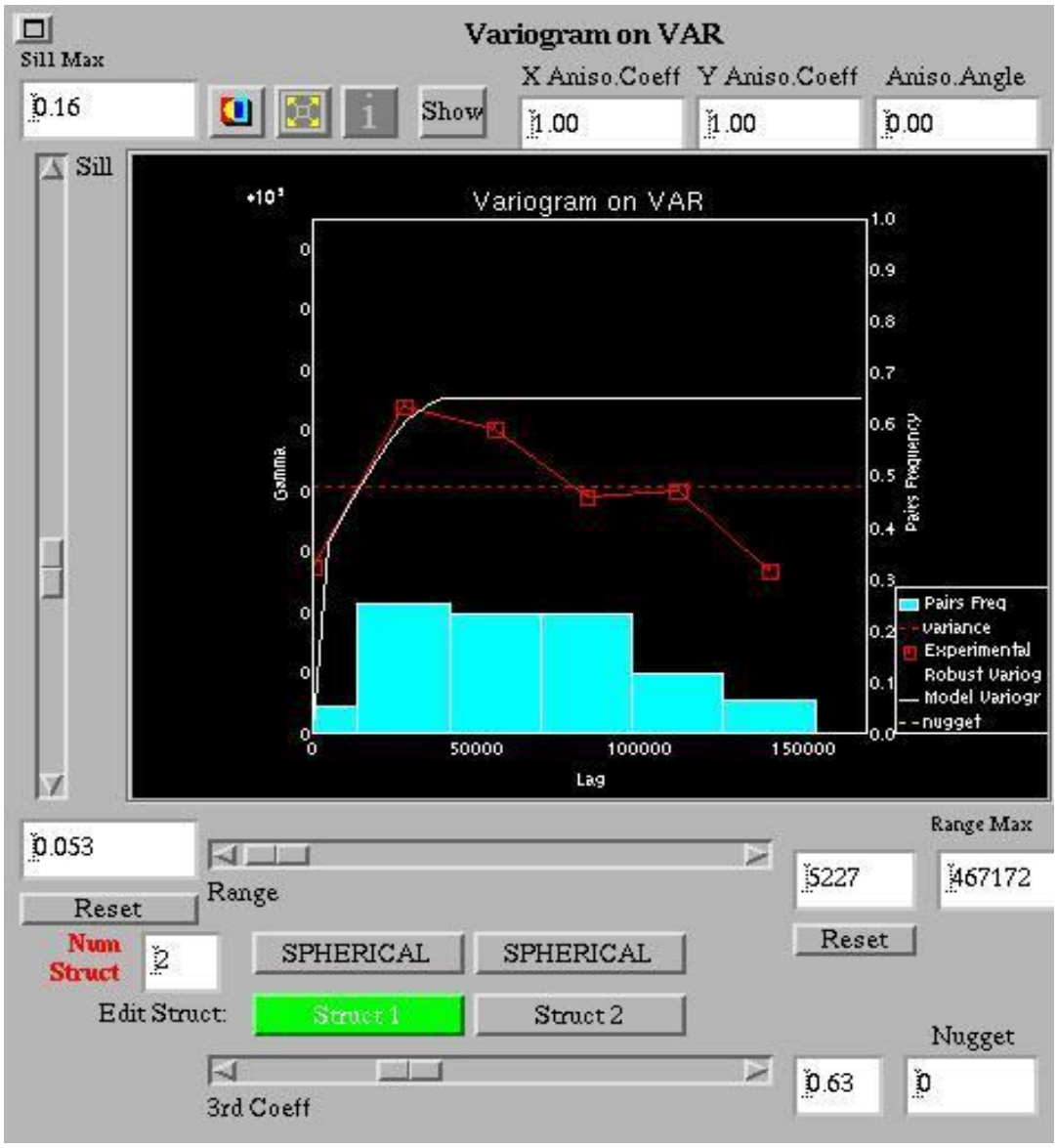

Fig. 5.4*: Experimental and theoretical semi-variogram referred one of the considered layer data; as it is possible to notice, its experimental trend does not approximate perfectely the theory, overall if not many data were available, as in this case. Reported theoretical semi-variogram has been constructed used two different spherical trends.*

6. Vsh DISTRIBUTION MAPS COSTRUCTION

In order to create Vsh distribution maps, an Eni internal software called Flow-map was used. Its most important feature is to take into account compositional variables and to estimates their spatial distribution using geostatistical methodologies.

The first step has been the uploading of the Western Desert grid map, and after that the available wells coordinates, with the corresponding Vsh values, were plotted **(Fig. 6.1)**.

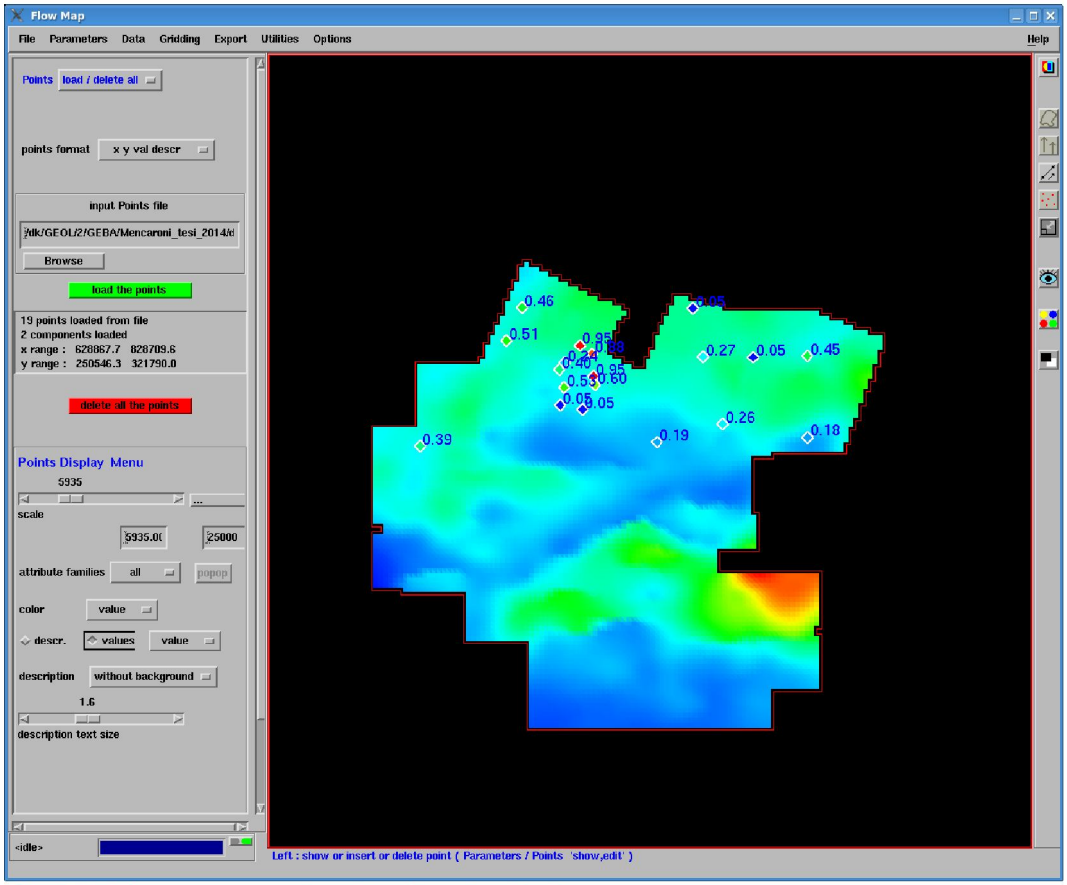

***Fig. 6.1**: Flow-map screenshot after the points loading.*

It's important to remember that we tested two different scenarios: the first one (Scenario A) is based on the formation tops directly measured from the wells, while in the second (Scenario B) depths have been extrapolated from the PSM 2009 GeoModel, and, because these data are in contrast, their calculated Vsh values are completely different.

Flow-map allows to choose from four different models (spheric, exponential, gaussian and cubic), based on our experimental semi-variogram, that were deduced, as previously explained, from Krig_tree. Besides the known values (i.e. the Vsh values reported in the wells points) and the semi-variogram model, in Flow-map it is necessary to provide a third parameter, drawing a vectors set that indicates the direction of local anisotropy used during estimation **(Fig. 6.2)**.

In this work, the criteria for establish vector directions are based on marine transgressions, known thanks to paleo-bathimetric charts that follow substantially a NE-SW direction in every time step.

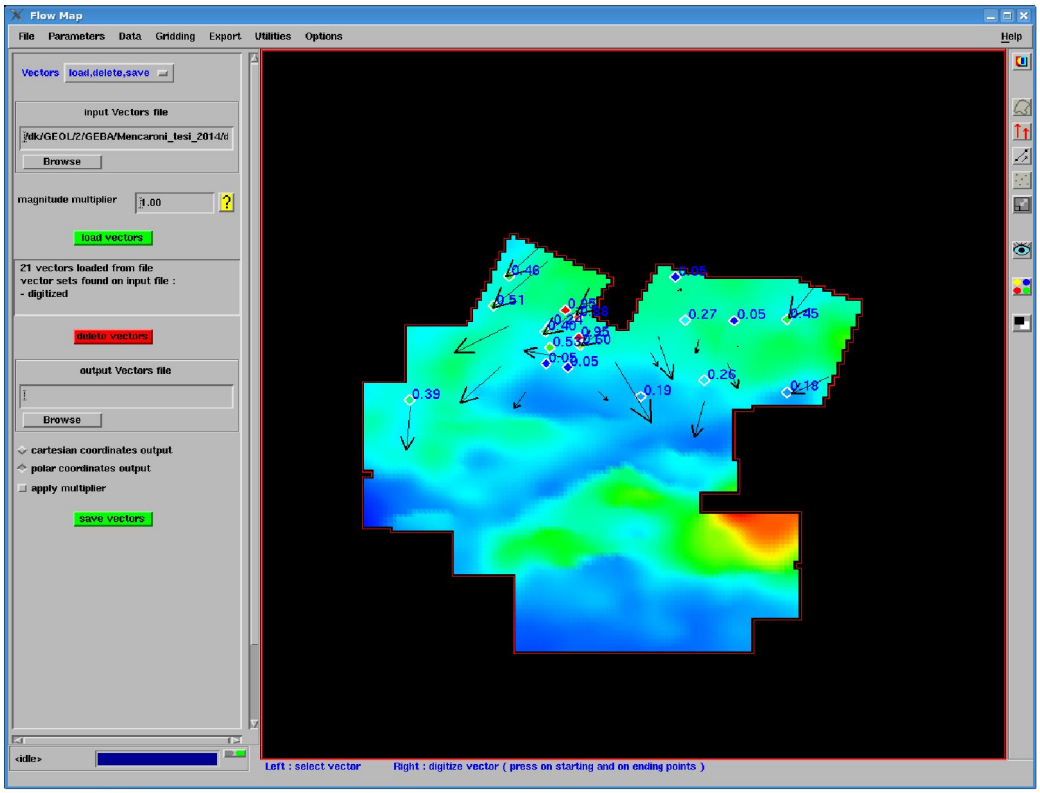

***Fig. 6.2**: Flow-map screenshot after the vectors loading.*

These parameters were adjusted until Vsh maps, that could represent a realistic sedimentological setting, were obtained; in order to reach this goal, with Flow-map it's possible to weight vectors and well data **(Fig. 6.3)**. Thanks to this it was possible to change the Vsh isolines paths.

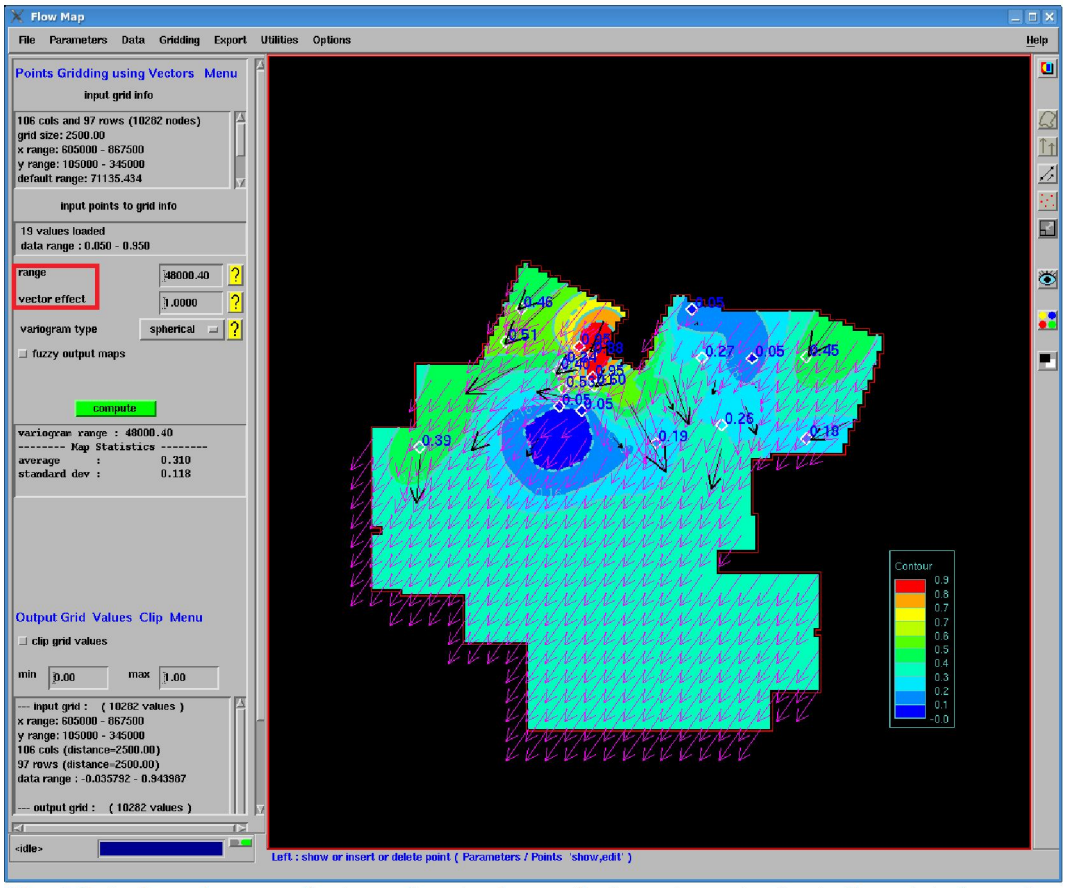

***Fig. 6.3**: in the red square, the two values to change the importance to give to the points (range) and vectors (vector effect) are visible.*

6.1 “SCENARIO A” MAPS

Based on the input information, Vsh distribution maps for six of the twelve GeoModel layers were estimated, in particular for the layers from 3rd to 8th. The reason why not all the layers have been characterized in terms of Vsh is that no sufficient gamma ray data for the lower layers were existing , while the higher layers are not interested from secondary migration processes. For this reason, they are not indispensable to be determinate in terms of Vsh distribution, because they will not influence the results. The following figures refer to the “Scenario A”.

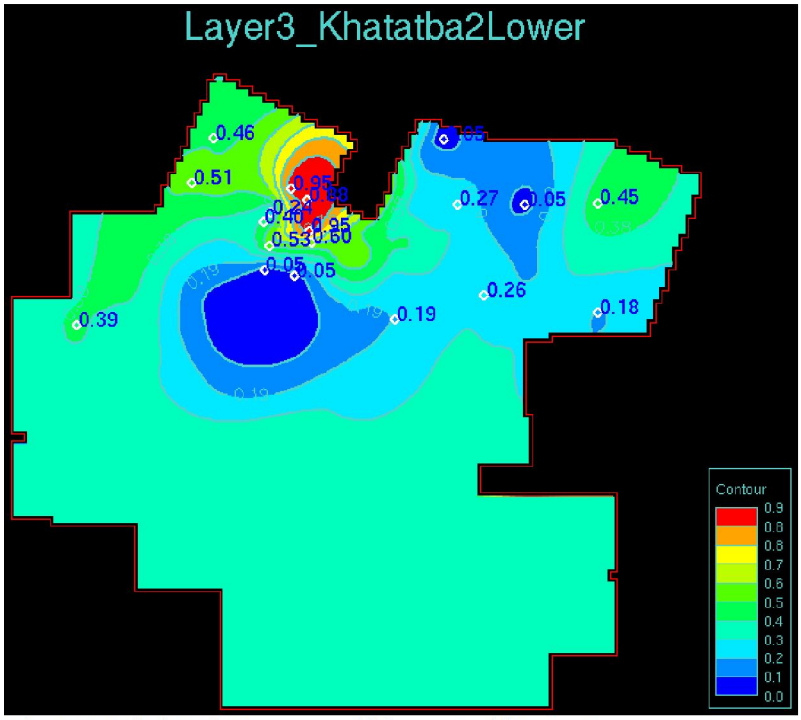

***Fig. 6.4**: Vsh distribution map of “Scenario A” Layer3*

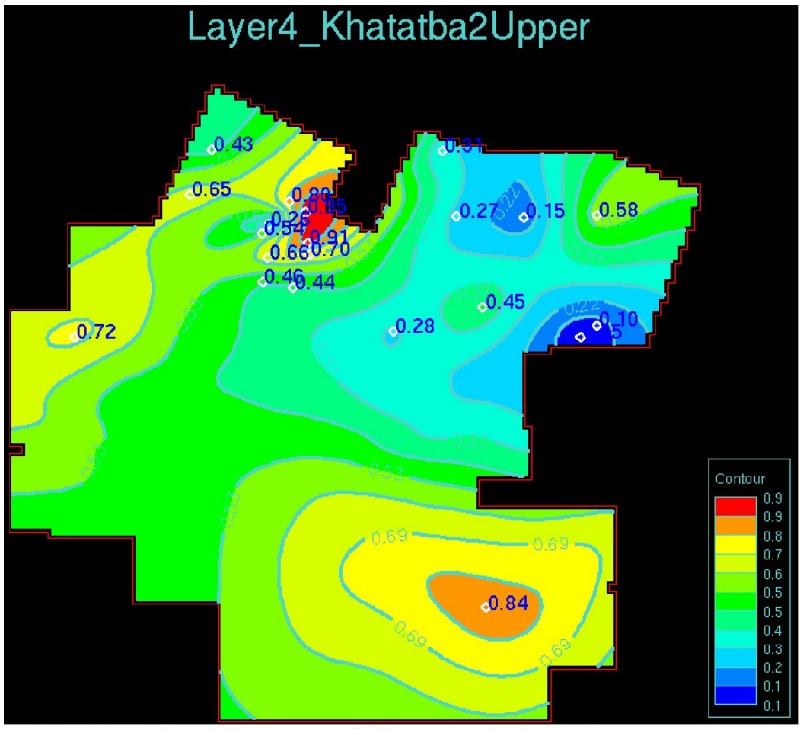

***Fig. 6.5**: Vsh distribution map of "Scenario A" Layer4*

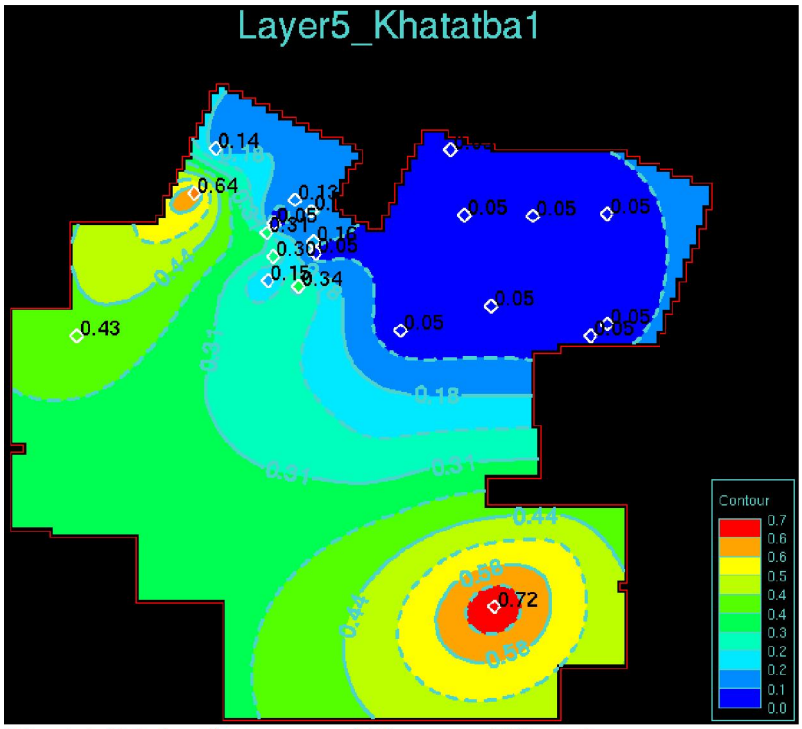

***Fig. 6.6**: Vsh distribution map of "Scenario A" Layer5*

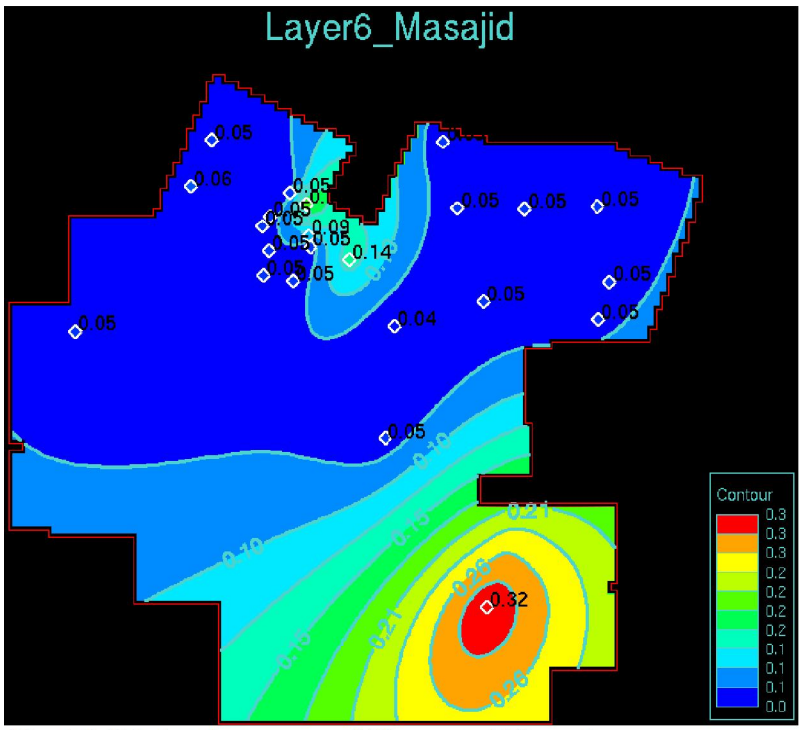

***Fig. 6.7**: Vsh distribution map of "Scenario A" Layer6*

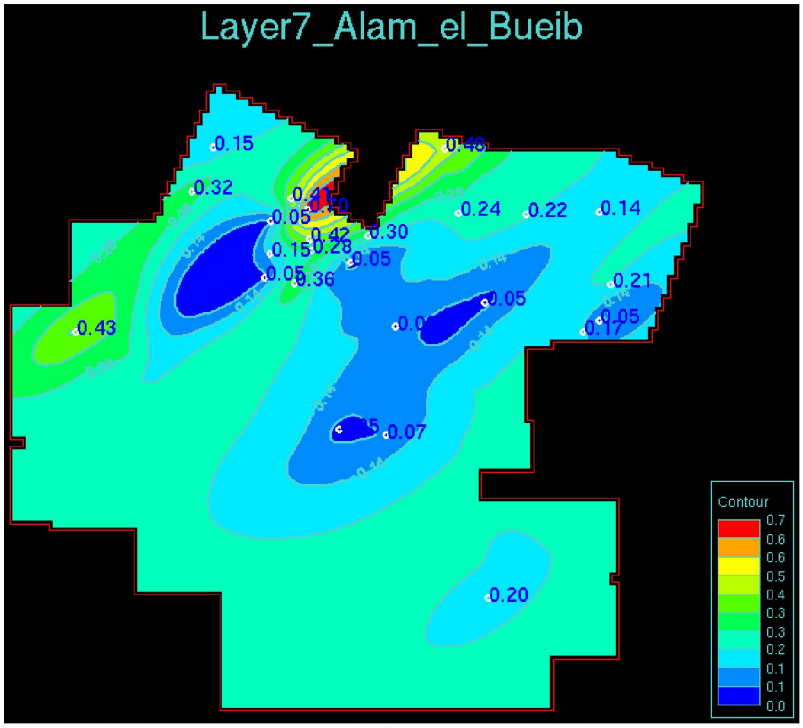

***Fig. 6.8**: Vsh distribution map of "Scenario A" Layer7*

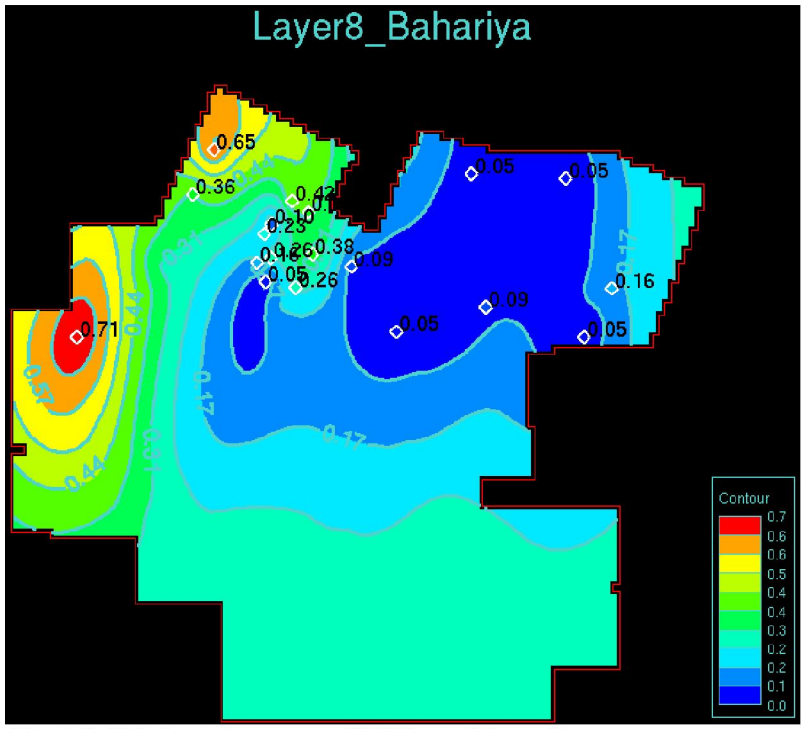

***Fig. 6.9**: Vsh distriution map of "Well tops" Layer8*

6.2 "SCENARIO C" MAPS

Once the Vsh distribution maps of "Scenario A" have been obtained, these were compared with facies distribution maps obtained from a detailed sedimentological report of the Western Desert area (Baruffini et al., 2012). These comparison was necessary in order to understand if, in terms of maps, the reached results were realistic, or if the available wells were been insufficient in number to have a good response from kriging, generating improbable results.

This check showed a comparison not completely satisfactory **(Fig. 6.10)**.

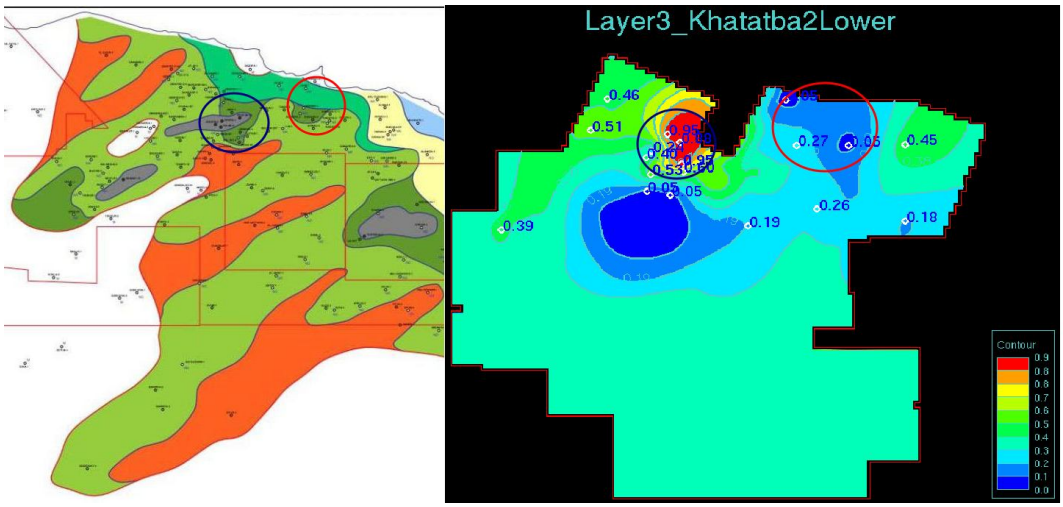

Fig. 6.10: *a comparison between the facies map (on the left) and the Vsh distribution map (on the right). The blue circles show a good correspondence between facies and Vsh values: the gray indicates deposition of "low density shale" and the dark green parts are "shale prone alluvial plane"; this high shale concentration is visible with the hottest color in the Vsh map with an optimal accordance. The red circles indicate instead a visible discordance: the aqua-green indicates "shaly low energy coasts with coal", that with the dark green theoretically involves in a important shale fraction, but it is not recorder in the Vsh distribution map.*

Based on these results, it was decided to consider another scenario for the tests; this new scenario was based on the available sedimentological information, comparing the wells data with the facies maps from the stratigraphic report. The aim of this scenario was to construct maps showing the most realistic Vsh distribution, trying to reproduce the facies distribution, respecting the starting Vsh data and adding artificial extra-wells value into the "Scenario A" maps, using the so-called "pseudo-wells" option.

Moreover, in order to reproduce the geometries of facies maps, some real well values were changed because they were in strong discordance with the facies theoretical value (**Fig. 6.11**).

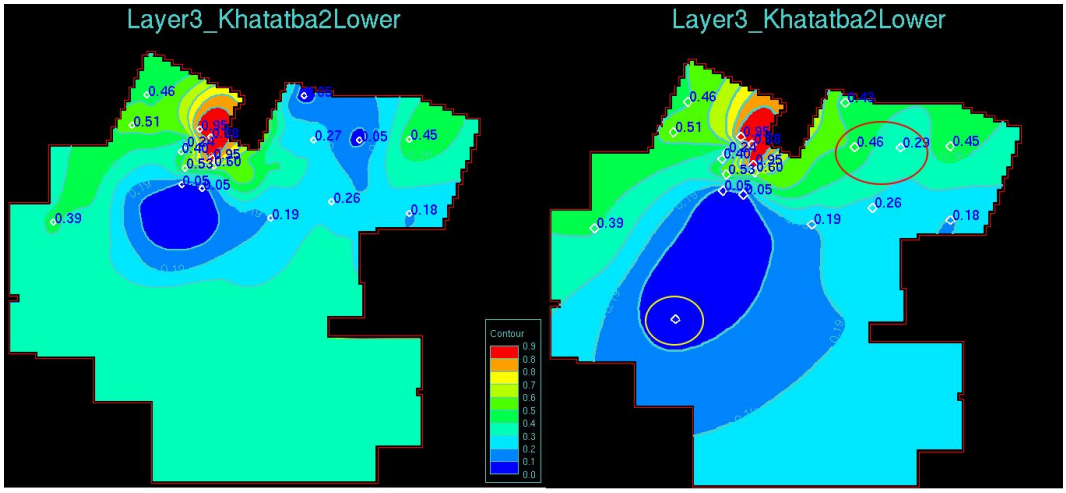

Fig. 6.11*: comparison between the Layer3 from the "Scenario A" (on the left) and the same layer modified (on the right). The red circles show two Vsh values changed and the yellow one shows an inserted "pseudo-well".*

These differences could be due to various reasons; on one hand, the problem could be a not perfect goodness and continuity of the gamma ray logs, that could implicate an incorrect Vsh evaluation. On the other hand, itis necessary to consider that facies distribution maps were done using both wells, seismic and field data, and they were not build to simulate the exact behavior of the formation, but just to have an idea of the sedimentological evolution of the formations in the Western Desert. The aim of this test was however to understand what is the different response of Migri at this Vsh values changes, and for this reason it was important to test it in different conditions. If the software will responses in a sensible way to these minimal changes, itis clear that in its application a detailed knowledge of the sedimentological settings will be necessary.

The comparison between Vsh and facies distribution maps allowed to construct the following maps. Unfortunately, the report from which these figures have been taken focused just on the lower target, until the Early Cretaceus formations. Moreover, the subdivision of Alam el Bueib Fm (layer 7) into a lot of sublayers implies that it was not possible to have information about this target, because of our impossibility to divide the layers in the GeoModel. In conclusion, this new

test scenario (that hereafter will be called “Scenario C”), shows just four modified maps (layers 3rd, 4th, 5th and 6th), while the layers 7th and 8th will be the same that the “Scenario A”.

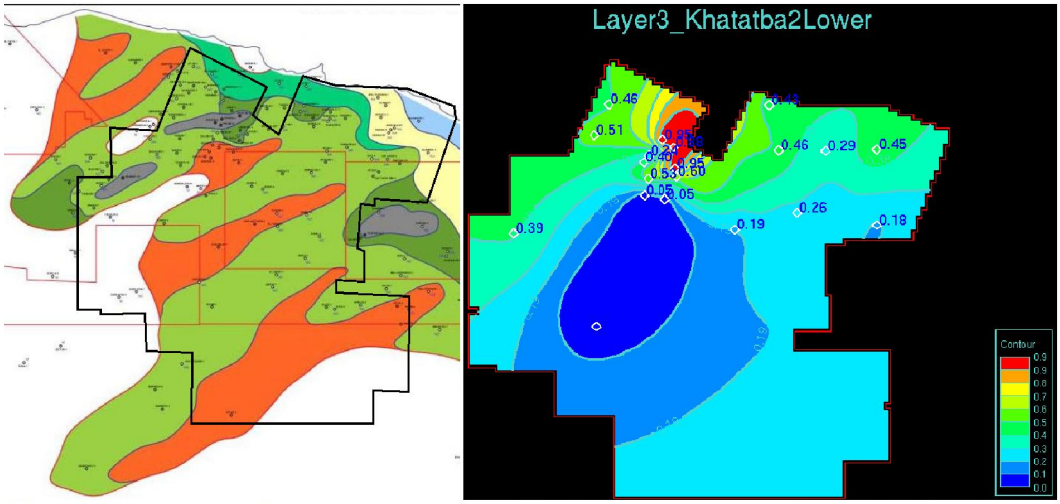

***Fig. 6.12**: comparison between facies map and Vsh distribution map of "Scenario C" in layer 3. The colours in the facies maps indicates: dark reen: shale prone alluvial plane; light green: sand prone alluvial plane; gray:low density shale; aqua-green: shaly low energy coasts with coal; orange: fluvial sheet sandstone; beige: shaly-sandy delta front; light-blue: marine shelf shale-limestone.*

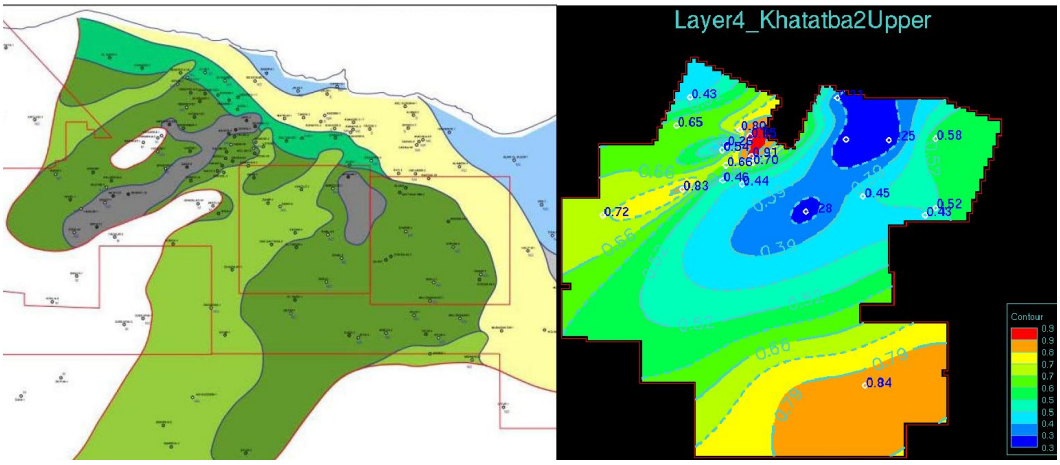

***Fig. 6.13**: comparison between facies map and Vsh distribution map of the "Scenario C" in layer 4. The colours in the facies maps indicates: dark reen: shale prone alluvial plane; light green: sand prone alluvial plane; gray:low desity shale; aqua-green: shaly low energy coasts with coal; beige: shaly-sandy delta front; light-blue: marin shelf shale-limestone.*

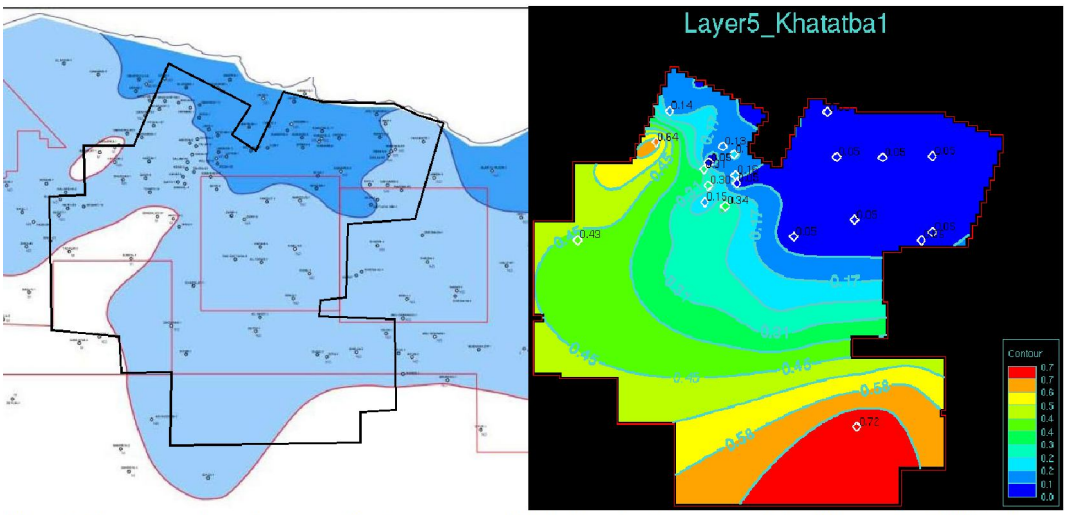

Fig. 6.14*: comparison between facies map and Vsh distribution map of the "Scenario C"" in layer 5. The colours in the facies maps indicates: blue: marine limestone; light-blue: open-marine shale-limestone.*

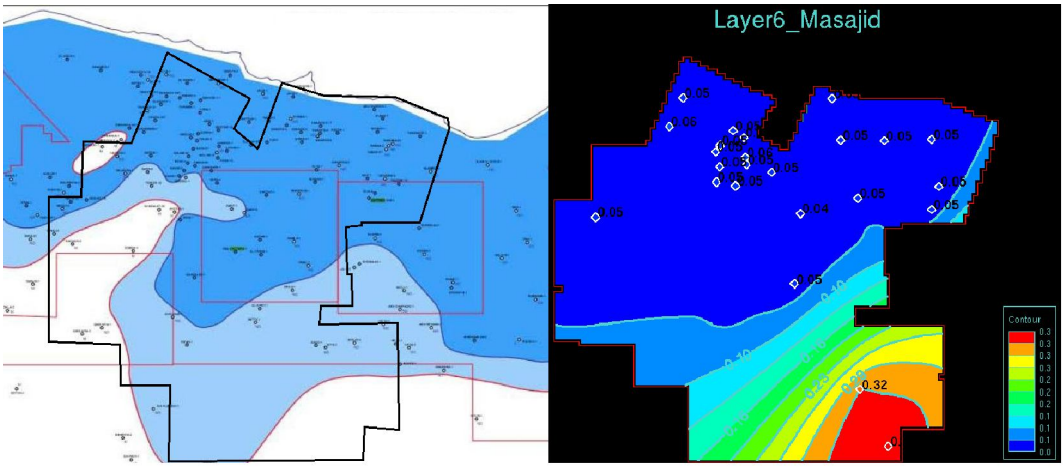

Fig. 6.15: comparison between facies map and Vsh distribution map of the "Scenario C" in layer 6. The colours in the facies maps indicates: blue: marine limestone; light-blue: open-marine shale-limestone.

6.3 THE “SCENARIO B” MAPS

The last Vsh distribution maps were those related to “Scenario B The log response shows clearly that this scenario is not realistic, because it is in discordance with the formations features. This test has been however continued in order to have another example about the software's behavior on Vsh changes. The following images are the corresponding Vsh distribution maps.

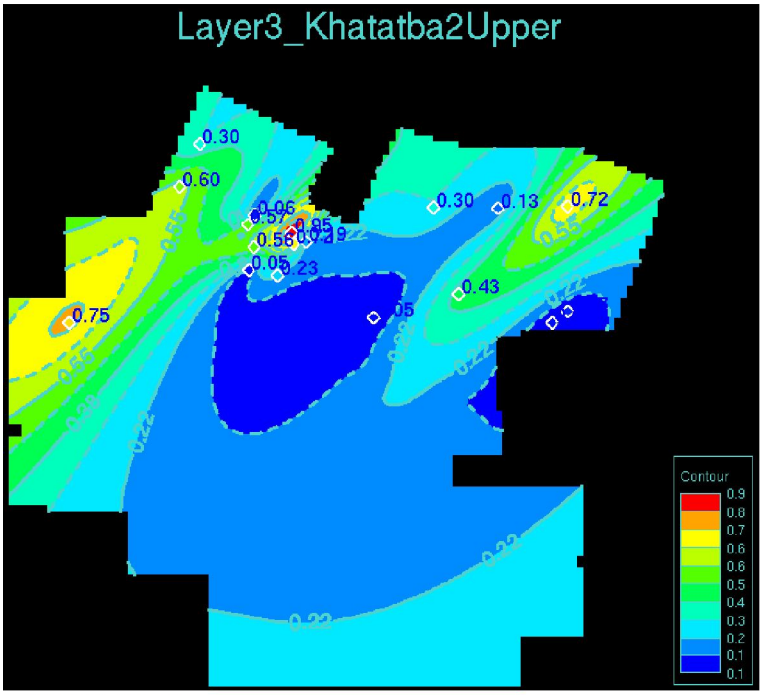

6.16: *Vsh distribution map referred to "Scenario B", layer3.*

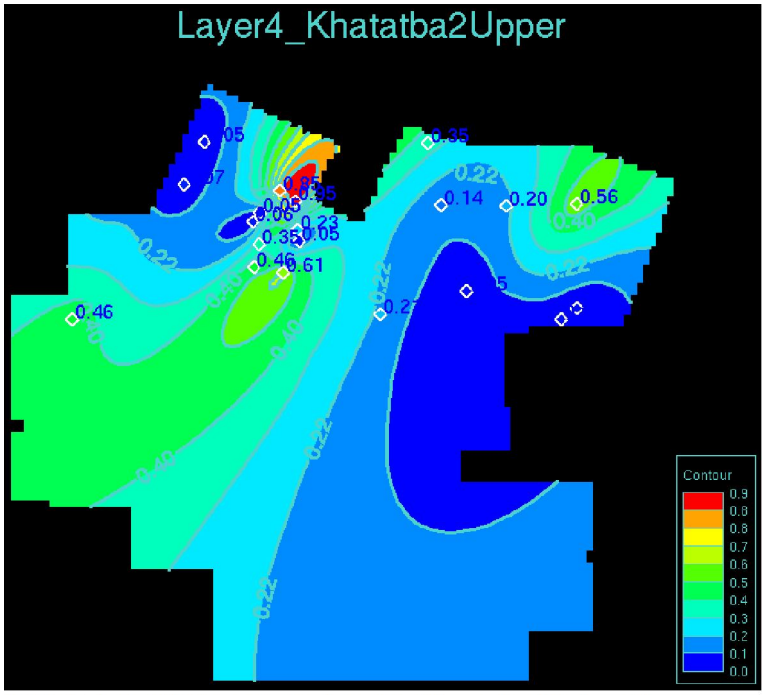

6.17: *Vsh distribution map referred to "Scenario B", layer4.*

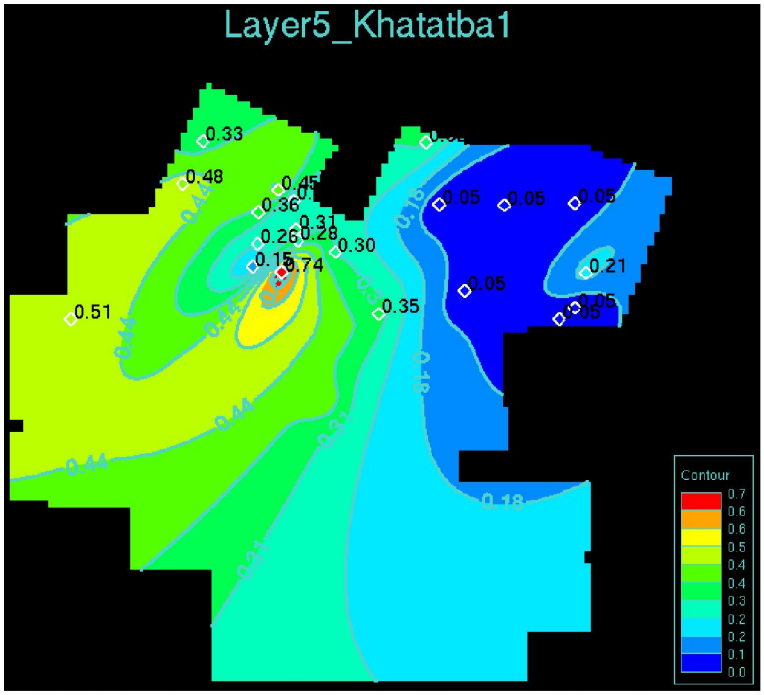

6.18: *Vsh distribution map referred to "Scenario B", layer5.*

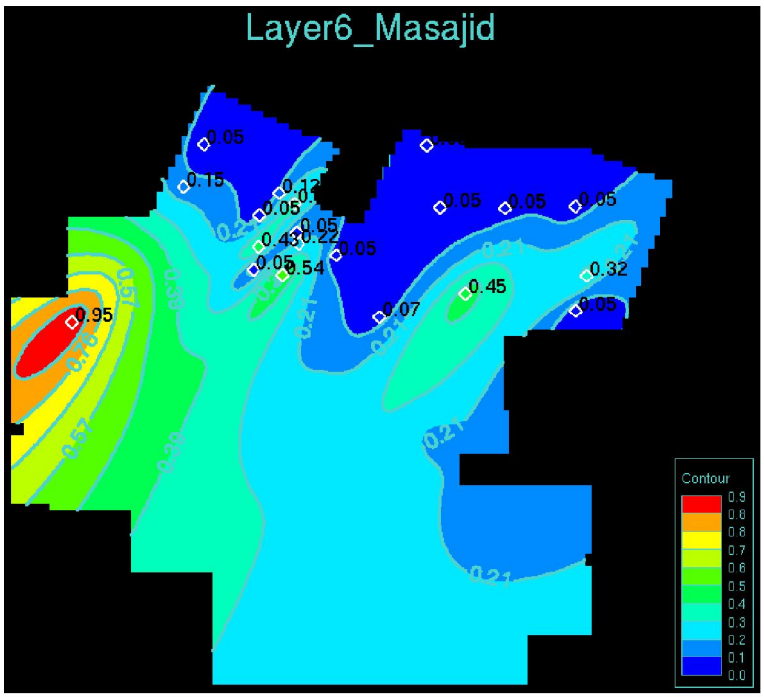

6.19: *Vsh distribution map referred to "Scenario B", layer6.*

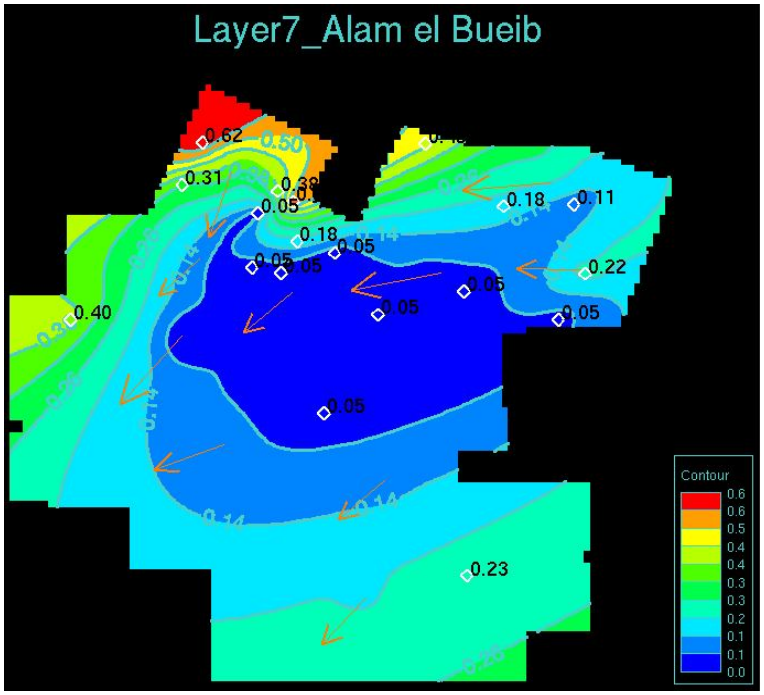

6.20: *Vsh distribution map referred to "Scenario B", layer7.*

7. "*MIGRI*": MODEL AND SIMULATION

In the previous chapter, construction of Vsh distribution maps was described. As already said, in this phase of the study Vsh maps will be inserted into the GeoModel constructed on *Migri*, a software that aim to simulate the secondary migration flow dynamics and to characterize position, volume and phase (oil, gas or both) of any accumulations. In particular, tests that will be described aim to a better knowledge about how the shale contents into the rocks influences flow and accumulations.

The input variables are many, often complex and difficult to obtain; as regards to the GeoModel base parameters as thicknesses, depths and faults permeability, they were assumed to be functional at past studies, that aimed at slightly different goals than the simulation we wanted to perform in this study.

We will only focus on the Vsh parameter, and the minimum target of our simulations will beto see the real reservoir rocks that compose the considered petroleum system charged, and the distribution of the accumulation decreasing from the lower layers to the uppers.

These minimum goals are however not trivial because with the secondary migration simulation software currently used by Eni, namely SEMI, the Vsh value is not an input data. In fact, a lithological characterization of the formation is not possible with SEMI, and the HC transfer from a layer to the upper is only regulated by faults permeability and by an abatement factor, arbitrarily assigned by users, that should simulate the different behavior of the formation respect to the hydrocarbon flow. For this reason, thanks to Migri, a satisfactory result of these tests could open, new perspectives about Petroleum System Modelling, with an approach which could be based on the effective geological situation of the studied area.

7.1 A NEW APPROACH IN THE SECONDARY MIGRATION SIMULATION: INPUT PARAMETERS

Migri is a released software still in development phase, developed by the Norwegian society Migris A.G. It presents itself like “a new approach to the hydrocarbon migration modeling, that could allow more accurate estimations about flow pathways, oil and gas losses and accumulation volumes, reducing in this way uncertainties and risks during the appraisal phases” (Øyvind et al., 2013).

The main innovation introduced by the software is the 3D GeoModel vertical subdivision in flow-units; these are sub-units that assign to any layer different flow conditions, based on the principle of the Darcy's law. Thanks to the input parameters, this software calculates relative permeability and capillary pressure that control oil and gas saturation, migration velocity, hydrocarbon column height and losses of every flow-paths.

Vsh value is one of the main factors influencing capillary pressure and permeability, and it is one of the driving parameters in this kind of approach to secondary migration.

Migri allows to insert a huge quantity of data, in order to increase the GeoModel realism, as visible in **Fig. 7.1.** Some of the values can just be uploaded from existing files, while others can be calculated by the software itself.

Fig. 7.1*: list of the input data allowed to be inserted on Migri*

For what concern this study, as previously mentioned, data derived from the 2009 PSM Western Desert project (De Poli et al., 2009). The aim of that study was the evaluation of different source rocks contribute to the hydrocarbons accumulations in the Western Desert area; secondary migration accumulation was performed through SEMI and internal developed software. In the next years, some corrected and more detailed version of the GeoModel have been developed, but it was not possible to use them, because they are not accessible because of industrial secret reason.

The most important parameter that was inserted during the migration phase has been the 4D GeoModel. It is a depth model that adds new strata and reproduces the

depositional and deformation history of the area. These maps were built, even for the 2009 PSM Western Desert project, through SIMBA, another modeling software developed by Eni.

Other important input parameters are those related to temperatures and sea bottom depth variations, besides the faults polygonal into the layers that were available (from layer 5 to layer 8).

At the end, lithologies were inserted; even if they were partially discordant respect to the sedimentological information we had and to the Vsh data acquired by logs, at first lithologies used during the SEMI simulation were assigned. The first test which was performed, in fact, aimed to compare results from SEMI with the Migri behavior, and in order to compare them it was needed to assign to Migri the same input properties of the SEMI simulation.

Then, our tests have been enriched with a new scenario, hereafter named “scenario D”, in which all the 3D GeoModel input data are derived from the model build on SEMI in 2009 PSM project. In this scenario, no Vsh maps have been inserted; this parameter, in fact, is automatically attributed by Migri based on the lithology assigned to each layer. Specifically, lithologies and consequent Vsh values assigned are summarized in **Tab. 7.1**:

Thanks to all these information, it was possible to build the “Scenario D” 3D GeoModel on Migri (**Fig. 7.2**):

LAYER NUMBER	LITHOLOGY	Vsh VALUE	EVENT BEGINNING (My)	EVENT END (My)
1	Sandstone	0.05+-0.05	590.00	245.00
2	Sandstone	0.05+-0.05	245.00	175.00
3	Sandstone/Shale (25/75)	0.75+-0.15	175.00	169.00
4	Sandstone/Shale (25/75)	0.75+-0.15	169.00	167.00
5	Sandstone/Shale (75/25)	0.25+-0.15	167.00	164.00
6	Limestone	0.05+-0.05	164.00	156.00
7	Sandstone/Shale (75/25)	0.25+-0.15	156.00	120.00
8	Sandstone/Shale (50/50)	0.5+-0.2	120.00	94.00
9	Limestone/Marl (50/50)	0.25+-0.1	94.00	86.00
10	Limestone	0.05+-0.05	86.00	33.90
11	Shale	0.95+-0.05	33.90	7.50
12	Shale	0.95+-0.05	7.50	0.00

***Tab. 7.1**: lithologies and default Vsh values assigned to each layer in "Scenario D".*

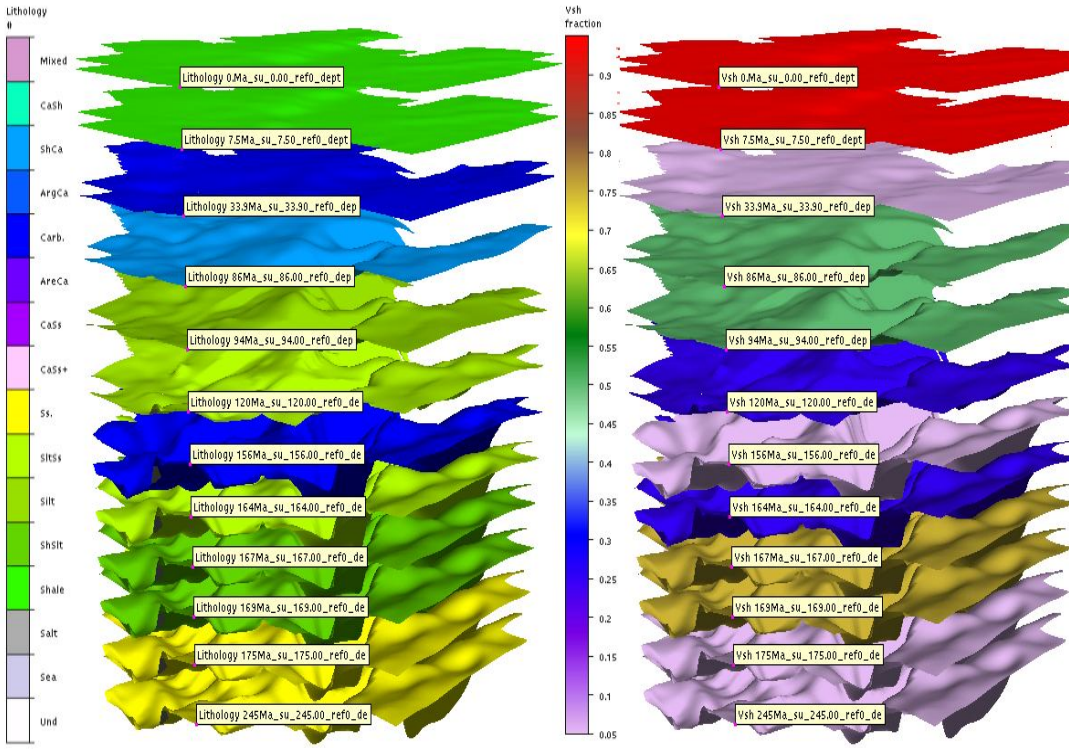

***Fig. 7.2**: "Scenario D" 3D GeoModel builded on Migri: on the left, the corresponding lithologies are shown; the model on the right shows Vsh values assigned by the software.*

Once the geological parameters were inserted with the greatest possible accuracy, even the element related with the petroleum system were considered.

At first it was needed to consider the available information about hydrocarbons expelled by the source rocks, still considering data deriving from the 2009 PSM project. At this step, a first substantial difference between the SEMI GeoModel and the one we build on Migri was found. In fact, the GeoModel used to perform simulations with SEMI showed all the main source rocks effectively present in the Western Desert petroleum system, namely two into the Khatatba Fm and one at Alam el Bueib Fm. The source rocks used in Migri are instead only referred to Jucassic, corresponding with the levels 2 and 3: the layers corresponding with the Alam el Bueib Fm have not been considered because of data availability reasons (**Fig. 7.3**).

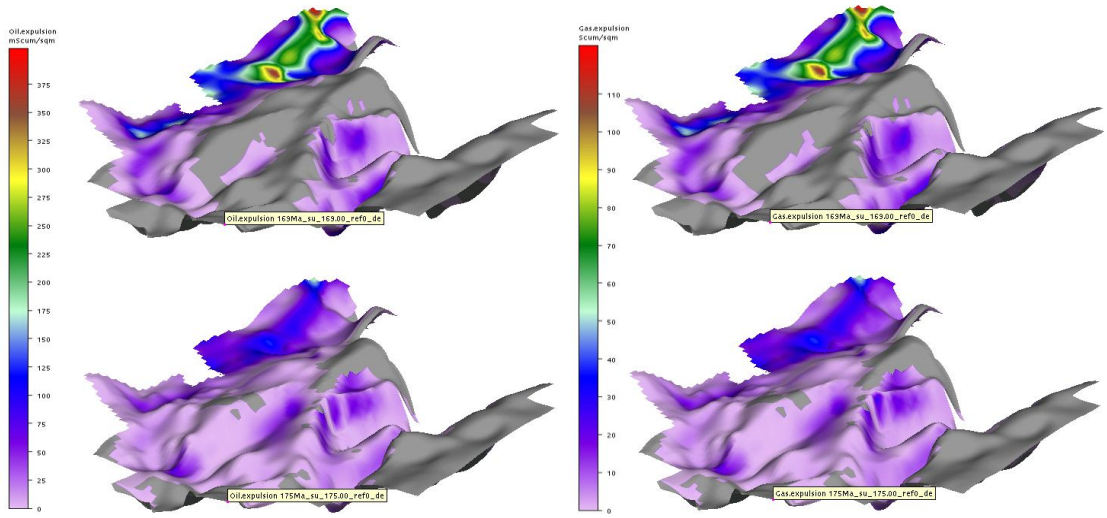

***Fig. 7.3**: Oil_expulsion (on the left) and gas_expulsion (on the right) of the two source rocks levels on Migri-builded GeoModel, corresponding with the layers 2 and 3.*

Other important parameters which have to be defined, in order to improve the GeoModel accuracy in the definition of the hydrocarbons up-flow, are those related with faults permeability. As previously said, the available fault polygons files were those referred to layers 5-6 (among them equal) and 7-8 (**Fig. 7.4**).

It was not possible to characterize the faults properties of that fault, because there

was not enough time to find literature information, and so to have accurate data of any specific fault. The only information which has been possible to know was that during the SEMI simulations, faults were considered open, and so fluids could pass through the layers mainly thanks to those.

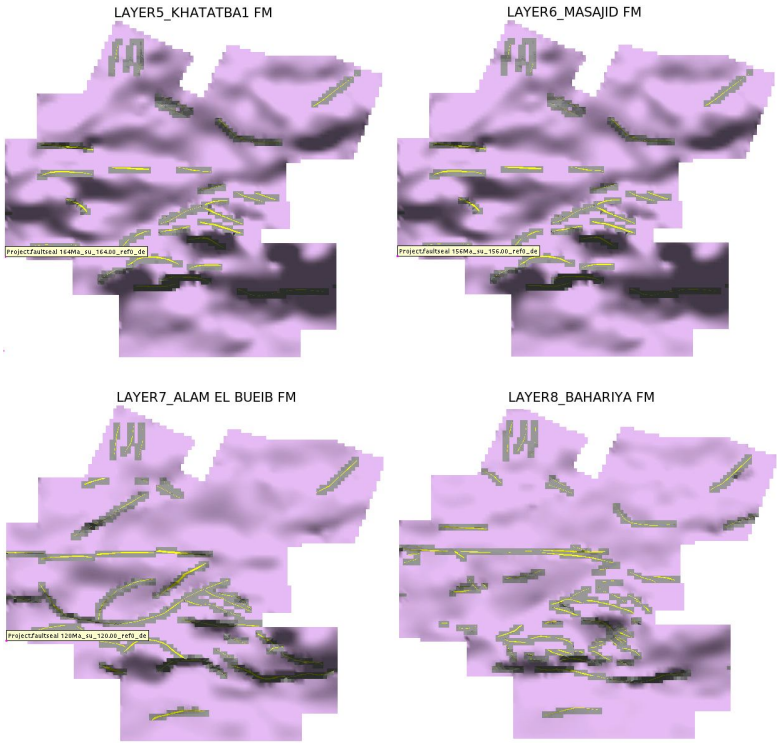

***Fig. 7.4**: faults displacement in the available layers.*

Even if this is a considerable approximation, it's necessary to remember that the aim of this phase of the study is to compare two simulations performed with quite identical input data but with different software, and therefore it's needed to maintain the same properties as more as possible.

The assumption of the open faults will be moreover used even in the construction of GeoModel improved with the Vsh maps, because they belong to the “basic” GeoModel (Scenario D) and the goal is to see what are the effects of the Vsh values, maintaining the same other input parameters.

7.2 THE SIMULATION

Once the model was characterized with all the available input data, it was possible to start with the software simulation of the "Scenario D" (Fig. 7.5):

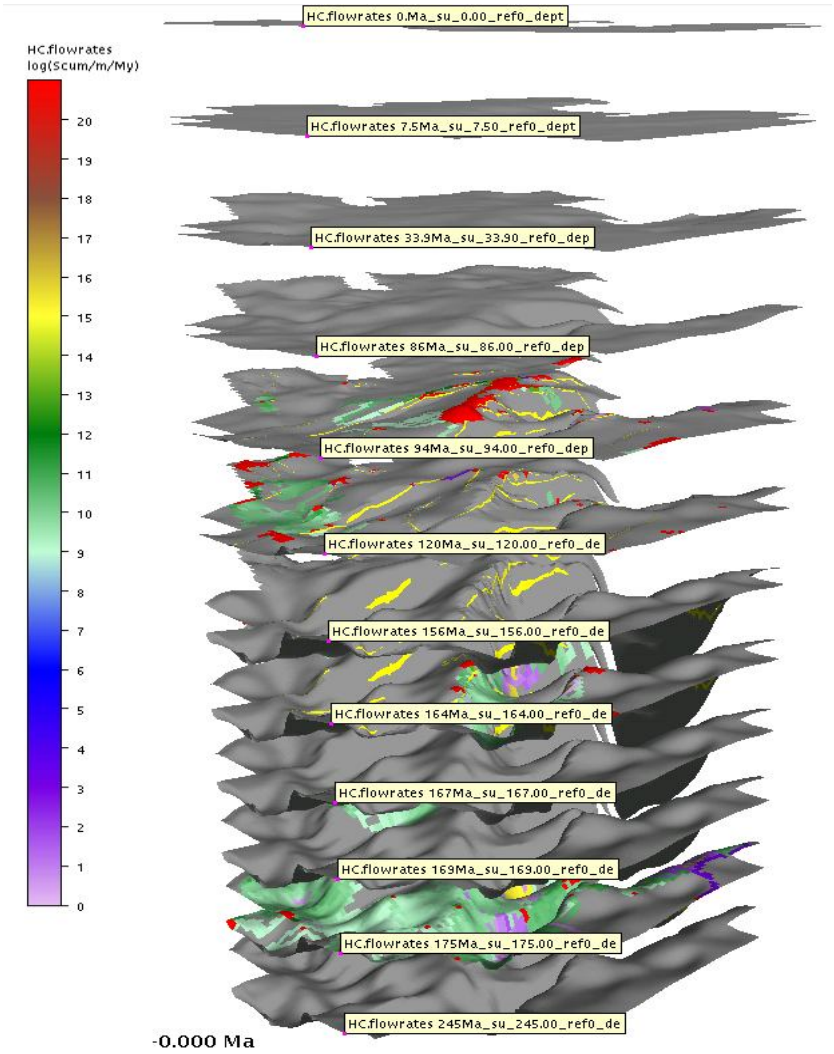

***Fig. 7.5**: Migri 3D GeoModel after the simulation was performad. This screenshot shows the Flow-rate maps for each layer.*

The model showed in Fig. 7.5 shows the final result of the temporal simulation. During the processing it is possible to see the evolution of the GeoModel for each time-step; it enriches with new layers during the time, including the hydrocarbon

expulsions with their flow path and accumulation for every temporal interval at which the layers referred.

The final result shows the flow-rate maps, that is a special Migri plot-type that aims to show many of the more important migration features in one single map, as it will be better explained in the following pages.

Once the simulation has been performed, position of hydrocarbon accumulations resulted by Migri were compared with the same results calculated by SEMI. In order to do this, "Trap_phases" maps, which show the positions of oil (green) and gas (red) accumulations, referred to layer 5 were used (**Fig. 7.6**).

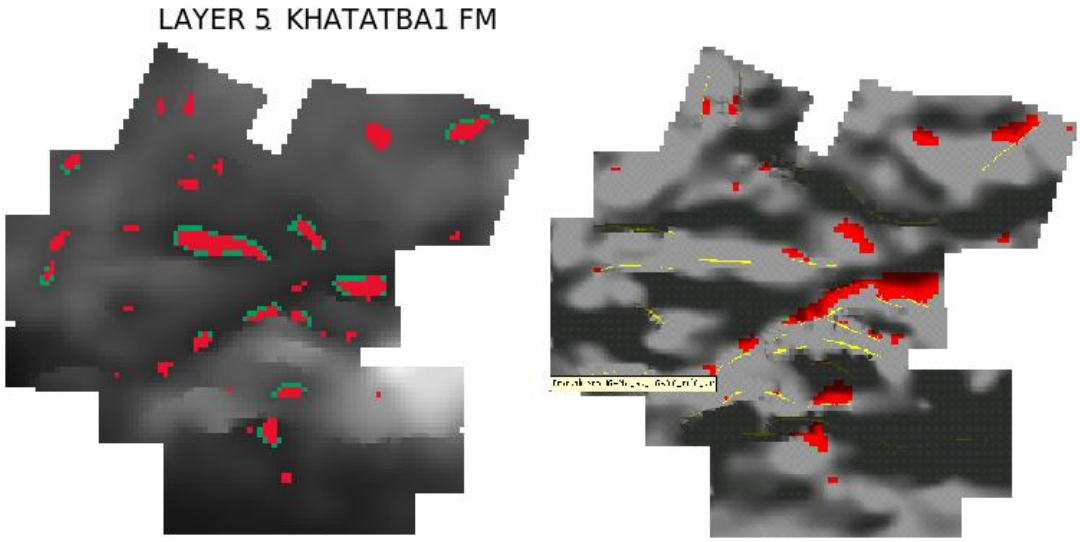

Fig. 7.6*: Comparison between trap_phases maps came from SEMI (on the left) and Migri (on the right) simulation, referred to the Layer5; the maps on the right referred to "Scenario D" conditions.*

Observing the maps, even if it seems clear that there are some differences in the accumulation distributions, there are anyway important similitudes between simulations performed with SEMI and with Migri.

Not identical results were however predictable and desirable, because of their different calculation techniques: Migri is a secondary migration simulation that works completely on 3D, while SEMI behavior is defined "2D and a half", because

it considers separately each carrier, and it doesn't consider at all the 3D model into which the carrier is inserted.

On the other hand, a good indicator of the constructed GeoModel reliability was represented by the not extreme discordance between the showed results., Build model is considered as reliable and was possible to evaluate the Vsh effect on the results, with the knowledge that the GeoModel on which this work has been performed is consistent.

Comparison between SEMI and Migri simulation results instead cannot be done for the upper levels. As previously explained, into the Migri GeoModel just the Jurassic source rocks were inserted, while in SEMI also the upper ones (contained into the Alam el Bueib Fm) were considered. For this reason, accumulation for the layers upper than the 5th resulting from the Migri simulation were volumetrically and quantitatively lower than those obtained with SEMI, as it is visible from the Layer 8 accumulation comparison (**Fig. 7.7**):

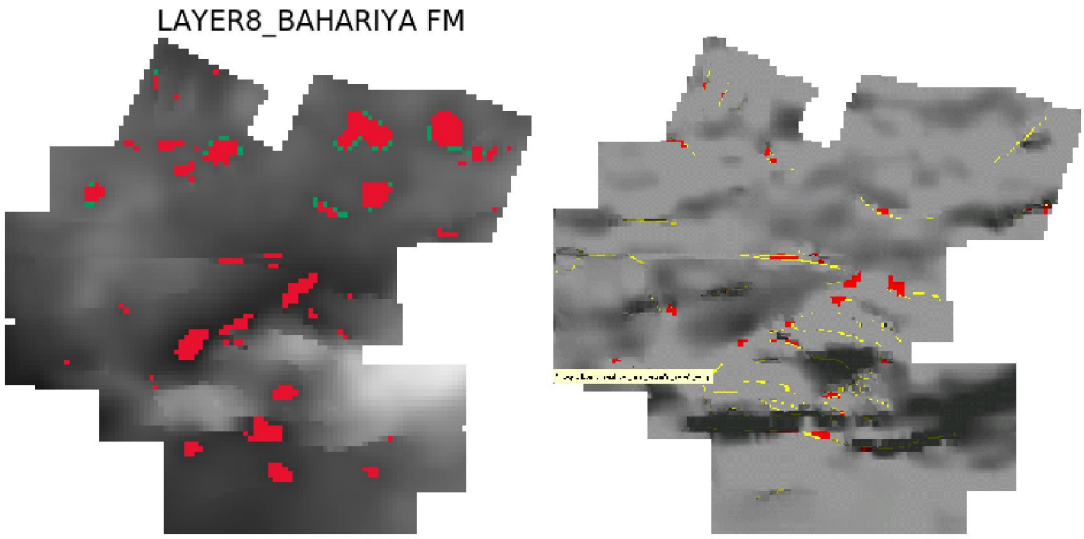

***Fig. 7.7**: Comparison between trap_phases maps came from SEMI (on the left) and Migri (on the right) simulation, referred to the Layer8; the maps on the right referred to "Scenario D" conditions.*

7.3 Vsh DISTRIBUTION MAPS INSERTION

In order to quantify an try to understand how the Vsh values can influence the simulation results, once the goodness of the GeoModel was verified, a comparison between simulation at different Vsh distibution has been necessary. In fact, comparing tests under slightly different Vsh conditions was the way in which the influence of the parameter and the limit values over which important changes in accumulation distributions and flow direction occurred were determined and understood.

Consequently, Vsh distribution maps referred to the others scenarios were added to "Scenario D" (**Fig. 7.8 - 7.9**). As explained in chapter 6, Vsh distribution maps build thanks to wells data has been those referred to layers from 3rd to 8th. In the layer in which a Vsh distribution map was not build, values adopted in the "Scenario D" were used. Based on the same principle, also the lithologies assigned at every layer are the same used for the "Scenario D" conditions simulation, assumed as a "base model".

This concept should be taken into account, and it will be taken up in the chapter 8. In fact, the choice to attribute a lithology or another to each layer, even if it doesn't change the Vsh values manually inserted, involves the automatic allocation of other default parameters, very important in migration processes, linked with the assigned lithology, that in this study has not been inserted manually because it was not possible to know them. The most important one is the carbonate volume fraction Vca, analogue at the Vsh but referred to carbonate.

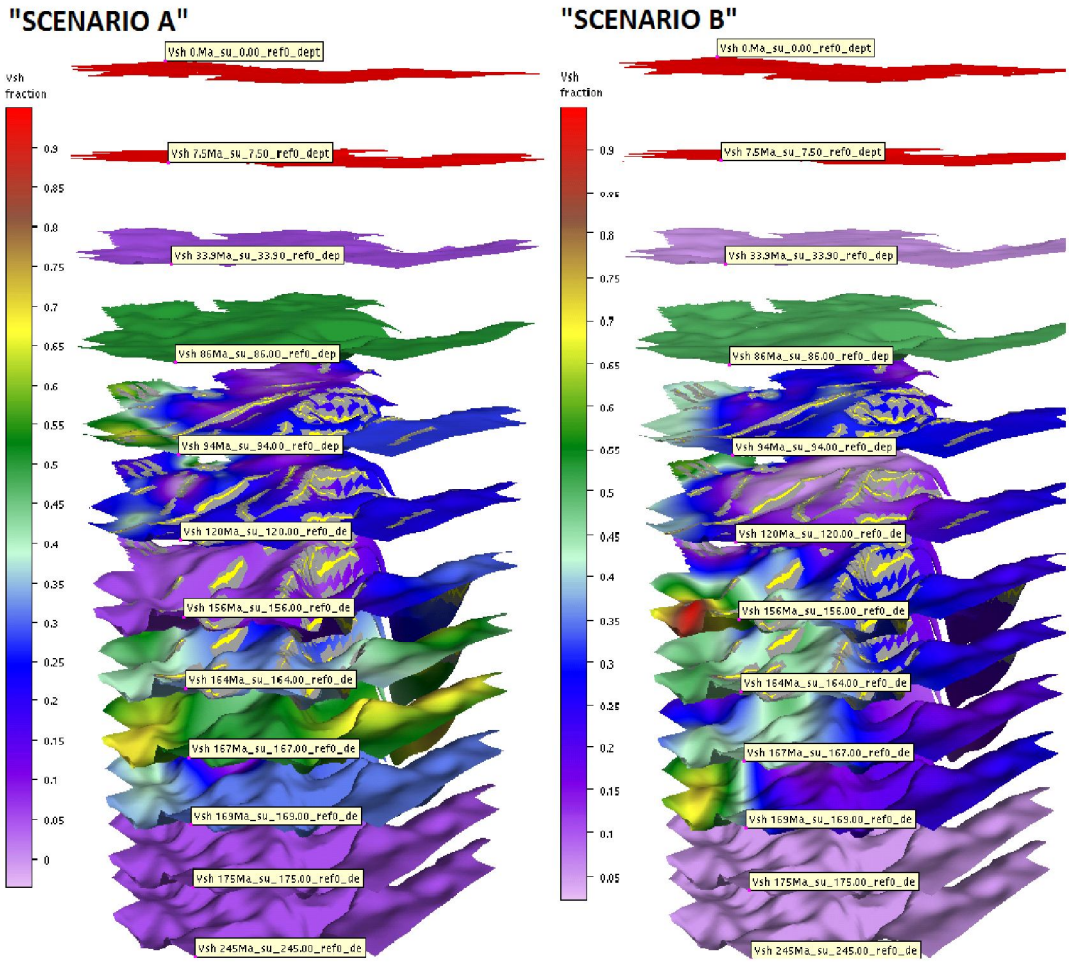

***Fig. 7.8**: Vsh distribution maps on 3D GeoModel on Migri; the images referred to "Scenario A" and "Sceenario B", and some Vsh distribution difference is visible also at this scale.*

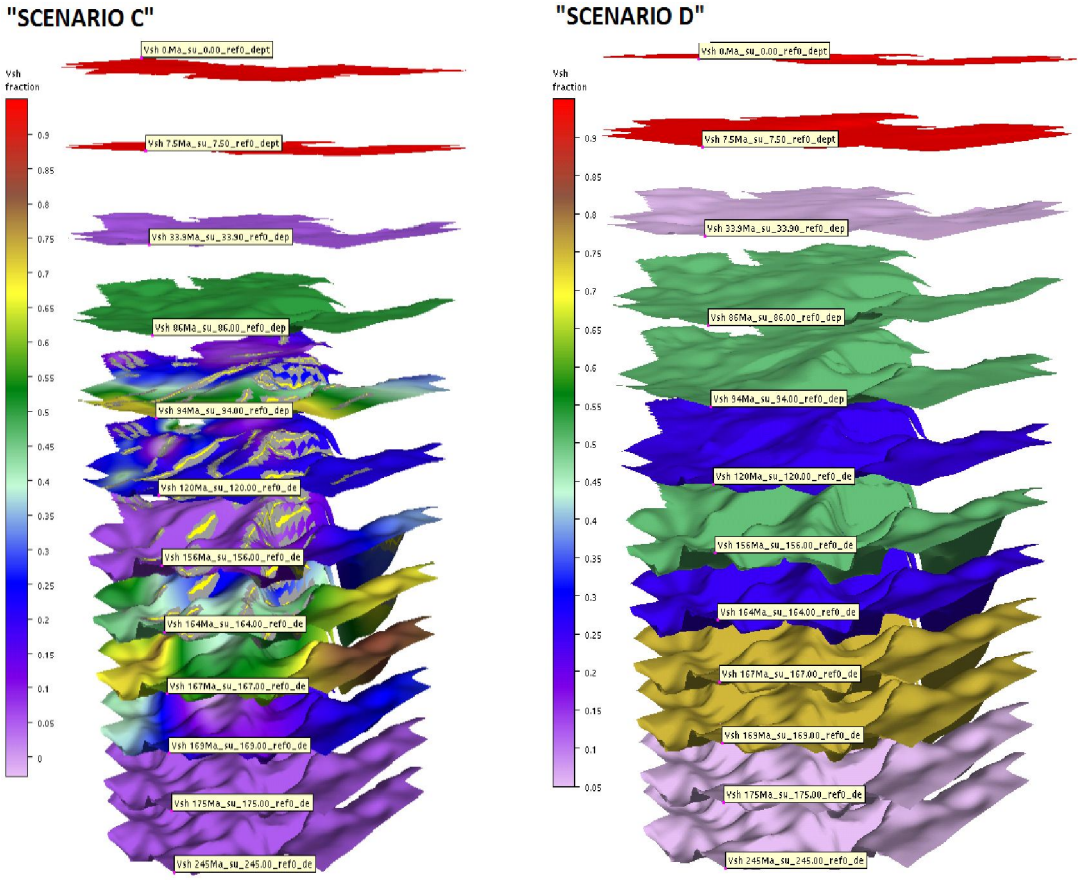

***Fig. 7.9**: Vsh distribution maps on 3D GeoModel on Migri; the images referred to "Scenario C" and "Scenario D".*

7.4 COLLECTION OF RESULTS

Once all the Vsh distribution maps were attributed to the corresponding scenario, simulations were performed, and their results are shown in the attachments.

In order to allow an easier view and understanding of the output maps, some short explanations about their meaning are reported in the following pages. These descriptions have been taken from the Migri's help, and the reported examples are referred to the Layer 5 of “Scenario A”.

- *FLOW-RATE*: As previously said, Flow-rate map is a special Migri plot-type that aims to show many of the more important migration features in one single map. In particular, it is possible to show the different phases of hydrocarbon accumulated: oil (dark green) and gas (red). Light green indicates the oil flow, yellow-brown gas flow and violet the mixed phase flow. Thanks to a logarithmic scale, flow rate is able to indicate with darker colors larger quantities of oil and/or gas migrating through that node (**Fig. 7.10**).

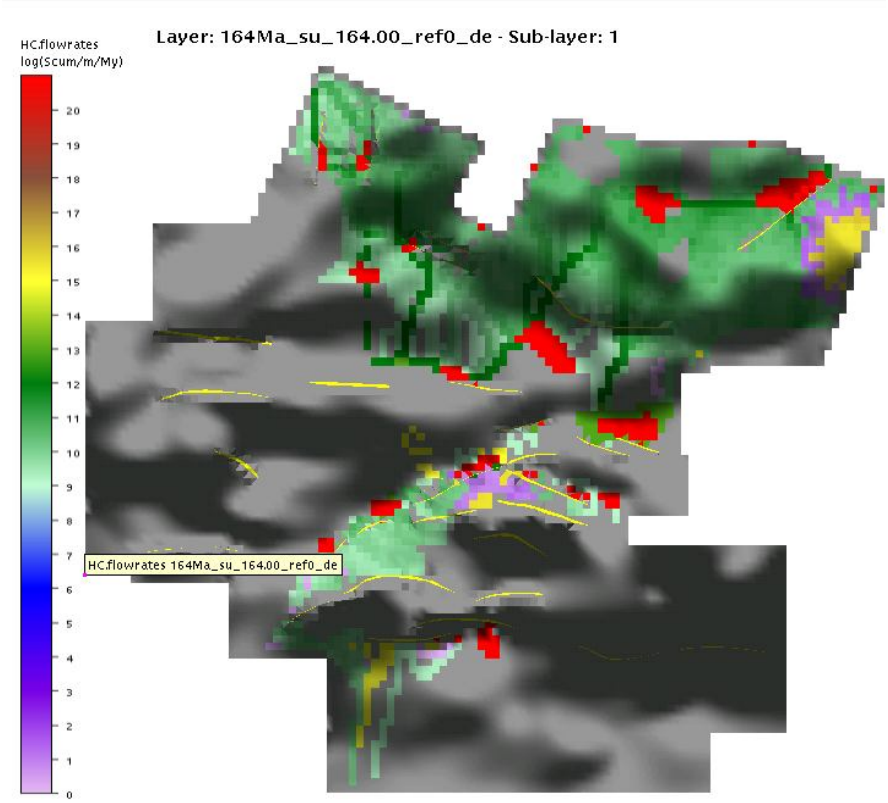

***Fig. 7.10**: Flow-rate example map, referred to Layer 5-Scenario A*

- *TRAP_PHASES*: It indicates the modeled phases of the traps. With red are shown gas accumulations, with green the oil ones (**Fig. 7.11**).

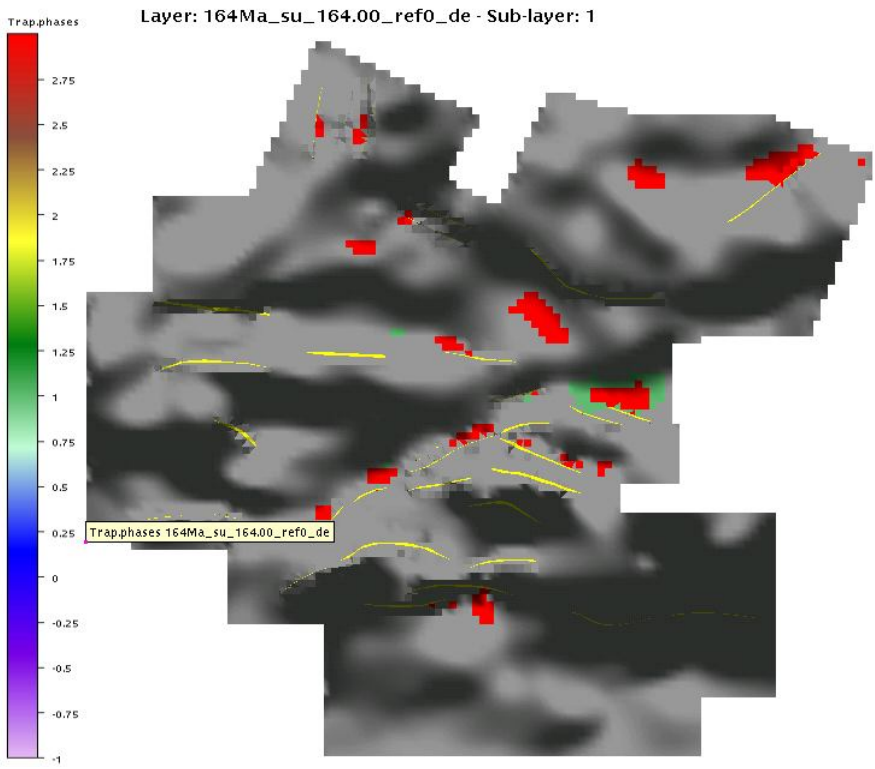

***Fig. 7.11**: Trap-phases example map, referred to Layer 5-Scenario A*

- TRAP_HC-COLUMN*:* the color scale indicates the modeled height of the trapped hydrocarbons column. The values are in meters, and the range is between 0 and 150 m (**Fig. 7.12**).

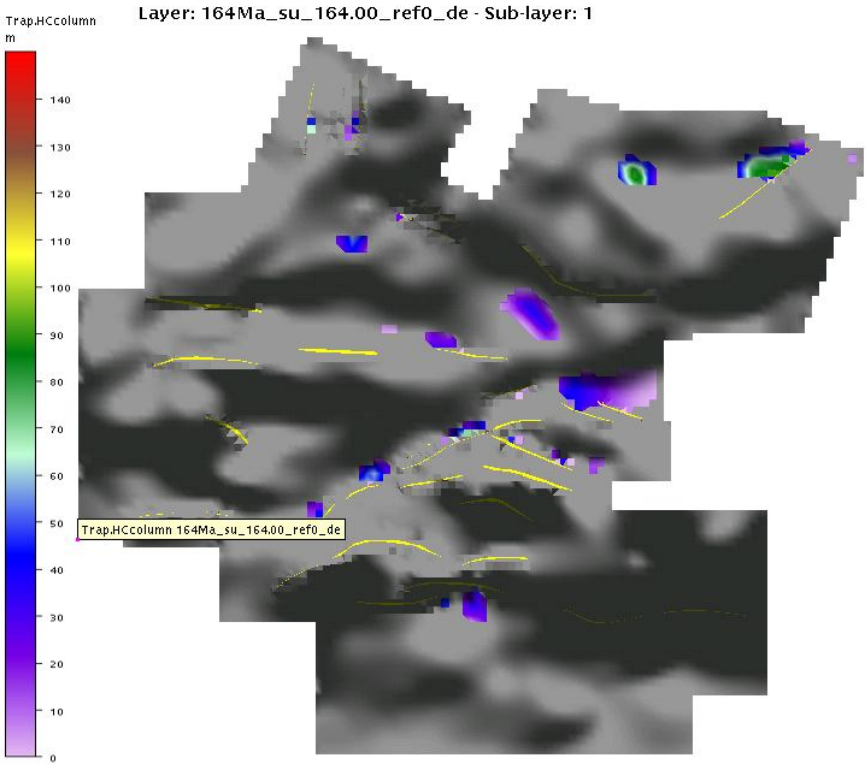

Fig. 7.12*: Trap-HC_column example map, referred to Layer 5-Scenario A*

- *STRUCTURAL_CLOSURE*: height above the structural spill point. In other worlds, the traps potential volume (**Fig. 7.13**).

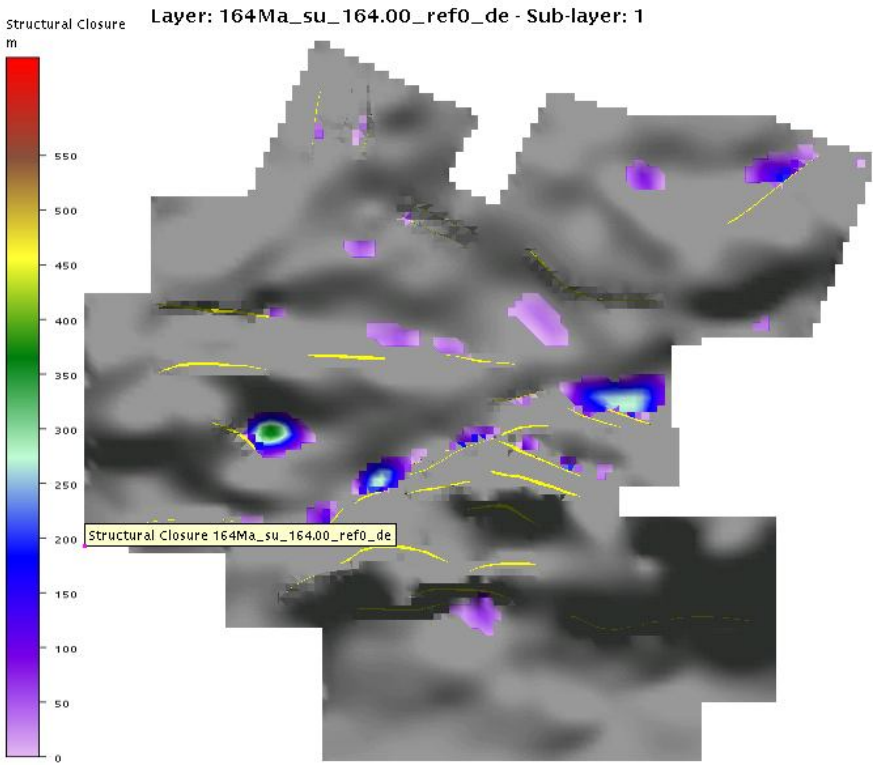

***Fig. 7.13**: Structural-closure example map, referred to Layer 5-Scenario A*

- *FLOW-DIRECTION*: potential direction of flow (yellow: lateral; red: upward; blue: downward); it isn't the effective flow direction, but the path it could take in the colored area. It's indipendent from the hydrocarbon quantity (**Fig. 7.14**).

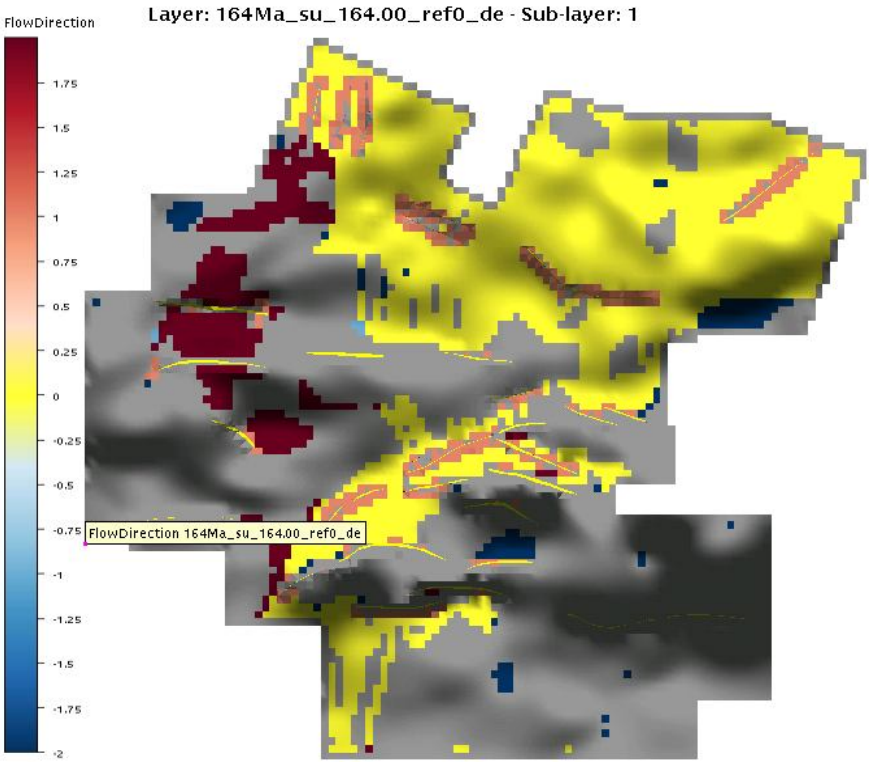

***Fig. 7.14**: Flow-direction example map, referred to Layer 5-Scenario A*

- *OIL AND GAS EXPULSION*: oil and gas volume expelled from the source. It depends from the histories that are defined for each modeled source rock unit (the figures referred to layer2 source rock) (**Fig. 7.15**).

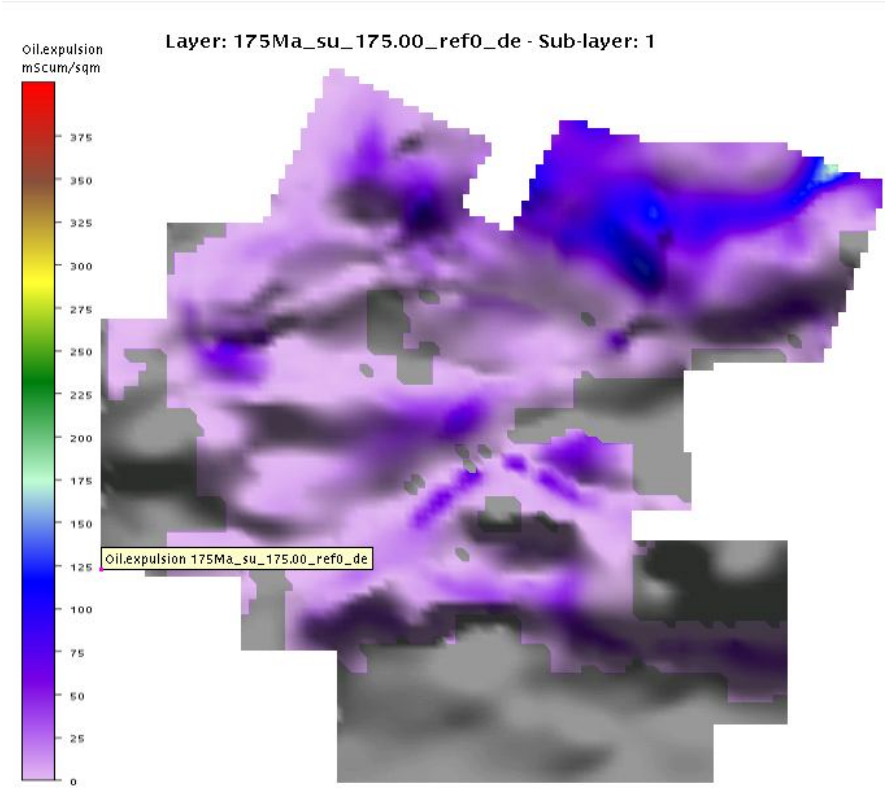

***Fig. 7.15**: Oil-expulsion example map, referred to Layer 2, lower source rock level*

8. RESULTS DISCUSSION

Starting from the different scenarios that were considered and from the related migration simulations, in this chapter the differences between calculated pool positions and volumes will be analyzed.

The layers considered for the hydrocarbons migration are the 5^{th}, 7^{th} and 8^{th}, namely the formations that constitute the main reservoir in the Western Desert petroleum system. They are in fact the layers that have been affected by hydrocarbon charging during the simulations: we can therefore consider the correspondence found between the layers charged in our simulations and the real data as a first goal achieved.

In this chapter, the hydrocarbon spatial distribution in the area will be evaluated, while accumulation volumes and their phase (oil, gas or both) will not be considered in detail. In fact, it was not possible to extend the comparison also to this kind of information as it can not be disclosed.

Verification about the goodness of test results will be focused on the 5^{th} layer, the upper carriers which, in fact, are receiving not only the hydrocarbons coming from the Khatatba Fm, but also from shallower source rocks. These have not been inserted in the GeoModel used in Migri, and therefore a comparison between the results of SEMI and Migri on upper reservoir charging is biased and can not be done.

Before starting to analyze the simulation results, it seems useful to remind the previously described scenarios, in order to better focus the conditions under which the tests have been performed:

- *SCENARIO "A"*: definition of the formation tops is given by the well interpretation and the Vsh values are associated to the corresponding layer in the PSM GeoModel, even if they could be at different depths.

- *SCENARIO "B"*: formation tops are derived from the PSM GeoModel and their depths are used to re-compute the Vsh values, disregarding well formation tops interpretation.

- *SCENARIO "C"*: its formation tops are the same as in Scenario "A", but the Vsh distribution maps of some layers are constructed taking into account the sedimentological information contained in the available facies maps.

- *SCENARIO "D"*: it is not characterized by any Vsh distribution maps, but only lithologies are assigned to each layer. Vsh values and the other input parameters are defined using Migri defaults parameters assigned for each lithology.

8.1 LAYER_5, KHATATBA FM

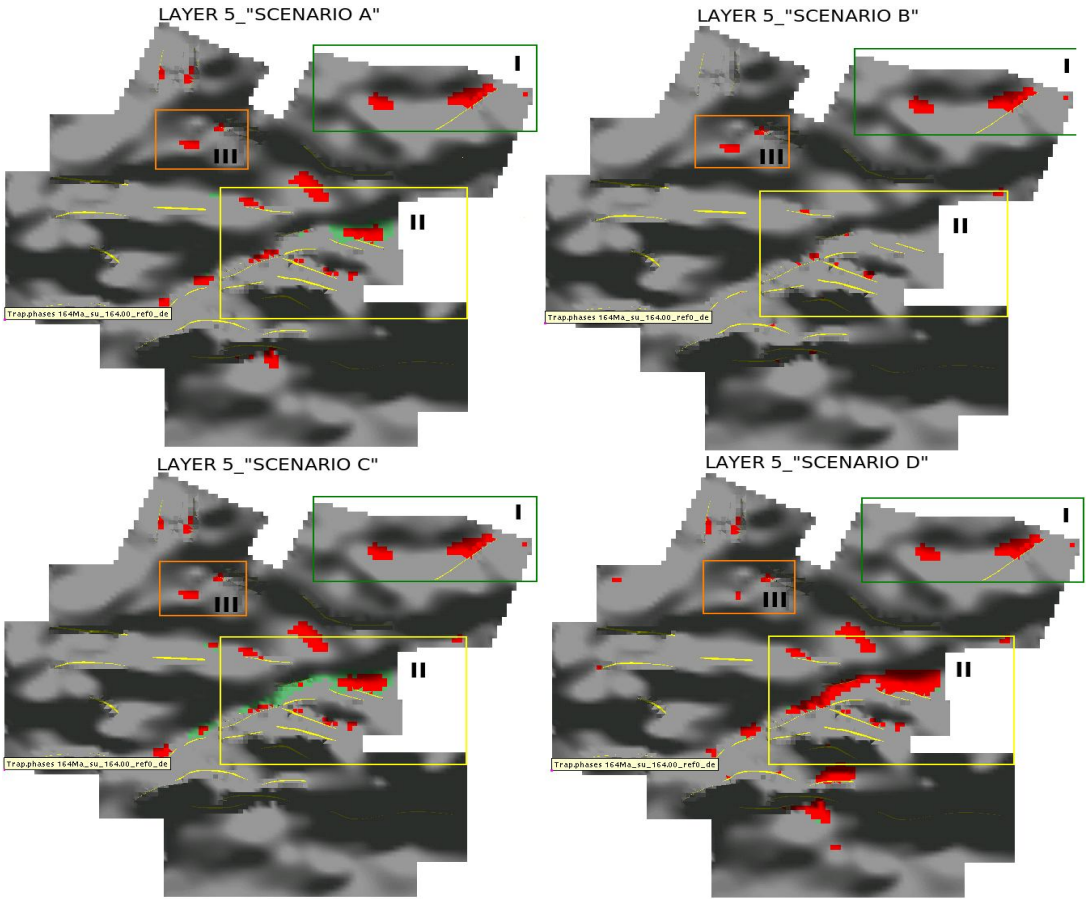

Fig. 8.1: *comparison between trap_phases maps of different scenarios referred to layer 5th*

8.1.1 ACCUMULATION "I" ZONE

The "trap_phases" map provides information about hydrocarbon phases distinguishing between oil (red) and gas (green).

In **Fig. 8.1** are presented the results for the 8th layer pools, resulting from the simulations for each of the above described scenarios.

As it is possible to note focusing on the "I" rectangle, in the North-East part of the study area, two big oil accumulations are present for each proposed scenario, also

with volumes more or less constant, as visible in the "trap_HC_column" maps (**Attachments 1 – 4 – 7 – 10**). Through the Migri 3D view it is possible to see which structures correspond to these accumulation (**Fig. 8.2**).

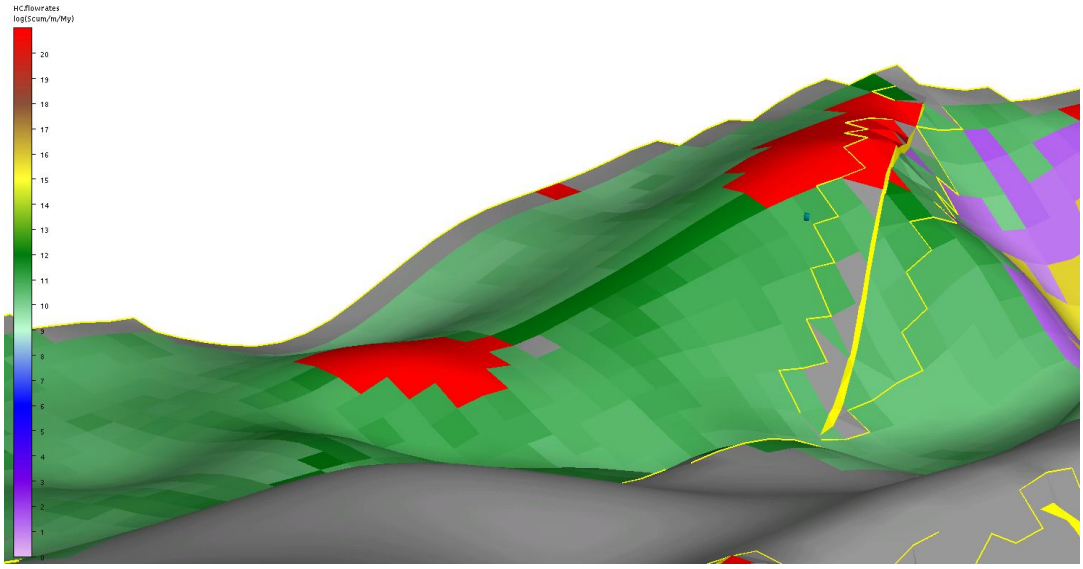

Fig. 8.2: *Migri 3D view showing which structure are related with the two hydrocarbon accumulation visible in all the scenarios, I zone.*

Observing the flow-path maps (**Attachments 1 – 4 – 7 – 10**), that show potential hydrocarbons movement direction, it is possible to see that these are more or less the same for each scenario. This correspondence is due to the more or less equal Vsh distribution in the zone. As it is possible to notice in the Vsh distribution maps, in fact, Vsh values are less than 1 for the scenarios "A", "B" and "C", while in "scenario D" this variable is constant equal to 0.25.

Because the Vsh parameter representsthe only difference among scenarios, that otherwise are described by identical properties, the equal accumulation distribution on this structures for all the scenarios is not a surprise.

Even if it was not possible to compare migration simulation output with the real filling situation measured in each well, however some observation about the trap filling of the two main Western Desert north-western structures were still possible.

For what concerns the easternmost accumulation, it is known that in the zone there are, or there were, productive wells extracting from the Khatatba Fm. The results of the migration simulation was found in agreement with the real situation, not referring to trapped hydrocarbons quantities. In fact, dimensions of these pools are probably too large to be realistic. On the contrary, pools present in the western part seem not to have a field confirmation. In this zone, in fact, only few exploration wells are present but, at the present day, they have not be productive.

This is in contradiction with the results of the migration simulations where some prospects were found. To better understand which was the reason for this inconsistency, it was decided to explore the possibility that it may exist a threshold Vsh value beyond which accumulations and flows are subjected to some critical changes. The threshold Vsh value should be greater than 0.25, that is the value that characterizes "Scenario D", as it produced similar results to the other three scenarios, marked by even smaller Vsh values.

Starting from this, new tests were performed with "Scenario D", progressively increasing the constant Vsh value, until some changes in the accumulations of the considered structures were observed (**Fig. 8.3**).

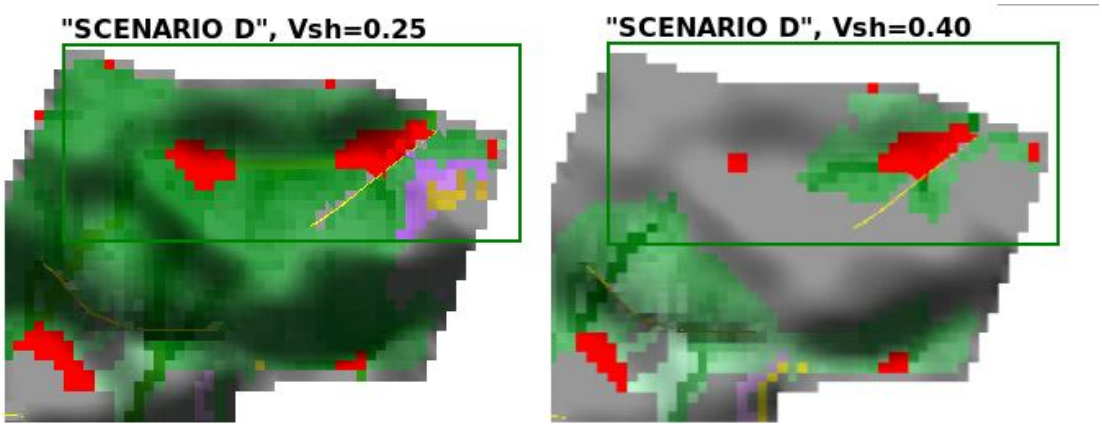

***Fig. 8.3**: flow-rate maps referred to rectangle "I" during increasing Vsh tests on "Scernario D". With red, gas accumulation are showed.*

As it is possible to notice from the pictures, a sudden change in flow and accumulation conditions is found comparing the same zone with Vsh values equal

to 0.25 and 0.40. During a third test, the simulation was performed at Vsh=0.30, without any differences respect to the Vsh=0.25 output. This suggests that the threshold Vsh value, over which the flow dynamic experiences critical changes, is between 0.30 and 0.40.

This is however only a synthetic analysis that shows that to explain the real data we are forced to introduce Vsh values far from measure ones from wells.

Trying to correctly interpret this kind of geological situation, marked by a great lithological heterogeneity, we have to refer back to Migri capability to use up to 7 possible components in the lithological description. These are: shale (Vsh), low-permeable carbonate (Vca), permeable carbonate (Vcp), organic matter (Vom), evaporites (Vev), igneous (Vig) and sand (Vss). The first six of these can be set as fractions for each layers, while sand constitute what is left after the other 6 percentage are defined. In many cases only Vsh or Vca will be used, and therefore the other parameters will be equal to 0.

In the case study, as described in the geological settings chapter, the upper part of Khatatba Fm is characterized, in its northern part (and therefore for the two considered prospect area) by significative carbonate percentages that alternate and mix with fluvial and deltaic sediments.

In conclusion, in order to explain real data we have to consider not only the Vsh value but also the carbonate volume fraction value (Vca) as both these parameters have a big importance in the secondary migration modeling, especially when in the GeoModel there are formations that are even partially carbonates.

In fact, in the previous described situations, three of the four scenarios are showing Vsh values much less than 1 in their North-West area. This would mean that they are very clean sandstones, characterized by excellent storage properties, if the actual carbonate percentage is not considered.

In Migri, all the lithological components that are not explicitly assigned by the user get a default value, for each of the 14 reference lithologies. Therefore, in the case of Layer 5, also the Vca is automatically assigned.

“Scenario D” will be the most sensible to default values assigned by Migri, because

in this case a Vsh map has not been loaded. However, a mixed lithology has been assigned, made by sandstone and limestone, such that resulting Vca was equal to 0.3.

As at the beginning of this study the main interest was focused on understanding the influence of Vsh on the migration processes, it was unfortunately not possible, for time reasons, to add an investigation about the percentage of carbonate respect to the terrigenous sediments.

The analysis of the results, however, clarified that the main factor that could have determined the discrepancy between migration simulation results and real data is the lack of the definition of Vca distribution. This was necessary as, the part of Western Desert enclosed by the "I" rectangle is characterized by an important carbonatic component. This lithological aspect influences the pore space and the permeability. In fact, if Vca is not considered, the resulting storage capacity is greater and the pool volume is overestimated, as the result of the migration simulations demonstrates.

As a first result of migration simulations, we may conclude that in model where there is an alternation between terrigenous and calcareous sediments, it is essential to define, besides the Vsh values, also the Vca distribution, loading both Vca and Vcp maps, so to improve the quality of the migration modeling.

8.1.2 ACCUMULATION “II” ZONE

In comparison with the previously described “I” zone, the “II” zone shows a filling situation more heterogeneous between different scenarios, even if also in this case Vsh distributions are quite similar and they have a value equal to about 0.3.

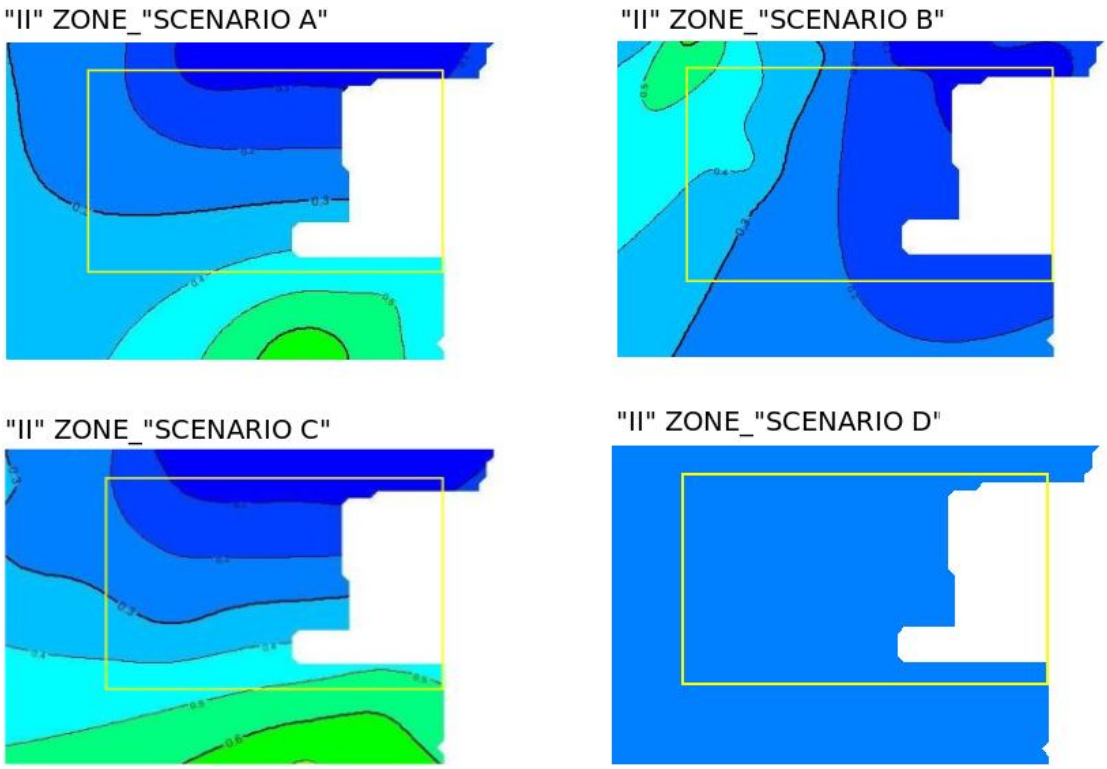

Fig. 8.4: *comparison between Vsh distribution map of different scenarios referred to “II” zone.*

Regardless to the different trends in the maps, the range of values is very similar, so to understand the differences among layers we need to look carefully at each scenario (**Fig. 8.4**).

The most voluminous hydrocarbon accumulations are found in correspondence of “scenario D”, characterized by a constant Vsh value of 0.25. Looking at the other images, it is possible to notice that the volume decreases progressively from “scenario C” to “scenario A”, and at least to “scenario B”. Pools visible in “scenario C” and “scenario A” are actually very similar, and they differ especially

for some gas accumulations resulting just in “scenario C”. This accumulation similitude can also be found in the Vsh distribution, very similar for both models, as it can be notice from the Vsh distribution differences map (**Fig. 8.5**).

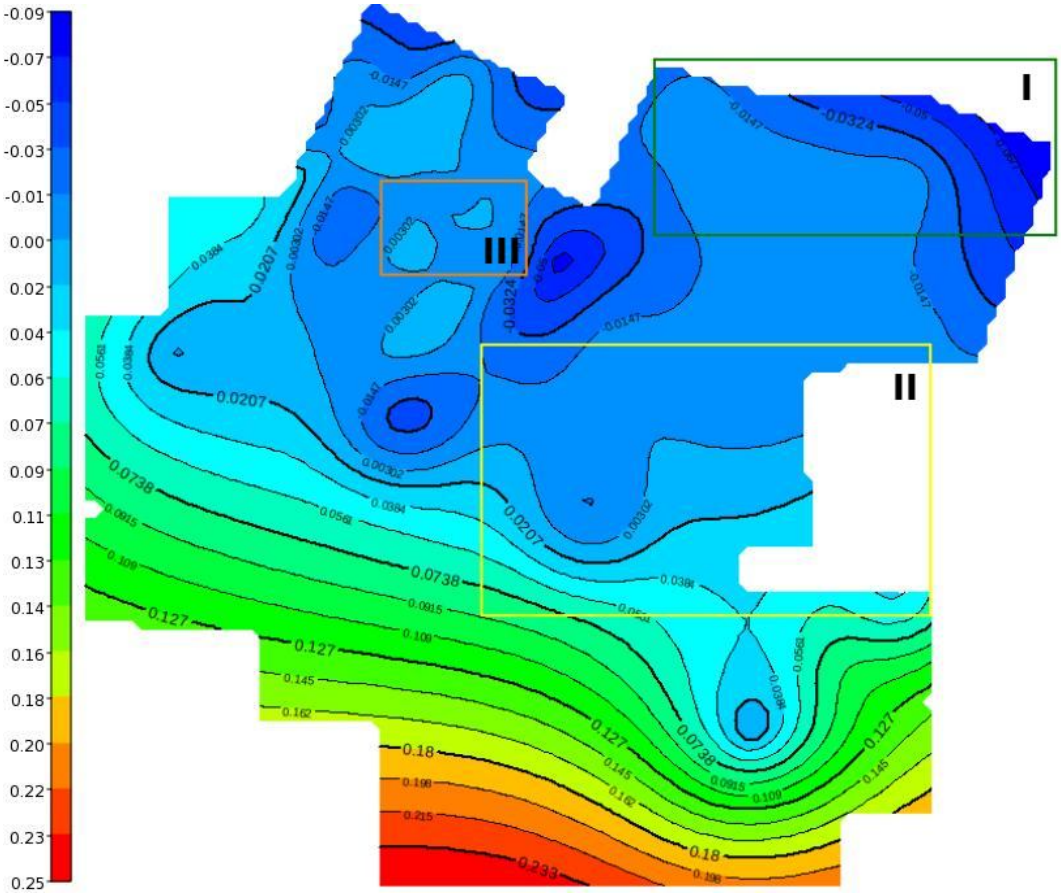

***Fig. 8.5**: Vsh distribution differences map between “scenario C” and “scenario A”*

On the other hand, when the Vsh differences start to become important, more discrepancies are visible, as showed by the pools distribution in “scenario D”, on which a smaller Vsh value (**Fig. 8.6)** led the formation of more extended pools into the rectangle “II” (**Fig. 8.1**).

The same behavior can be seen in the southern part of the maps, where some pools are present just in the Layer5 maps referred to “scenario D” and “scenario A”: on the other hand, smaller Vsh values in “scenario D” (0.25) allowed bigger pools formation, and just small in “scenario A”, where Vsh in greater.

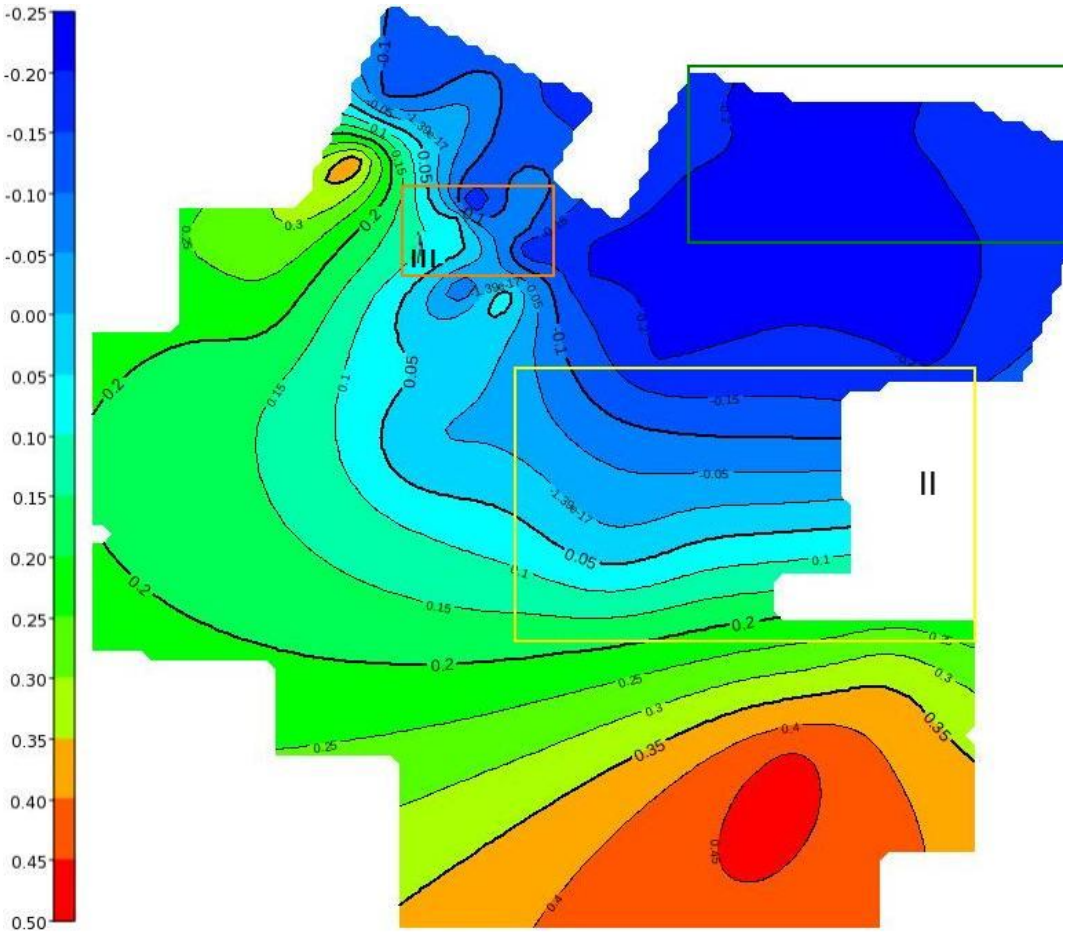

Fig. 8.6: *Vsh distribution differences map between "scenario C" and "scenario D"*

Comparing this last scenario with the similar "Scenario C", it's possible to notice how in the southernmost pools areas "scenario A" Vsh value is more or less 0.45, while in the other scenario it is about 0.65 (**Fig. 8.5**). Respect to the example referred to rectangle "I", in which a Vsh value of 0.4 does not allowed hydrocarbon accumulation, in the southernmost part of the "scenario A" map one pool is present even if the Vsh value is greater. The reason of this discrepancy could be the closeness of this accumulation to the near faults system. In fact, the consequence of an high Vsh value is to not allow the hydrocarbon flow, and stop them at the lowest layer, but in this case faults allow the flow to the 5th layer, and because Vsh values are not extremely high in "scenario A", the accumulation in this zone has been

possible. Conversely, in the situation described in “scenario C” an higher Vsh value doesn’t allow the storage.

This situation is also proved looking at the southern parts of flow-direction maps (**Fig. 8.7, Attachment 1 – 7**): in “Scenario C”, the high Vsh values, instead of allowing the accumulation (yellow color means horizontal movement) may generate a downward flow (blue colour), while in “Scenario A” an horizontal movement is allowed.

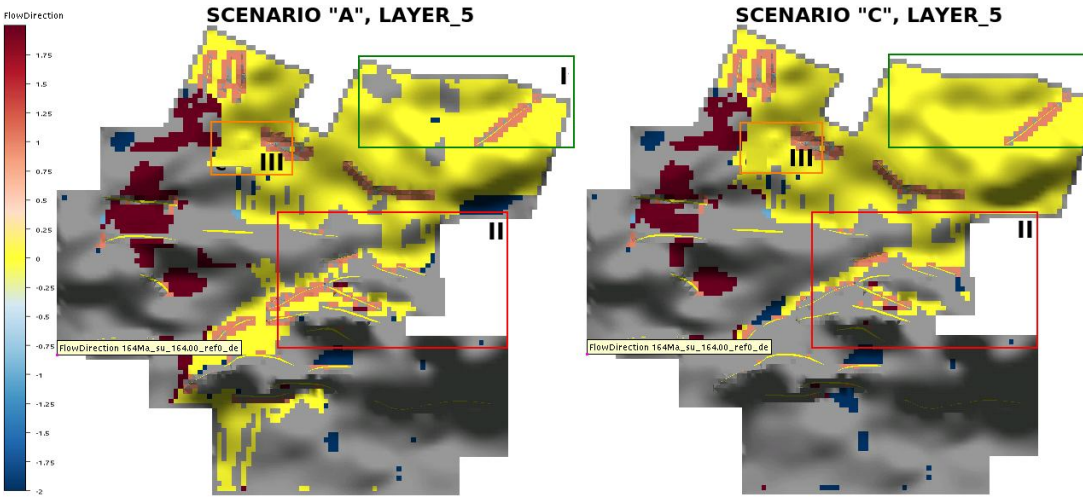

Fig. 8.7: *comparison between Flow-direction maps of “Scenario A” and “Scenario C” referred to Layer5*

A separate discussion has to be done to “Scenario B”; although the low Vsh value, the accumulation in this case has not been possible. This result is not due to some kind of software anomalies, but to the unrealistic Vsh starting data which characterized this scenario. Due to this reason, in fact, most of the hydrocarbons has not been able to reach Layer5, but stopped in the lowers.

8.1.3ACCUMULATION “III” ZONE:

As previously observed considering the “A” zone, also in the “C” zone a good homogeneity in pools distribution can be notice between different scenarios.

This zone corresponds to the “Meleiha group” fields, a really important production site, about which it is easier to have information about hydrocarbon presence, thanks to the several studies that have been made in order to define its structural conditions and petroleum potential.

Respect to the other two zones, “III” zone accumulations seem to be smaller and with a constant extension, but actually this kind of pool volumes is more realistic than the previous considered, as it is possible to understand from **Fig. 8.8**, in which the E-W total extension are reported both for the whole Western Desert and for the Meleiha group zone.

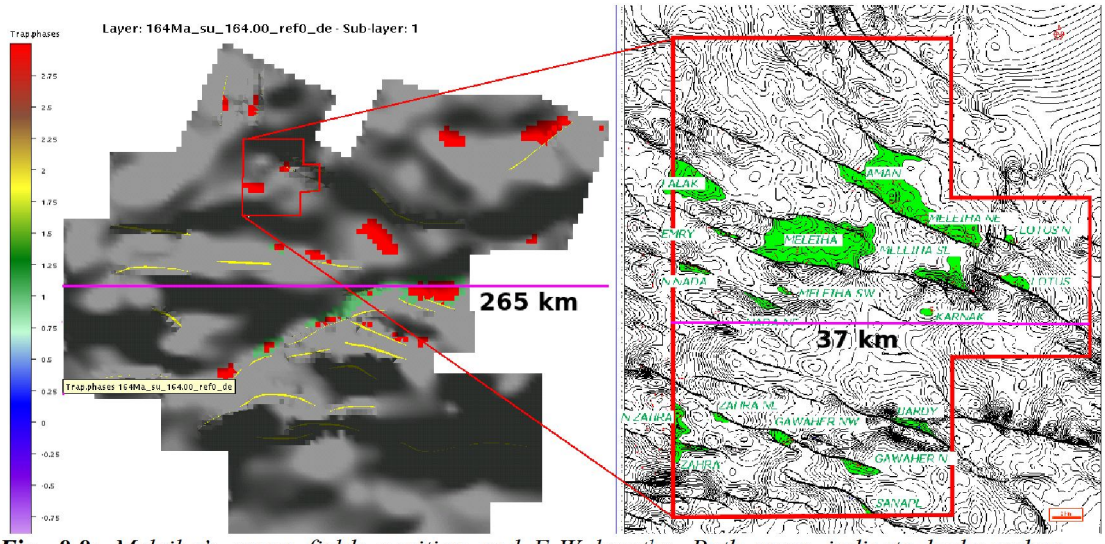

***Fig. 8.8**: Meleiha's group fields position and E-W lengths. Both maps indicate hydrocarbon accumulations.*

It is also evident how the few pixels resulting from Migri calculation in this area, overestimate the real accumulation areal extension (indicated with green colored zones), that indeed are distributed in smaller pools. Looking at the reported real distribution, resulting from a detailed study of this zone (Baiocco et al, 2010), it

seems to be clear that it is quite impossible to reproduce the same distribution in our model. In fact, the lack of minor structures in the regional map implies that all the hydrocarbons of this zone accumulate just into the two main structures, making a so irregular distribution impossible to reproduce.

For this reason, looking at the comparison between simulation results and real situation, it is possible to notice that the obtained accumulations approximate only roughly the real pools distribution, because they accumulate in two macro-structures (**Fig. 8.9**).

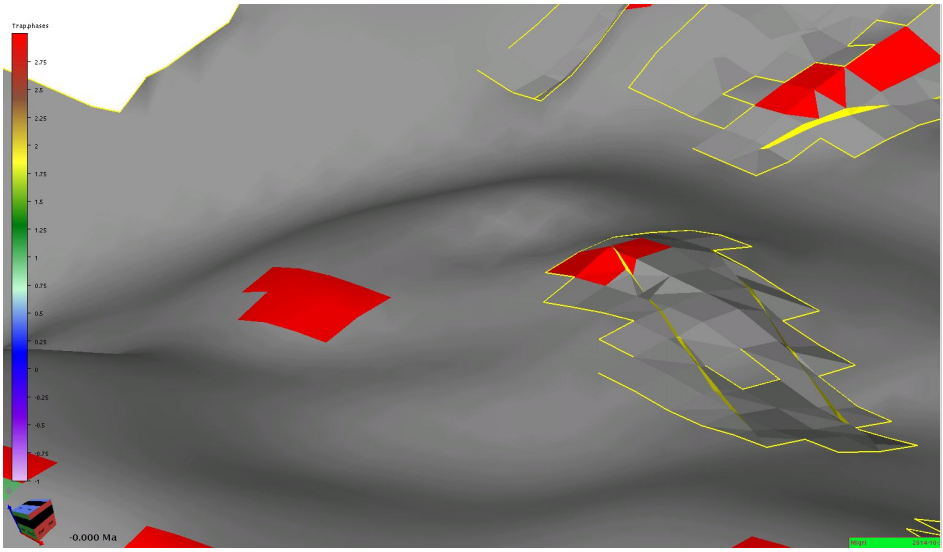

***Fig. 8.9**: "III" zone; pools 3D distribution referred to Layer 5.*

Trying to quantify the detail loss in the hydrocarbon distribution between the used maps and the real situation, a comparison between the 3D GeoModel used in this study and the detailed one used to observe the structure filling in Meleiha (Baiocco et al, 2010) has been done (**Fig. 8.10**).

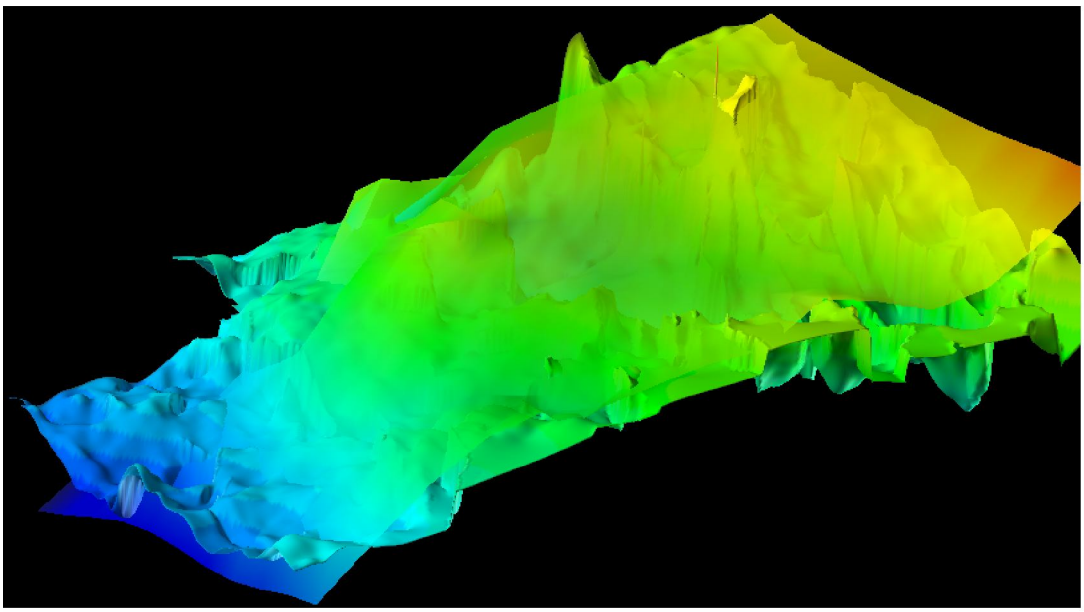

Fig. 8.10: *comparison between a detailed 3D Geomodel, used for a study about Meleiha, and a small portion of the smoother regional GeoModel used in this stud. Detail differences are clear.*

Looking at the differences between real and calculated distribution, and observing the detail gap between a regional map and a smaller one, it is possible to confirm the impossibility to reach accurate results without an adequate detail in the GeoModel. In fact, the mesh step of the regional used model is 4000 m, while in the reported detailed map is 250 m.

On the other hand, it seem necessary to remember that this is a study about secondary migration referred to a regional scale, and so it was never pretended to reach the same detail of the real hydrocarbon distribution. Moreover, with the current technologies it is not yet possible to work on a so detailed mesh for the entire extension of a work like this, because of huge amount of data processing that would become the file so heavy and unusable.

As regards with the relationships between layer5 Vsh distributions and hydrocarbon accumulation, in this case is not possible to have many information; resulting accumulation are very similar and they reflect a Vsh distribution almost equal between the scenarios, all characterized by low values in this zone.

8.2 LAYER_7, ALAM EL BUEIB FM

As previously said, it is impossible to compare simulation results referred to layers 7th and 8th with the reality, because in the Western Desert petroleum system just in correspondence of layer 7th other source rocks are present, but they have not been considered in the GeoModel. For this reason, to figure out what is the hydrocarbons contributions from the Jurassic source rocks accumulated in these layers would be an extremely complex operation. According to some studies carried out on the contribution of the different source rocks in the reservoirs, Jurassic ones resulted to be the most productive in the area, and they provide most of the oil and gas even in the shallower layers (De Poli et al., 2009). The first important result achieved could therefore be considered the correspondence between the layers charged from the deepest source rocks in the simulation and in reality (5th, 7th and 8th).

Considering the differences in the various scenarios accumulations, “B” and “D” seems to be unrealistic, because of their extremely large pools.

Some considerations could instead be done about “A” and “C” scenarios (**Fig. 8.11**).

As already explained in chapter 6th, it was not possible to construct a new “scenario C” Vsh distribution map referred to layer 7th and based on facies distribution, because the available facies map referred to this layer is divided in many sub-units, with characteristics also very different. These sub-layers reflect the different sedimentation phases that interested the Alam el Bueib Fm during the time, but unfortunately it was not possible to divide that layer on Migri, because of temporal and data acquisition reasons.

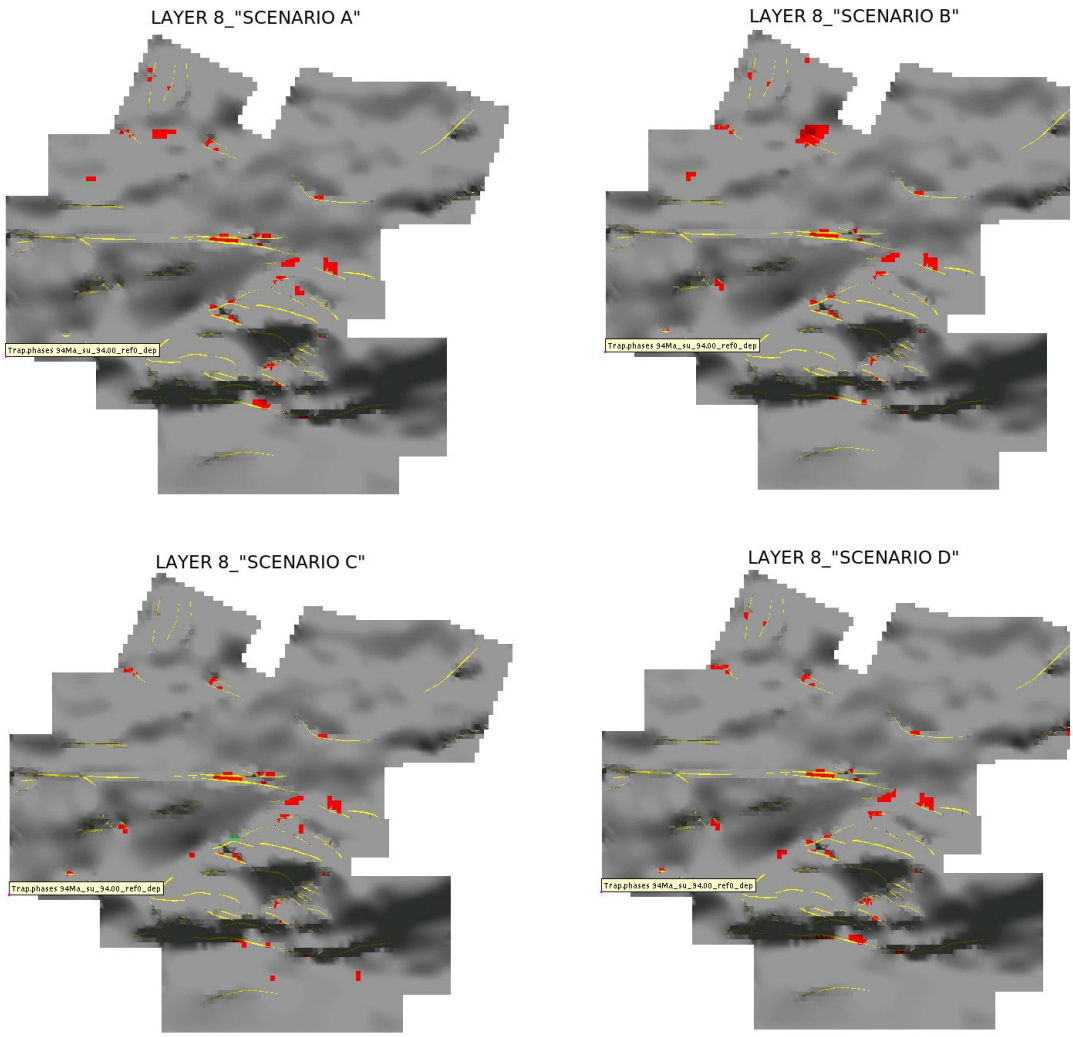

***Fig. 8.11**: comparison between trap_phases maps of different scenarios referred to layer 7th*

Moreover, because of the extreme Vsh variability of the different sublayers, it was not possible to approximate this lithological properties in a single map, and, accordingly, Vsh distribution map of layer 7th referred to "Scenario A" and "Scenario C" are equal. For this reason, accumulation differences visible in this layer derive only from hydrocarbon flow that has interested the deeper layers.

The first thing that can be notice on the trap_phases maps is the southern accumulation which is present in "scenario C" and absent in "scenario A". This situation seems to be opposite to the layer 5 pools distribution, in which an accumulation was present in the same area, but it interested "scenario A".

The absence of the southern accumulation on the layer 5th in “scenario C” implies that there would be more available hydrocarbon in the upper layers, but in volumetric terms this reason does not justify the so bigger accumulations characterizing “scenario C”, especially in the central part of the map.

A possible explanation about this behavior could be that layer 8th referred to “scenario C”, that is the Bahariya Fm, would be characterized by an average Vsh value greater than the same layer in “scenario A”, and this could act as a seal and allowed the greater charging of this layer. Actually, just looking Layer 8th accumulation in “scenario C”, it is possible to understand that even in this case the pool volumes are greater for the “scenario C” with respect to “scenario A”, as visible in their trap_HC_column maps (**Attachment 3 - 9**) and so the greater Vsh value characterizing the upper layer does not influenced the pools creation capacity in “scenario C”.

In order to evaluate the discrepancy between the pool volumes affecting scenarios “A” and “C” it was necessary to consider the accumulations into the Jurassic source rocks levels. By definition, in fact, it is normal that the source rocks are characterized by a greater Vsh values, and due to this reason not all the expelled hydrocarbons are subjected to secondary migration flow, which will be in part retained within the layers. It was therefore necessary to check if the evident lesser amount in the Layer 7th “A” scenario is due to this first migration phase and if the lowest layer would have trapped a greater percentage of fluids (**Fig. 8.12**).

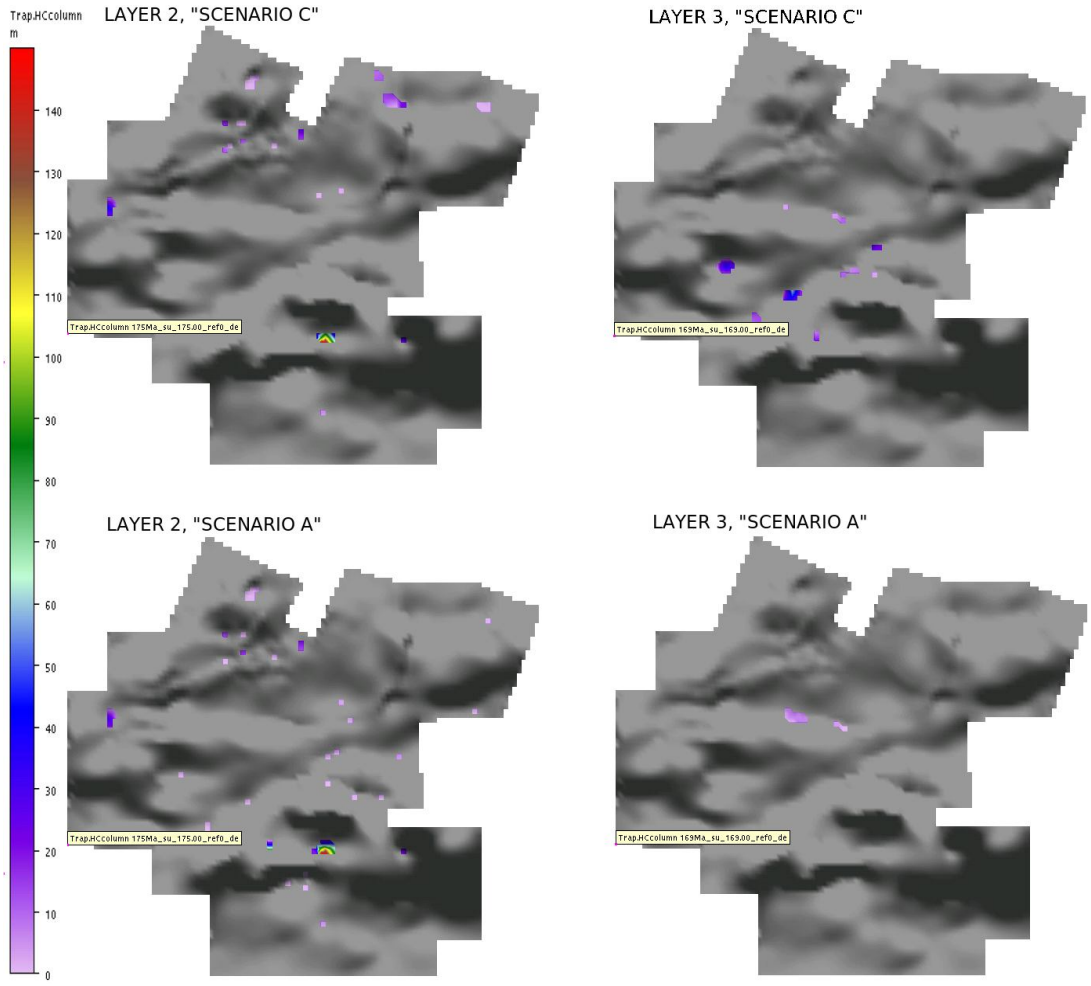

***Fig. 8.12**: Trap_HC_column comparison between the different scenarios*

As it seems evident from Fig. 8.12, which indicates the hydrocarbons column heights corresponding to the lowest source rock level, the hypothesis that the hydrocarbons deficit affecting “scenario A” respect to “scenario C” would be due to the first migration phase has not been confirmed. On the contrary,, it is evident how even in this lower layers the pools volume is greater in “scenario C”.

At this point, the fact that during the tests the hydrocarbon volumes have not been maintained constant seems to be clear. Once it was verified that the expelled hydrocarbon volumes has been constant for all the layers, as visible thanks to the “oil_expulsion” maps available in all the attachment, the only explanation about

this behavior is that a lateral flow outside the map has been allowed during the simulations.

Effectively, through a more accurate observation about the input parameter inserted on Migri, it was verified that the simulation has been defined to allow the flow leakage, if the GeoModel condition would pretend it.

For this reason, new tests, with the borders as barriers, were performed, and their results showed a greater amount of hydrocarbons accumulated on every layer, even if they generated unrealistic situation, as huge pools aligned close to the borders.

In conclusion, it is possible to say that the assumption used by the software to allows the fluids leakage is realistic, but the calculation of the amount of lost fluids has not been possible. Nevertheless, in a new version of Migri, a new tool can be used to quantify the losses, but because it has been released at the end of this study, this information could not be known.

8.3 LAYER_8, BAHARIYA FM

Progressive decreasing of fluids amount going through many layers until the 8th, beyond which no more hydrocarbon is accumulated, neither into the GeoModel nor in reality, makes the pools of this layer much smaller than the lower ones for all the scenarios.

From **Fig. 8.13** it is possible to observe that accumulations distribution, even if it is different from one scenario to another, seems to be characterized by small pools extended to the whole area, and the differences between the various scenarios are constituted just by small accumulations.

Looking at where their distribution, it is evident that they are most of all close to the faults, unlike the previous examples, in which accumulation were found even far from faults.

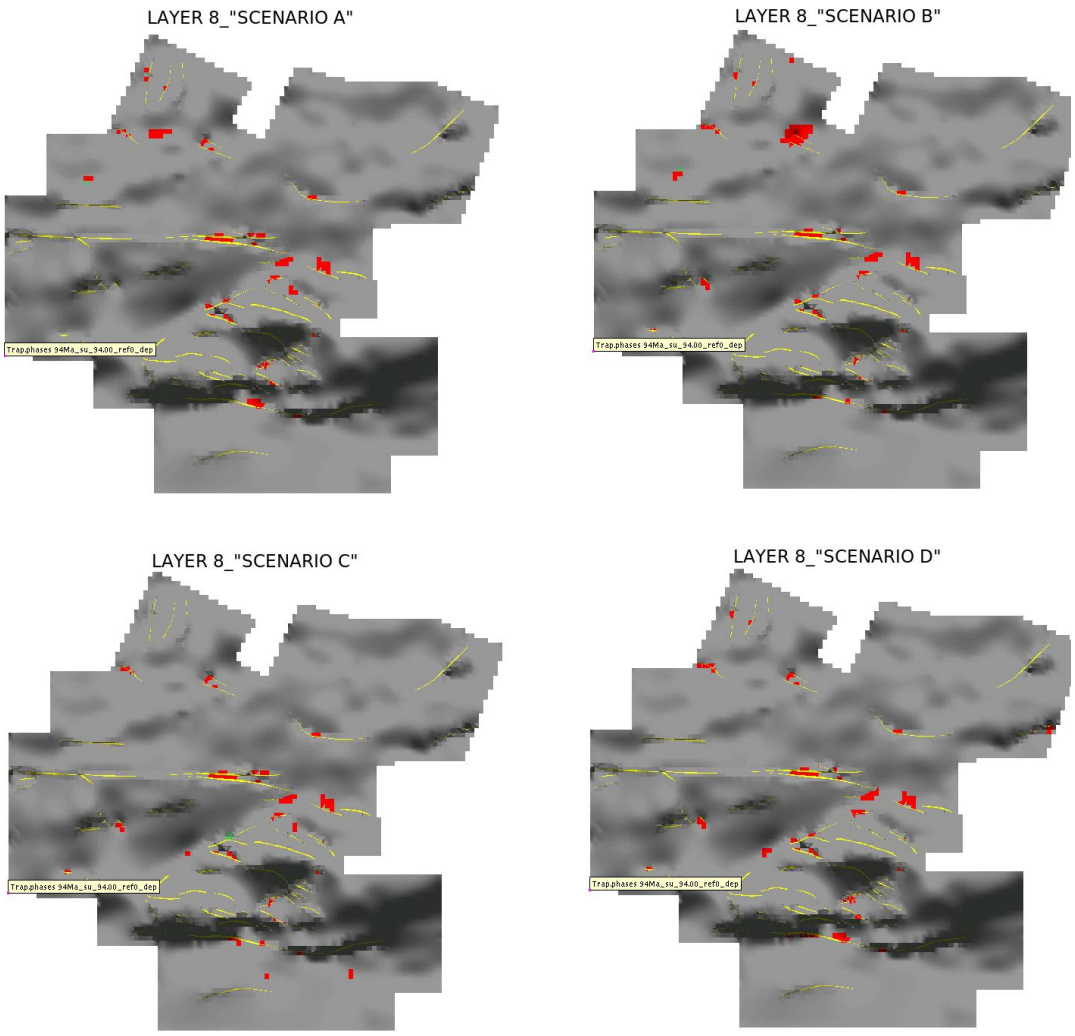

***Fig. 8.13**: comparison between trap_phases maps of different scenarios referred to layer 7th*

From this observation, it is possible to do some considerations about flow dynamic calculated by the software. In fact, it seems that decreasing the fluid percentage into the 3D GeoModel, going from lower to higher layers, Vsh influence as a flow driver loses its importance, and the only flow driver seems to become movement across faults. One of the reasons could be that decreasing the available hydrocarbons, a decrease of structure filling occurred and then spill-out movements do not experience. This fact could reduce horizontal movements into a layer, and so also in areas far from the faults.

9. CONCLUSIONS AND FUTURE DEVELOMPENTS

From the observation of the migration modelling results, some important information about the behaviour of the software Migri has been derived.

The first conclusion is that the use of Vsh distribution maps allowed to obtain a greater detail in the accumulations distributions, as it is clear comparing “Scenario D” pools, that appears too large to be considered realistic, with a more detailed distribution resulting from “Scenario A” and “Scenario C” tests.

With regard to the information about the influence of Vsh parameters on the flow dynamic within the model, the most important observation has been the definition of a Vsh threshold value between 0.3 and 0.4, beyond which hydrocarbon flow and accumulation seems to be prevented.

During the same test, however, it has been observed that this threshold value has the effect of a lithological barrier. In fact, a fault system may become the main flow path for hydrocarbons, nullifying the Vsh effect on the secondary migration flow, and allowing the formation of pools in correspondence of Vsh values even higher than 0.4.

It is therefore possible to affirm that these tests have been useful to clarify that in hydrocarbon migration modelling, like in Migri, it is difficult to forecast which will be the final effects of a given Vsh distribution. In fact, hydrocarbon paths are modified by a number of variables that all contribute to the final result. For this reason, in thise final chapter we will suggest which could be the most critical elements that may improve the migration modelling results and help to better understand the behaviour of Migri software.

- **STARTING GEOMODEL ADJUSTMENT RESPECT TO THE WELL TOPS:**

In chapter 3 the discrepancies, sometimes important, between depths of formations top measured from log data and those derived from the Migri GeoModel were described. In order to manage these differences, two scenarios, named “A” and “B”, were introduced to compare the two main options that may help in solving this issue.

In the case of Scenario “A” the assumption is to maintain the coherence of the lithological definition, accepting a discrepancy between well logs true depths and GeoModel depths. This assumption however will not guarantee that in general we will maintain the same layer thickness (between well data and the GeoModel), with a bad influence on the simulation accuracy.

In the case of Scenario “B” the assumption is to maintain the coherence between the GeoModel depths and the wells cuts, recalculating Vsh values. This assumption may contradict the expected lithological behaviour for the migration flow, with erroneous results.

In conclusion, the first improvement is the consistency between the starting model depths and formation tops calculated in the wells, improving the coherence between GeoModel geometries and the properties associated to them.

- **Vca CHARACTERIZATION:**

As it was seen in chapter 7, the assumption of a representative lithology for each layer implies the assumption of given default values from Migri. The most important of these are the Vsh, Vca (the decimal fraction of impermeable limestones volume) and Vcp (permeable limestones).

Even if this study was focused only on Vsh definition in the GeoModel, the tests clarify that it is not possible to define the lithological layer properties just with that

value. In fact, as previously mentioned, Migri defines the lithology as a sum of components: shaly, calcareous and sandy, where the sum must be equal to one. For this reason, it would be necessary to create not only a Vsh map, as described in this thesis, but at least a similar map of Vca, in order to have a complete lithological characterization of the layers. In fact, the third map for the sandy component can be obtained from the constrain that the three maps have to sum to one in each node. This improvement may allow to refine the flow simulation also in layers with a limestone component.

- **FAULTS PERMEABILITY REFINEMENT:**

In the GeoModel used for the tests, faults has been considered as open conduits, able to transfer fluids from the lower layers to the upper ones with no resistance. This approach has been assumed because it was one of the conditions to allow the comparison with SEMI results.
This simplification has certainly overestimated the permeability from one layer to the upper, and it is clear that more accurate fault permeability values should have being assigned, at least for the more important fault systems. For this purpose, however, it would be necessary to carry out a study about fault properties of the model.

- **SUB-LAYERING:**

Some of the formations that constitute the GeoModel were characterized by a great vertical heterogeneity, and, due to this reason, it was not correct to assign a single Vsh value for the whole layer thickness. On the other hand, a modification of the layers structure of the GeoModel would be a really complex operation, and it would need a huge amount of data and time, which unfortunately was not available.

In order to construct a more detailed model, and to have more accurate results, it seems clear that a further subdivision of these layers would be necessary, in particular for Layer 7, that is strongly heterogeneous and for which some information about possible sublayers is available in bibliography.
Moreover, in order to obtain a better lithological characterization, it would be useful if a sublayering could be introduced for any thicker and laterally continuous shale level visible in the gamma ray log.

- **GRID RESOLUTION:**

As said looking at the Layer 5 results, another parameter that influences the simulation accuracy is the grid resolution. In fact, comparing results coming from Migri with the more detailed maps used in a previous basin study (described in Chapter 8), it is clear that an accurate pools distribution cannot be obtained until the map used in the modelling are describing only the larger structures, not considering also the minor structures that may have effect on the migration paths.
On the other hand, remembering that this is a regional study, we may accept some imprecisions in the results as it would never be possible to conduct this kind of work with a refined mesh grid, because it would became too heavy in terms of computational times.
However, this observation aimed only to point out that any possible improvement in the grid resolution, like for example introducing a parallel computation in the migration, would result in a better quality of the results, and it would have allowed us to consider also the effects coming from the filling of the smaller structures.

REFERENCES:

- Adeoti L., Ayolabi E.A., James P.L. (2009) – *An Integrated Approach to Volume af Shale Analysis: Niger Delta Example, Orire Field*. World Applied Sciences Journal, Vol. 7 (4), pp. 448-452
- Ahmed M.A. (2008) – *Geodynamic evolution and petroleum system of Abu Gharadig Basin, North Western Desert, Egypt*. PhD Thesis Applied Geophysics, Rwth Aaten University, pp. 239.
- Albritton C.C., Brooks J.E., Issawi B., Swedan A. (1990) – *Origin of the Qattara Depression, Egypt*. Geological Society of America Bulletin, Vol. 102, pp 952-960.
- Asquith G., Gibson C. (1984) – *Basic Well Log Analysis for Geologists.* The American Association of Petroleum Geologists. 216 pp.
- Baiocco T., De Poli A., Elias R. (2010): *Petroleum System Modeling for Meleiha Development Lease; Egypt, Western Desert.* Eni E&P, GEOL-GEBA Internal Report.
- Balestra M. (2013) – *Studio regionale comparato della storia termica in Egitto.* Master thesis, Università La Sapienza Roma, pp. 129.
- Baruffini L., Trincianti E. (2012) - *Egypt, Western desert: Regional Stratigraphic and Sedimentological Study of the Jurassic and Early Cretaceous Series for Residual Prospectivity Assessment*. Eni E&P, SGEG-SPES, Internal Report, pp. 77.
- Bassiouni Z. (1994) – Theory, Measurement and Interpretation of Well Logs. Society of Petroleum Engineers, 372 pp.
- Bayoumi T. (1996) – *The influence of interaction of depositional environment and synsedimentary tectonics on the development of some Late Cretaceous source rocks, Abu Gharadig basin, Western Desert, Egypt.* Vol. 2, pp. 475-496.

- Bevan T.G., Moustafa A.R. (2012) - *Inverted rift basin northern Egypt. Regional Geology and Tectonics: Phanerozoic Rift Systems and Sedimentary Basins.* Bosward, pp. 482-507.
- Bumby A.J. & Guiraud R. (2005) - *The geodynamic setting of the Phanerozoic basins of Africa.* Journal of African Earth Sciences, Vol. 43, pp. 1–12.
- Carminati E., Cuffaro M., Doglioni C. (2012) - *Western Desert, Egypt: geodynamics & basin analysis.* Eni E&P, Internal Report, pp. 132.
- Clark I. (2001) – *Practical Geostatistics,* Geostokos limited, pp. 119.
- De Poli A., Elias R., Baiocco T. (2009): *Egypt, Western Desert: Regional Geochemical and 3D PSM Studies.* Eni E&P, GEOL/GEBA Internal report, pp. 147.
- Deaf A.S. (2009) – *Palynology, palynofacies and hydrocarbon potential of the Cretaceous rocks of northern Egypt.* PhD Thesis, University of Southampton, pp. 348.
- Doering S., Dalla Rosa M., Ruffo P. (2014): Global PSM - *Residual Exploration Potential in Mature Basins. Western Desert case of study.* Eni, SGEG-GEBA Internal Report.
- El-Sadek M.A., Ammar A.A., Omraan M.A., Abu Elkheir H.M (2007) – *Exploration for hydrocarbon prospects using aerial spectral radiometric survey data in Egypt.* Kuwait Journal of Science, Vol. 34 (2A), pp. 133-160.
- El Sisi Z., Hassouba M., Oldani M.J. Dolson J.C. (2002) - *The Geology of Bahariya Oasis in the Western Desert of Egypt and its Archeological Heritage*. Field Trip No. 8, Cairo 2002 International Conference and Exhibition.
- Gadallah M.M., Samir A., Nabih M.A. (2010) - *Integrated Reservoir Characterization Studies of Bahariya Formation in the Meleiha-NE Oil Field, North Western Desert, Egypt.* Journal of King Abdulaziz University: Earth Sciences. Vol. 21, n.1, pp. 111-136.

- Gindy A.R., El Askary M.A. (1969) - *Stratigraphy, Structure, and Origin of Siwa Depression, Western Desert of Egypt*. The American Association of Petroleum Geologists Bulletin Vol. 53, No. 3, pp. 603-625.
- Gindy A.R. (1991) – *Origin of the Qattara Depression, Egypt: Discussion and reply*. Geological Society of America Bulletin, Vol. 103, pp 1374-1376.
- Guiraud R. (1998) - *Mesozoic rifting and basin inversion along the northern African Tethyan margin*. The Geological Society, London. Special Publication Vol. 132, pp. 217–229.
- Gluyas J., and Swarbrick R. (2004) – *Petroleum Geoscience. Blackwell Publishing, 2004.* Blackwell publishing, pp. 347.
- Guiraud R., Bosworth W. (1999) - *Phanerozoic geodynamic evolution of northeastern Africa and the northwestern Arabian platform*. Tectonophysics Vol. 315, pp. 73–108.
- Guiraud R., Issawi B., Bosworth W. (2001) - *Phanerozoic history of Egypt and surrounding areas*. Memoires du Museum national d'histoire naturelle, Vol. 186, pp. 469-509.
- Guiraud R., Bosworth W., Thierry J., Delplanque A. (2005) – *Phanerozoic geological evolution of Northern and Central Africa: an overview.* Journal of African Earth Sciences, Vol. 43, 83-143.
- Hammada G.M (1996) – An Integrated Approach To Determine Shale Volume and Hydrocarbon Potential in Shaly Sand.
- Harms, J.C., and Wray, L.J. (1990) – *Nile Delta.* In Said, R. (Ed.), Geology of Egypt (329-344), Balkema, Rotterdam.
- Lüning S., Craig J., Loydell D.K., Štorch P., Fitches B. (2000) – *Lower Silurian "hot shales" in North Africa and Arabia: regional distribution and depositional model*. Earth-Science Reviews, vol. 49, pp. 121-200.
- Mohamed S. Abu El Ghar (2012) – *Sequence stratigraphy and cyclicity in the Middle Eocene of Fayoum ranges, Western Desert, Egypt: Implication for regional sea level changes*. Marine and Petroleum Geology, Vol. 29, pp.

276-292.

- Neftex (2013) – *Chronostratigraphic Chart, North Africa*. Eni E&P Internal Report.
- Øyvind S., Are T. (2013): *A novel adaptive gridding approach to hydrocarbon migration.* Migris A.S., Poster.
- Paleoservice (1986) – *The hydrocarbon potential of the Paleozoic rocks of the Western Desert, Egypt.*
- Said R. (1962) - *The Geology of Egypt.* Elsevier, 377 pp.
- Said R. (1990) - *The Geology of Egypt.* Balkema, Rotterdam, 729 pp.
- Saputra I. (2008) – *Shale Volume Calculation*. HRS Jakarta, March 2008
- Sestini, G. (1995) - *Egypt. Regional petroleum geology of the world, part II: Africa, America, Australia and Antarctica.* Vol. 22, pp. 66-87.
- Stampfli G.M., Borel G.D. (2002) - *A plate tectonic model for the Paleozoic and Mesozoic constrained by dynamic plate boundaries and restored synthetic oceanic isochrons. Earth and Planetary Science Letters, 196, 17-33.*
- Tantawy A.A., Keller G., Adatte T., Stinnesbeck W., Kassab A., Schulte P. (2001) – *Maastrichtian to Paleocene depositional environment of the Dakhla Formation, Western Desert, Egypt: sedimentology, mineralogy, and integrated micro- and macrofossil biostratigraphies.* Cretaceous Research, vol. 22, pp. 795-827.
- Younes M.A. (2012) – *Hydrocarbon Potentials in the Northern Western Desert of Egypt.* In Younes M.A. (Ed.), Crude Oil Exploration in the World, InTech.
- Zaher M.A., Senosy M.M., Youssef M.M., Ehara S. (2009) – *Tickness variation of the sedimentary cover in the South Western Desert of Egypt as deduced from Bruguer gravity and drill-hole data using neural network method.* Earth Planets Space, vol.61, pp. 659-674.

ATTACHMENT 1

SCENARIO “A”
LAYER 5_Khatatba1 (164 My)

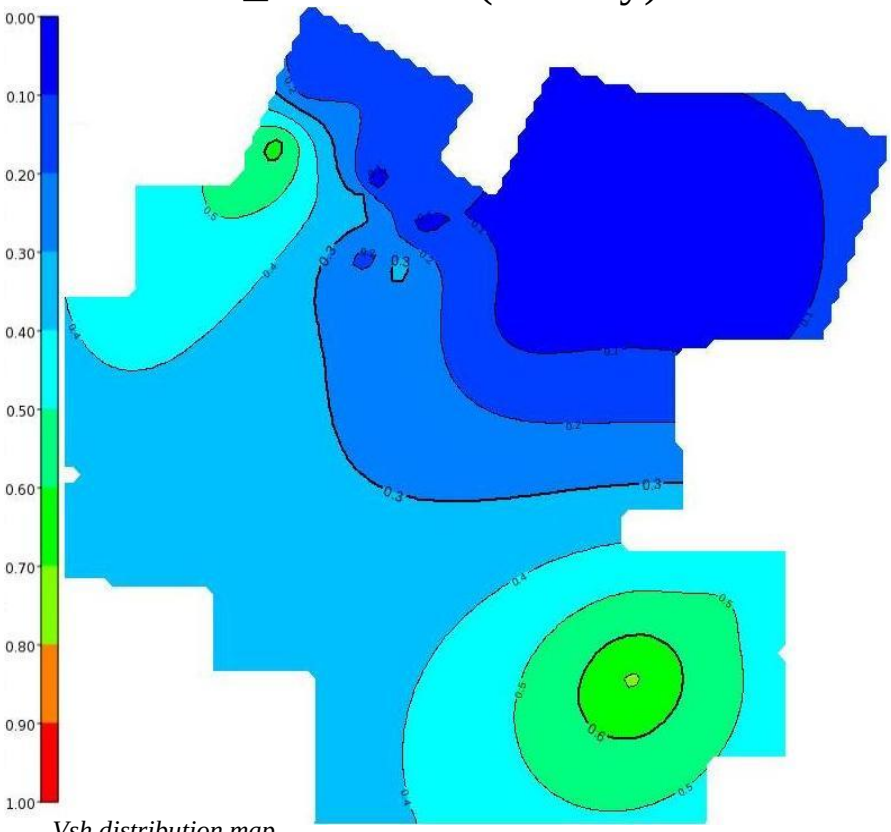

Vsh distribution map

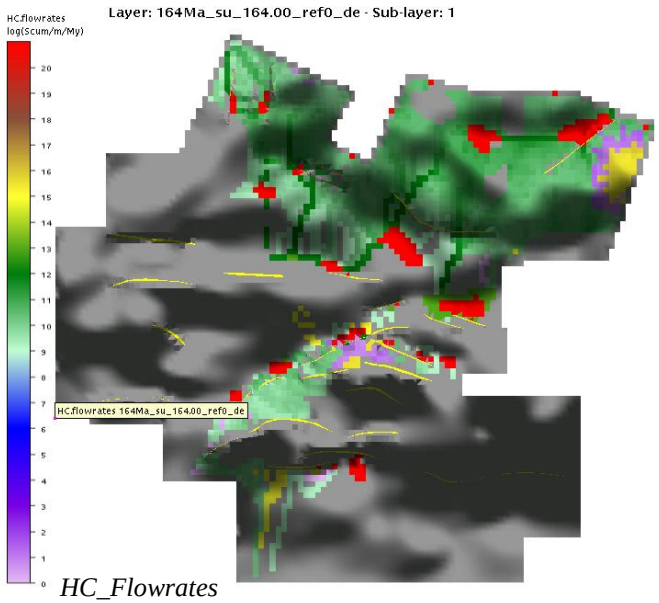

HC_Flowrates

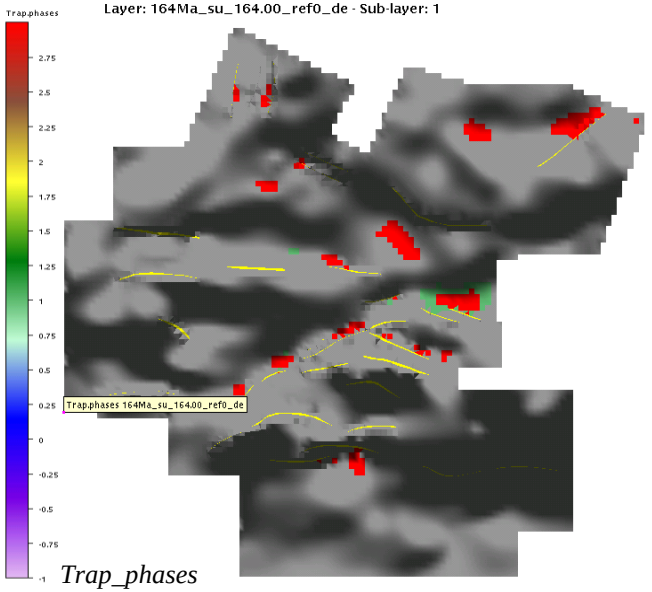

Trap_phases

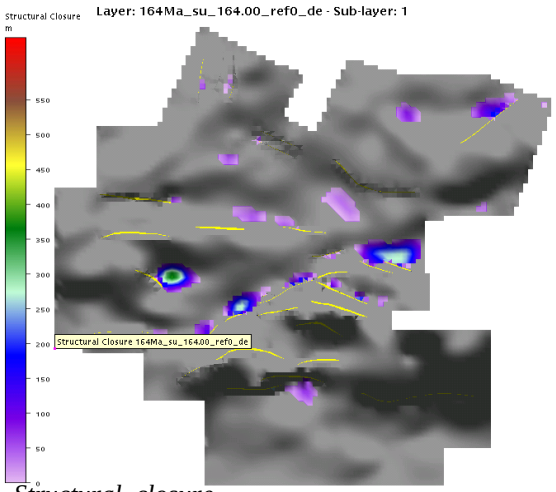

Structural_closure

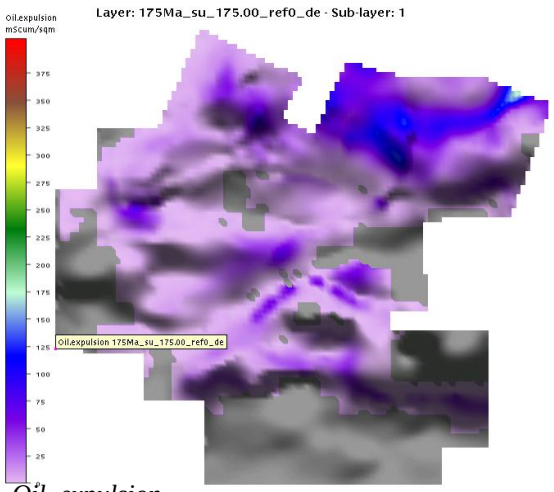

Oil_expulsion

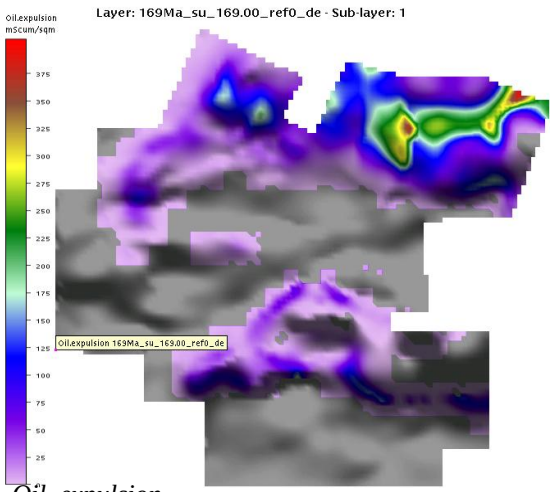

Oil_expulsion

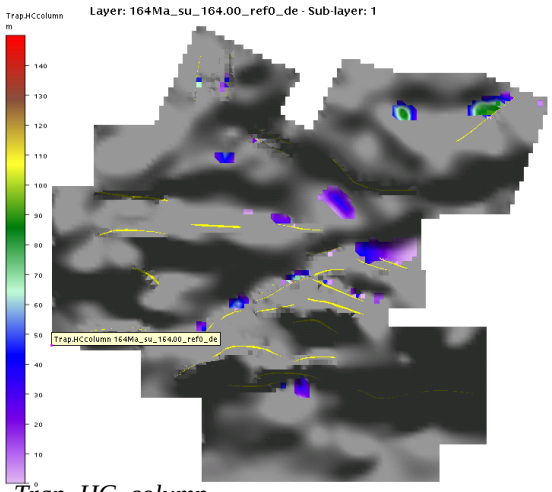

Trap_HC_column

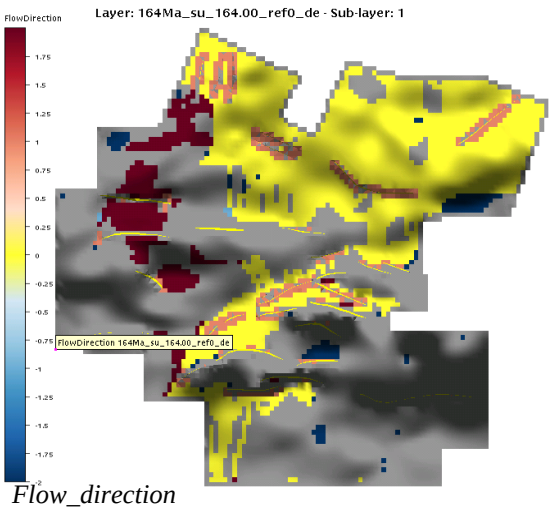

Flow_direction

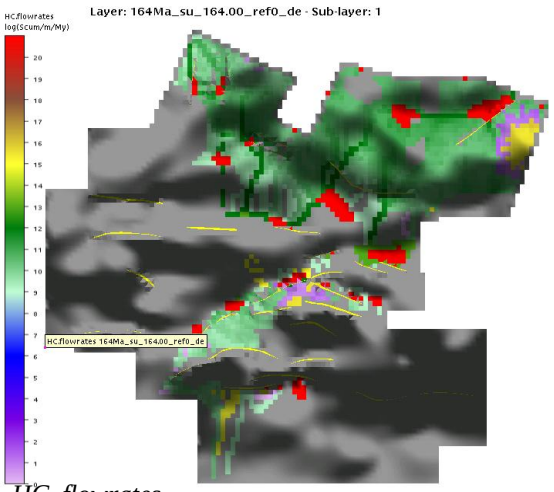

HC_flowrates

ATTACHMENT 2

SCENARIO “A”
LAYER 7_Alam el Bueib (120 My)

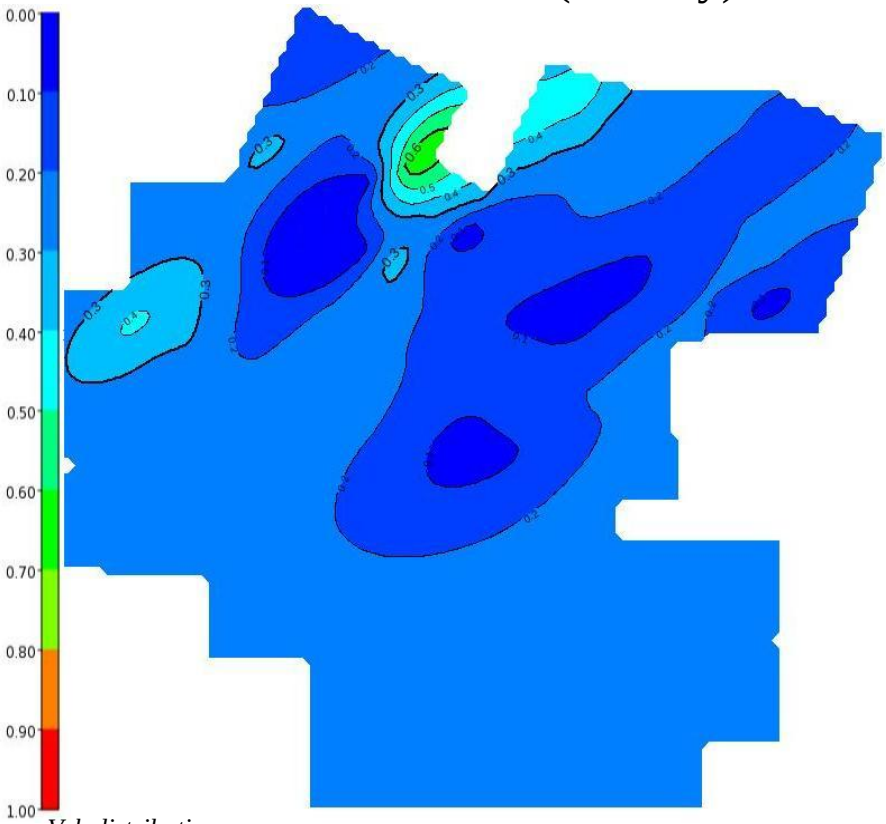

Vsh distribution map

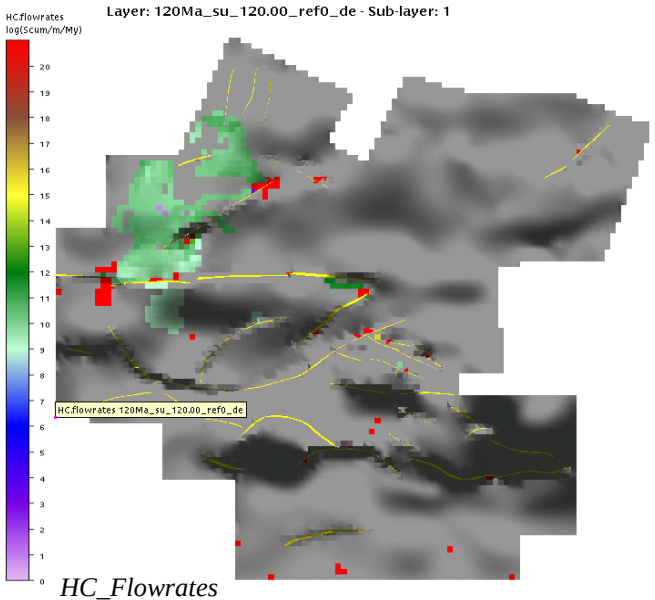

HC_Flowrates

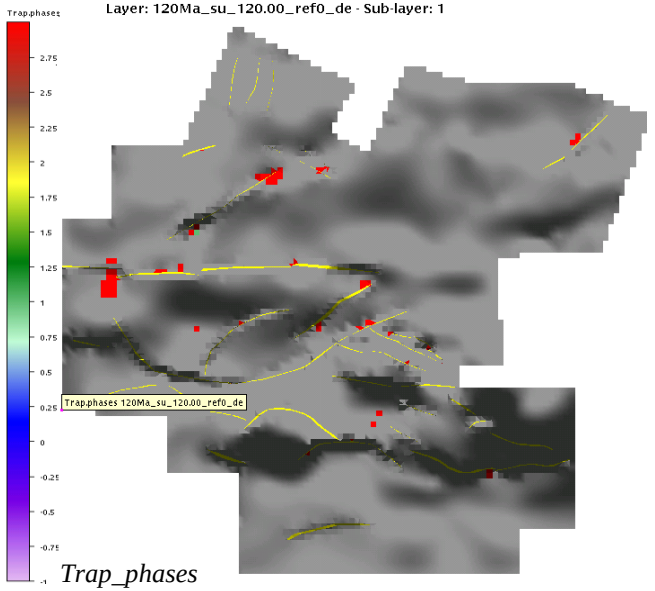

Trap_phases

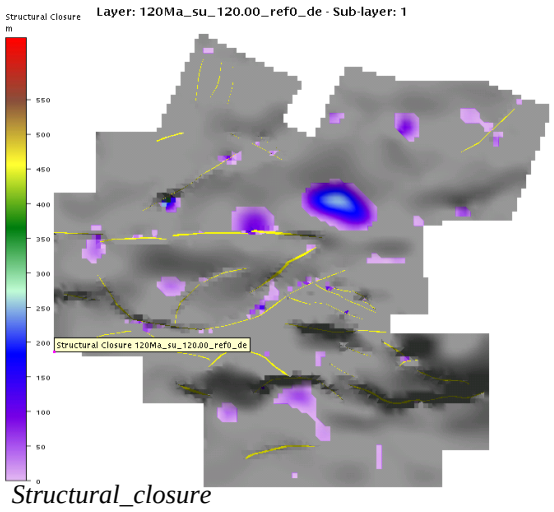

Structural_closure

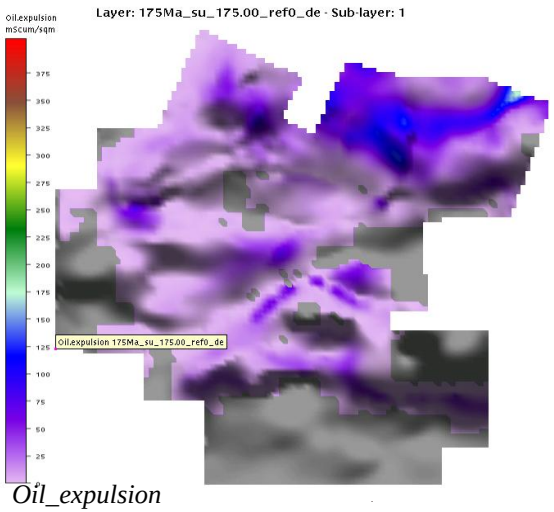

Oil_expulsion

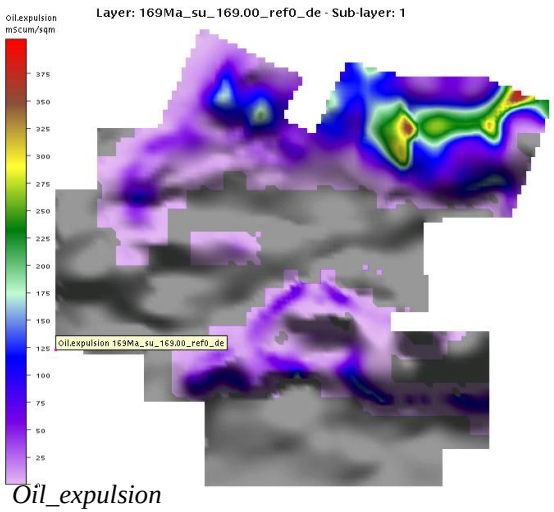

Oil_expulsion

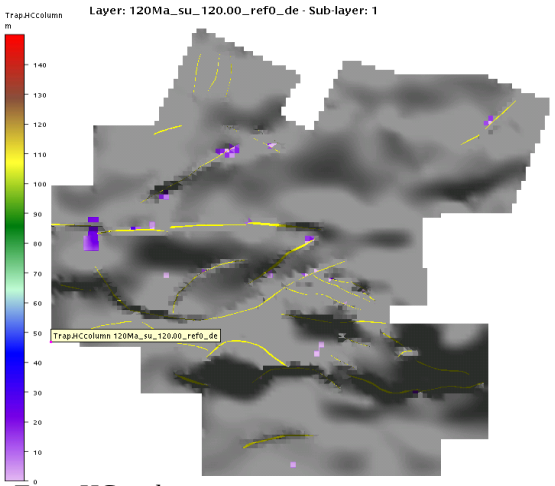

Trap_HC_column

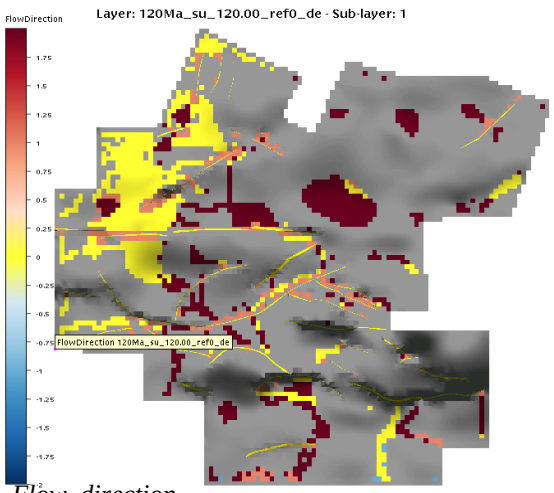

Flow_direction

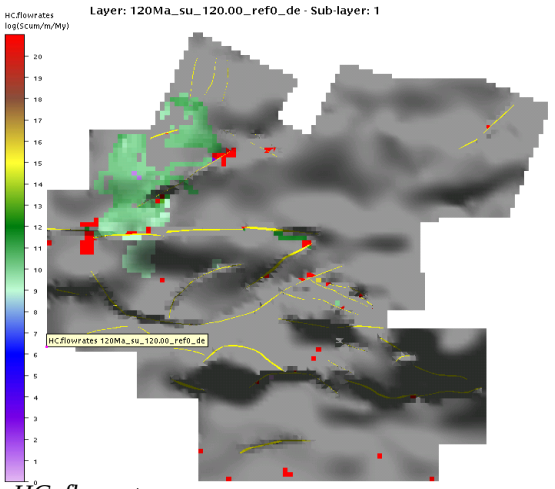

HC_flowrates

ATTACHMENT 3

SCENARIO “A”
LAYER 8_Bahariya (94 My)

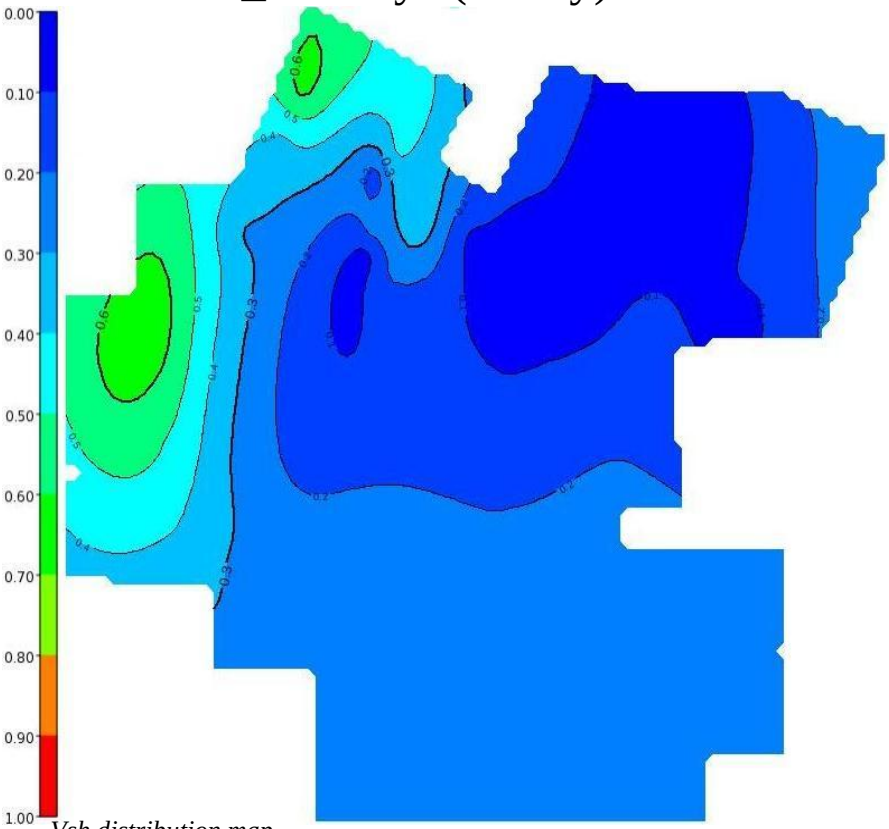

Vsh distribution map

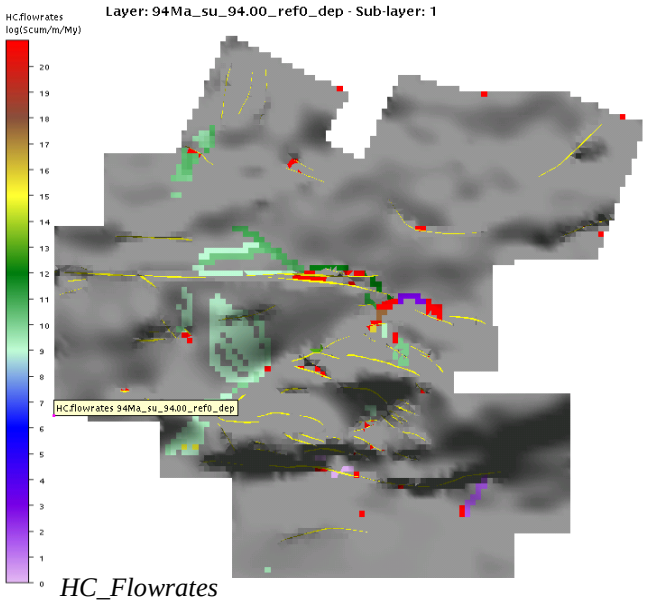

HC_Flowrates

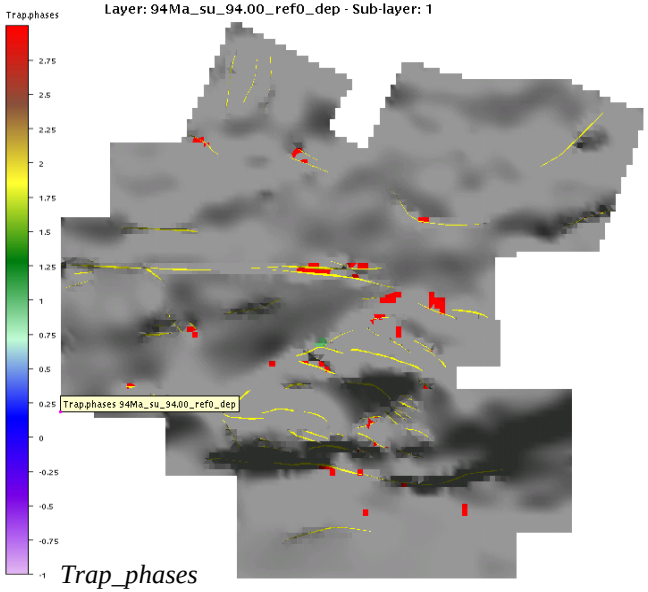

Trap_phases

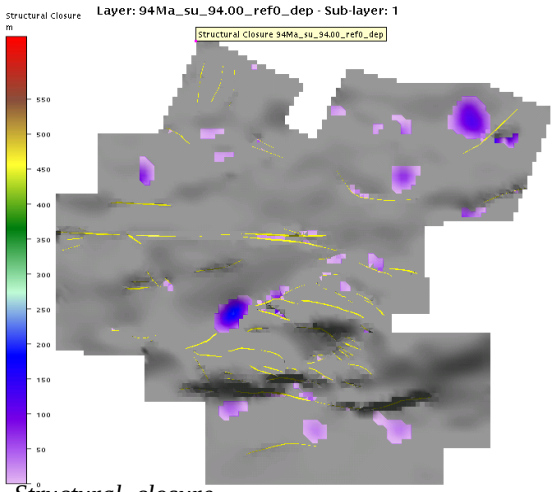

Structural_closure

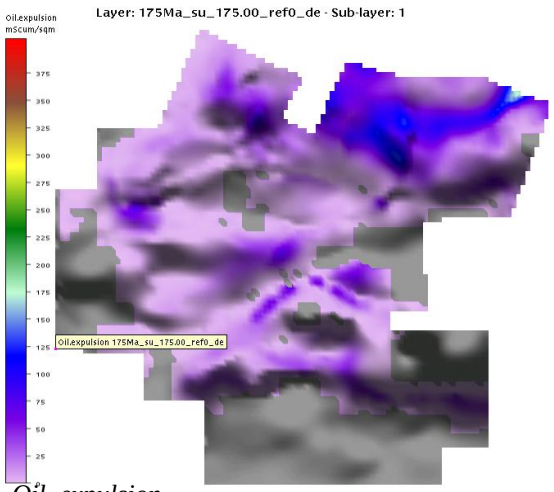

Oil_expulsion

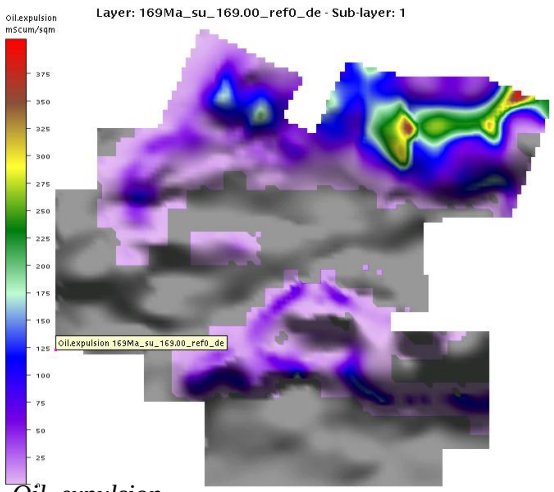

Oil_expulsion

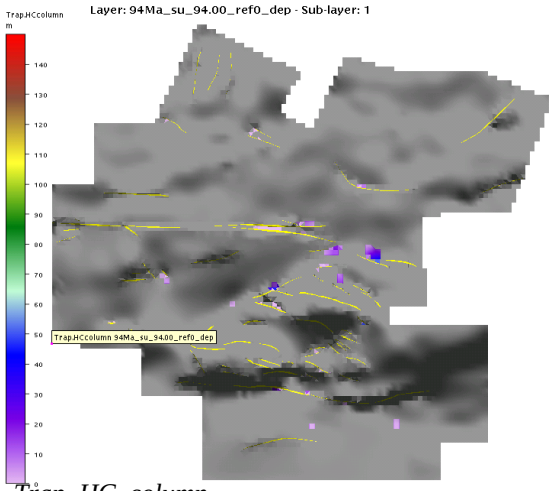

Trap_HC_column

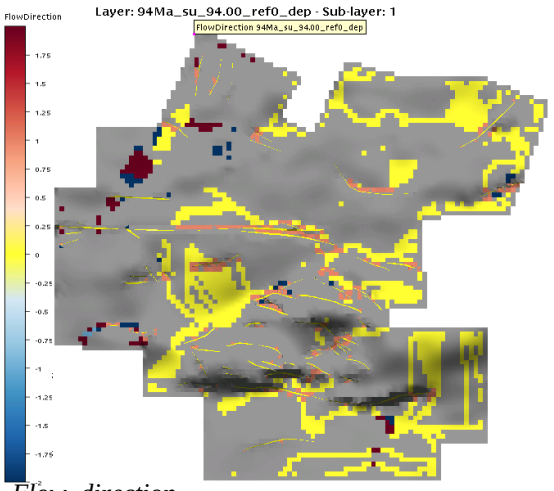

Flow_direction

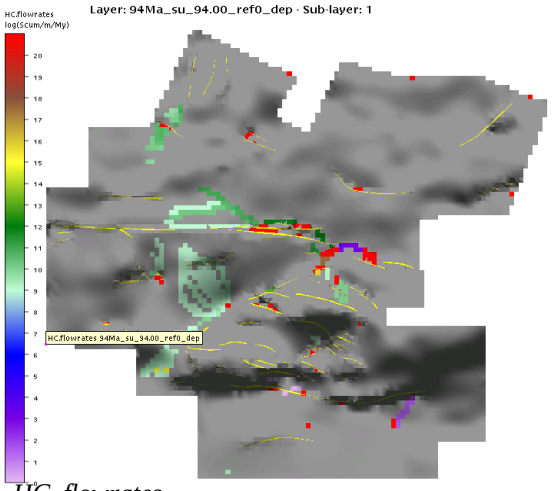

HC_flowrates

ATTACHMENT 4

SCENARIO “B”
LAYER 5_Khatatba (164 My)

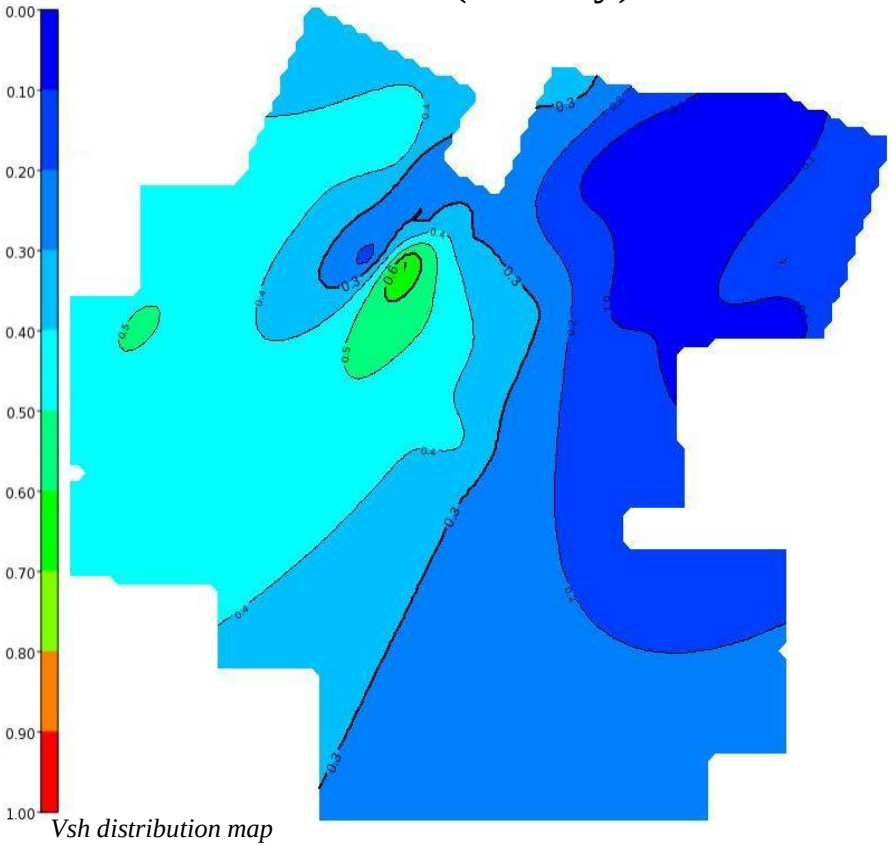

Vsh distribution map

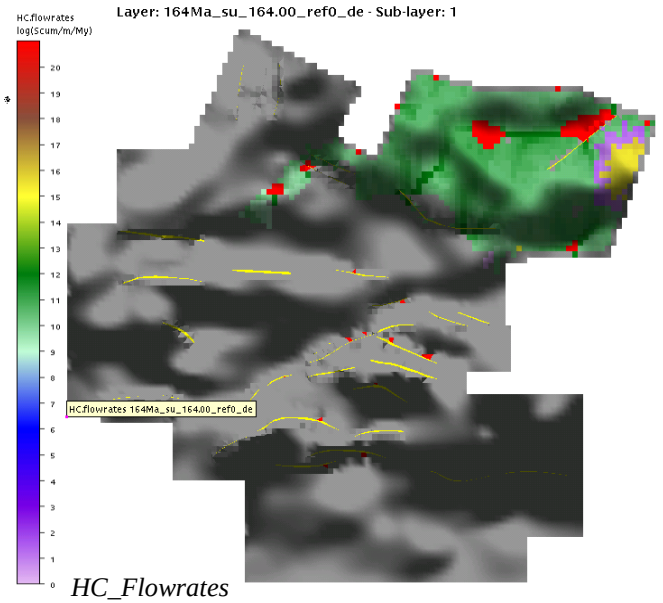

HC_Flowrates

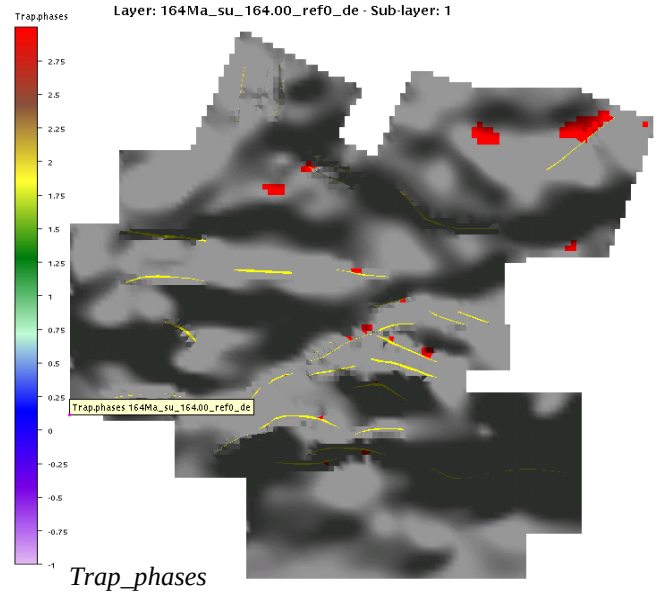

Trap_phases

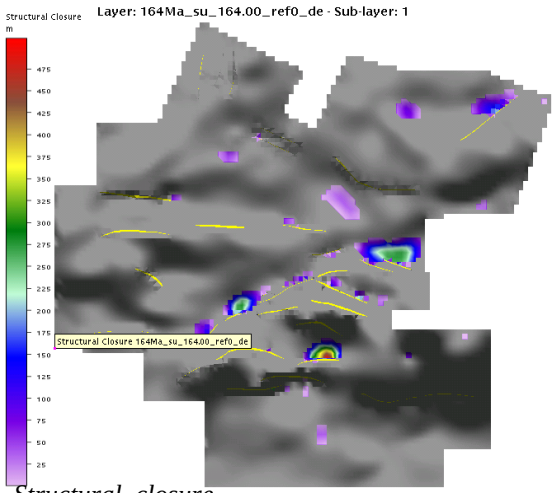

Structural_closure

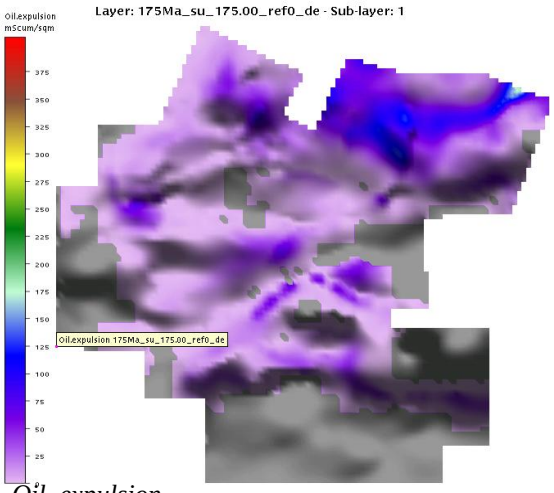

Oil_expulsion

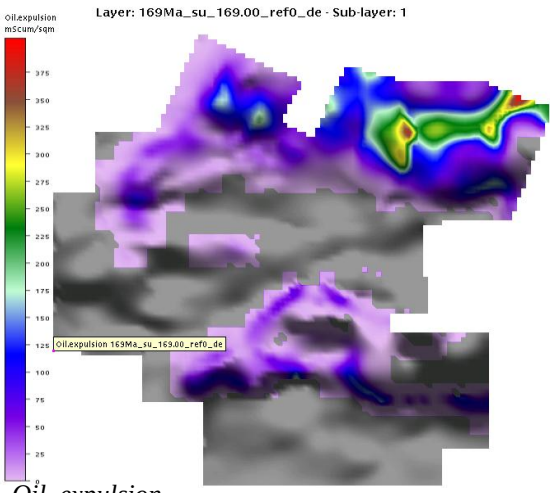

Oil_expulsion

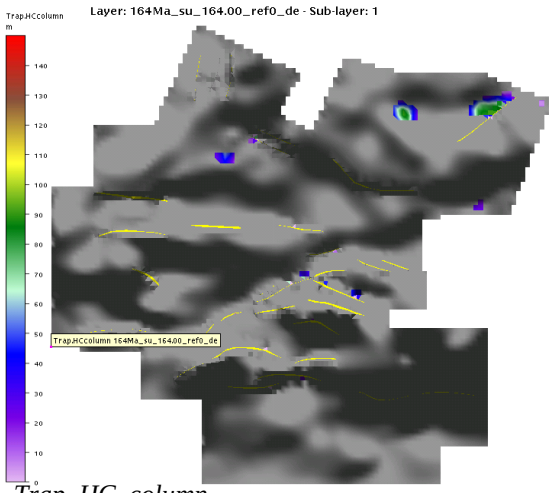

Trap_HC_column

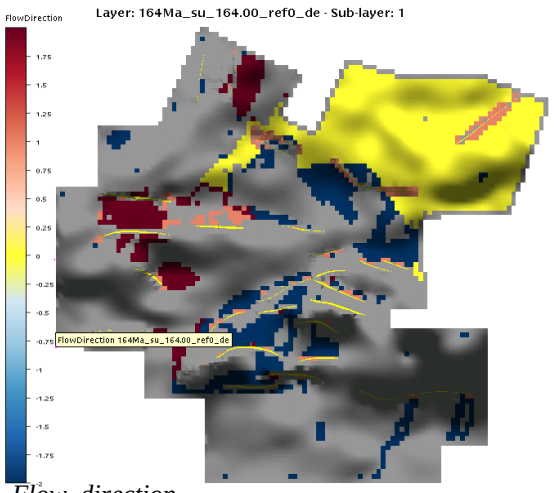

Flow_direction

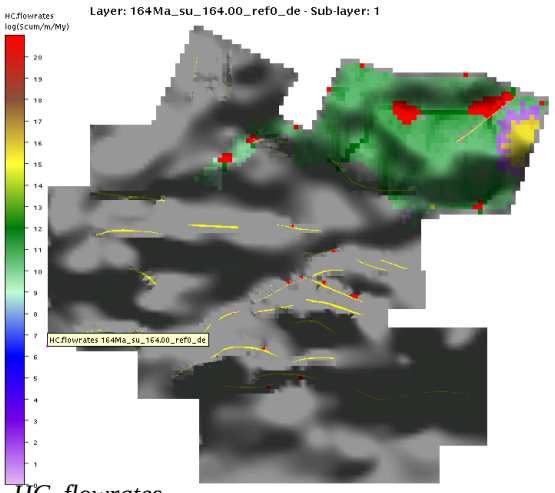

HC_flowrates

ATTACHMENT 5

SCENARIO “B”
LAYER 7_Alam el Bueib (120 My)

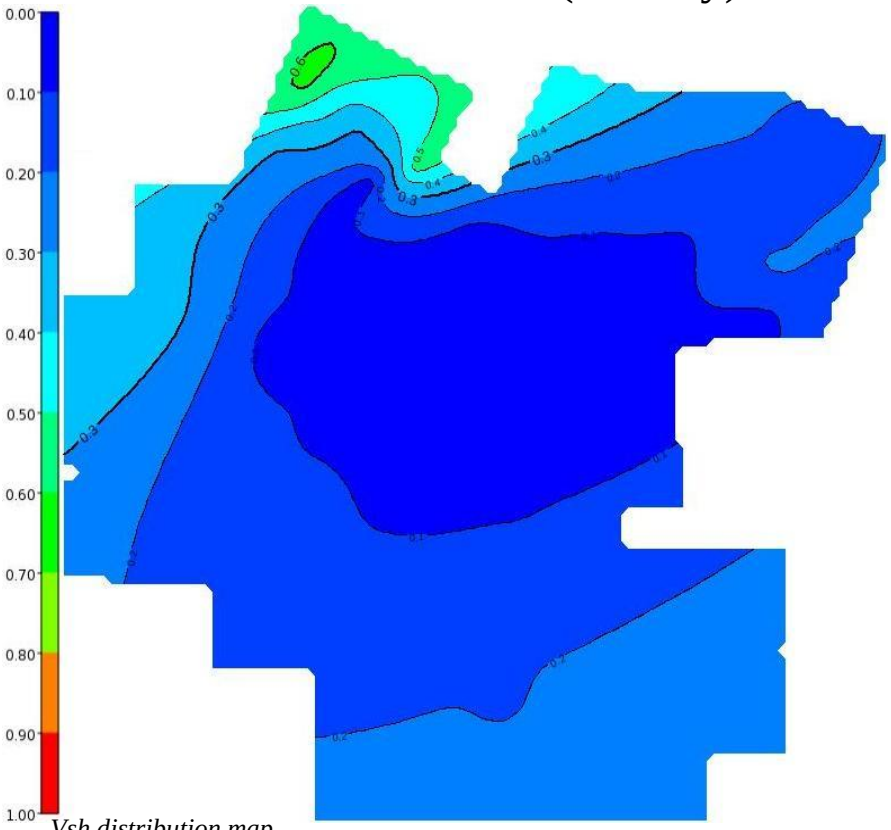

Vsh distribution map

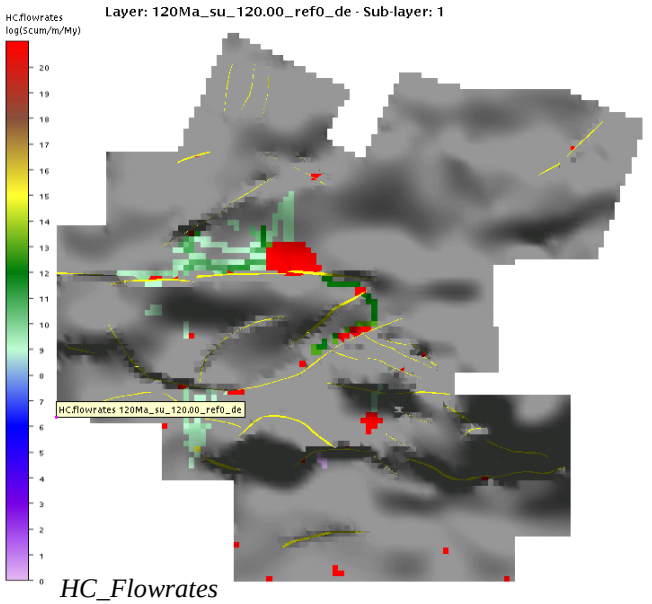

HC_Flowrates

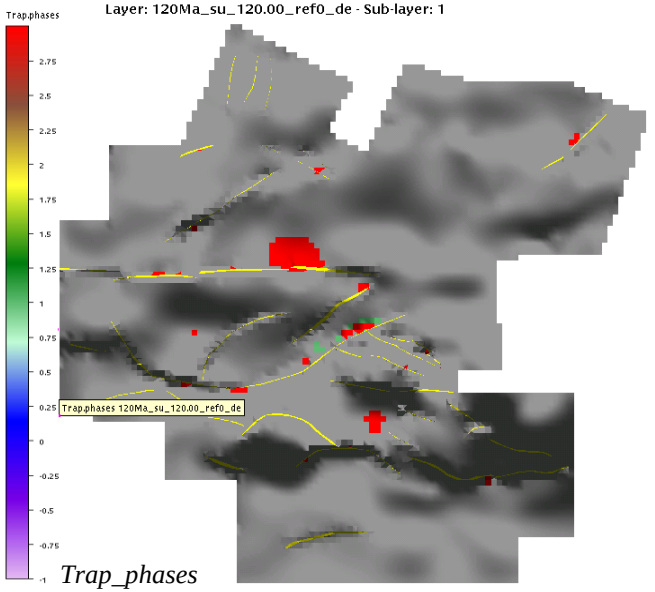

Trap_phases

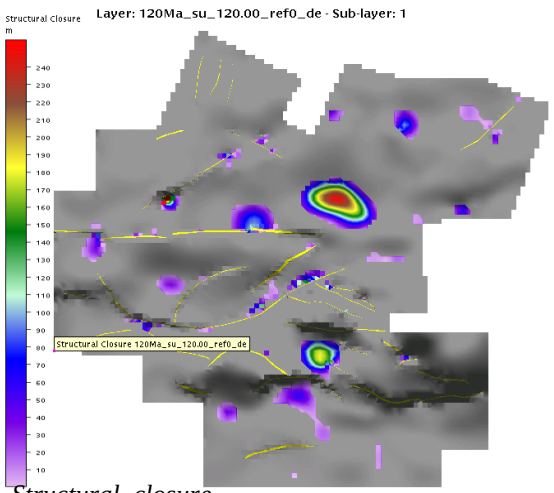

Structural_closure

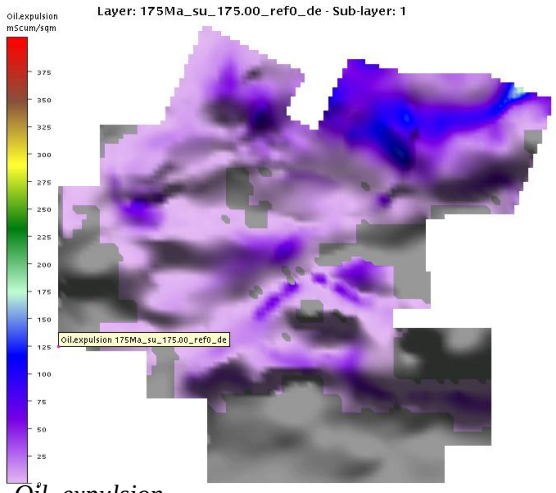

Oil_expulsion

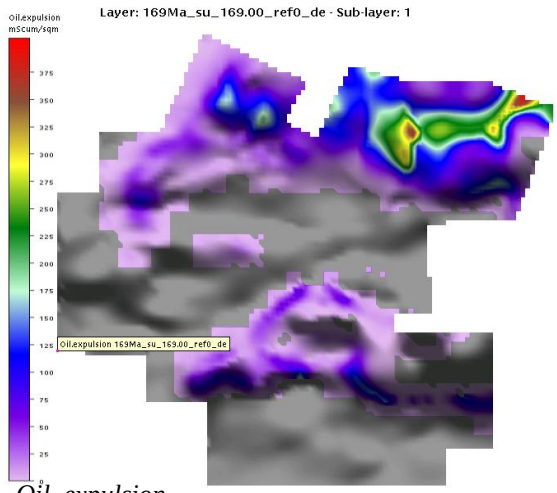

Oil_expulsion

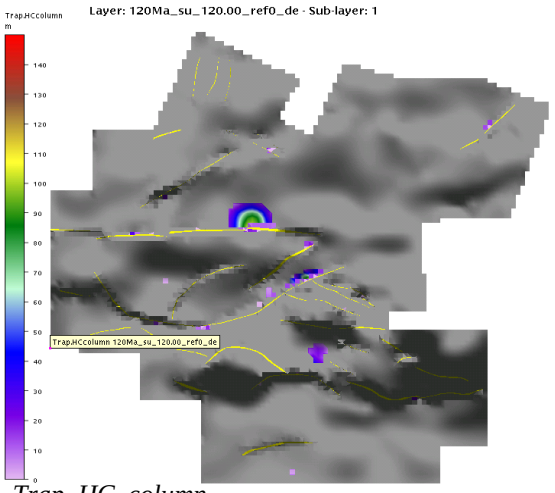

Trap_HC_column

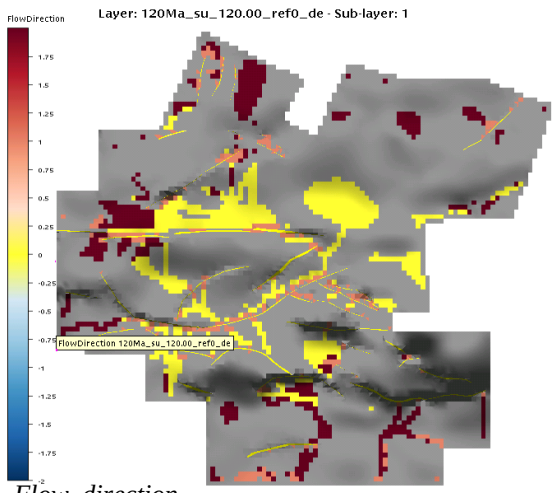

Flow_direction

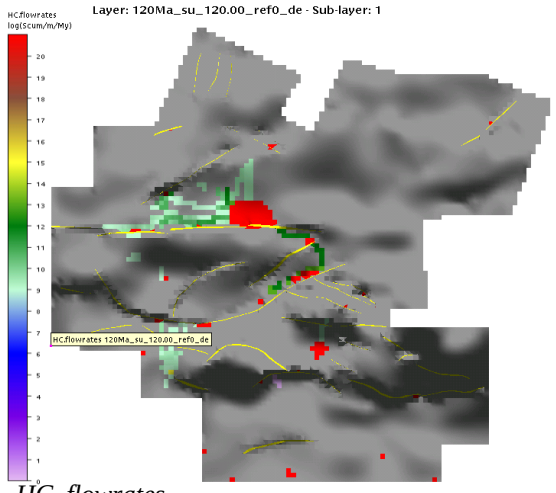

HC_flowrates

ATTACHMENT 6

SCENARIO “B”
LAYER 8_Bahariya (94 My)

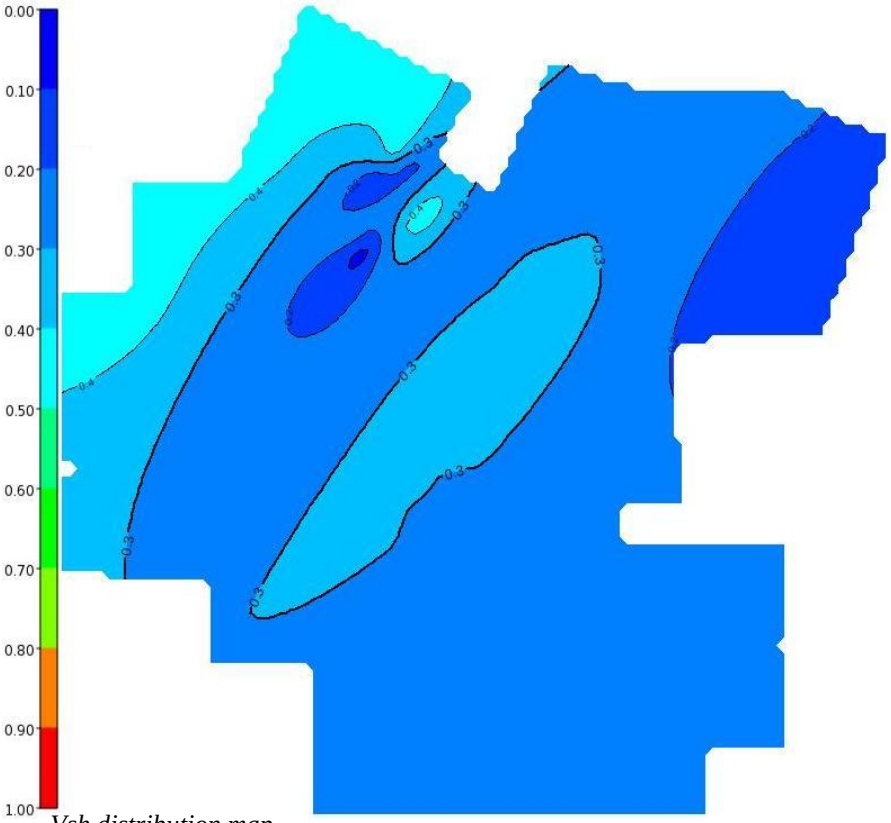

Vsh distribution map

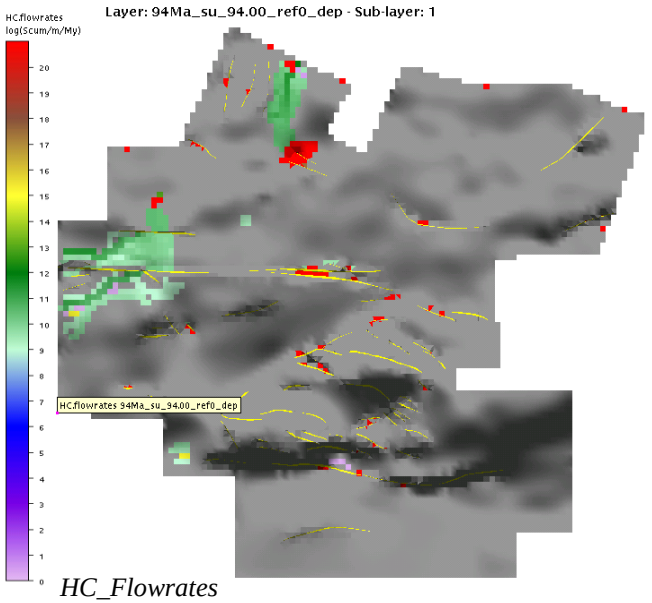

HC_Flowrates

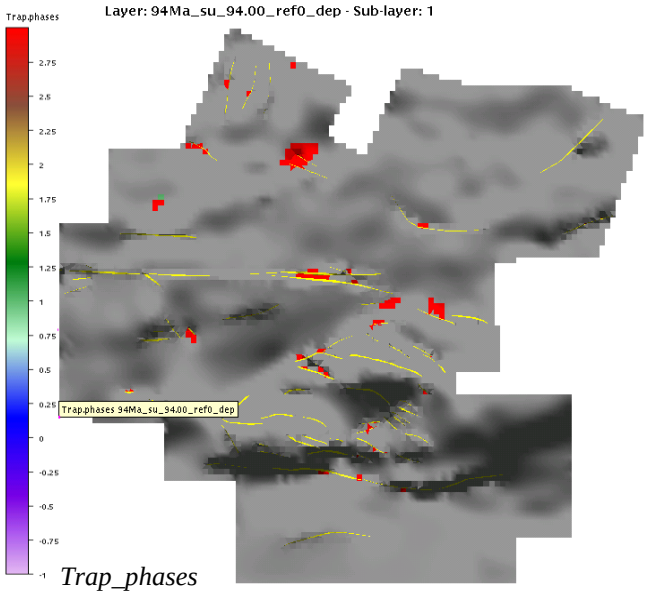

Trap_phases

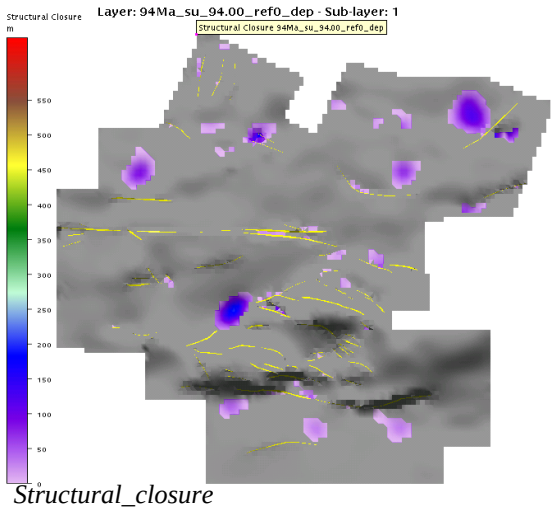

Structural_closure

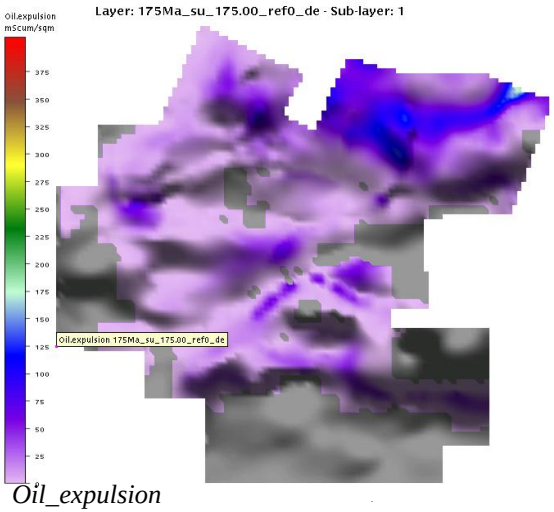

Oil_expulsion

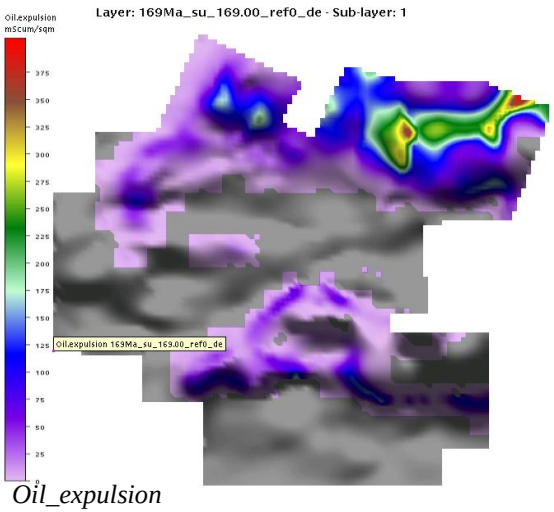

Oil_expulsion

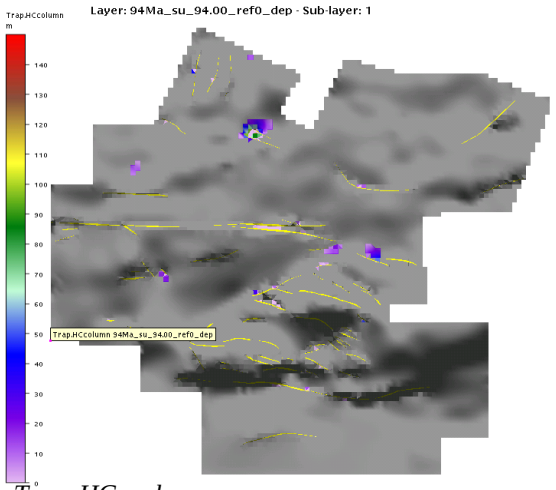

Trap_HC_column

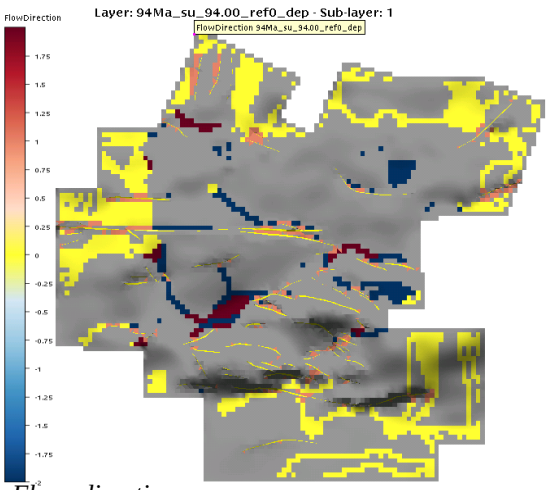

Flow_direction

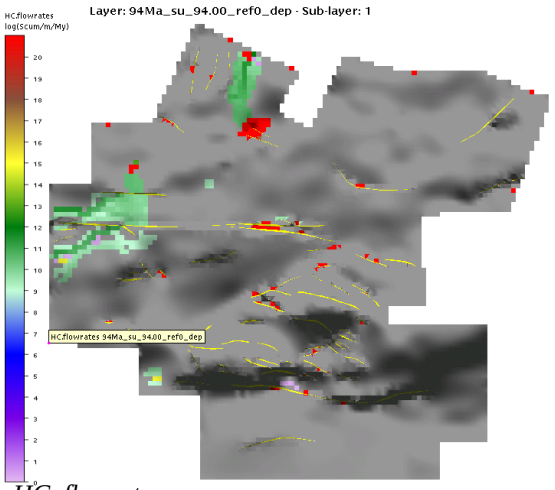

HC_flowrates

ATTACHMENT 7

SCENARIO “C”
LAYER 5_Khatatba 1 (164My)

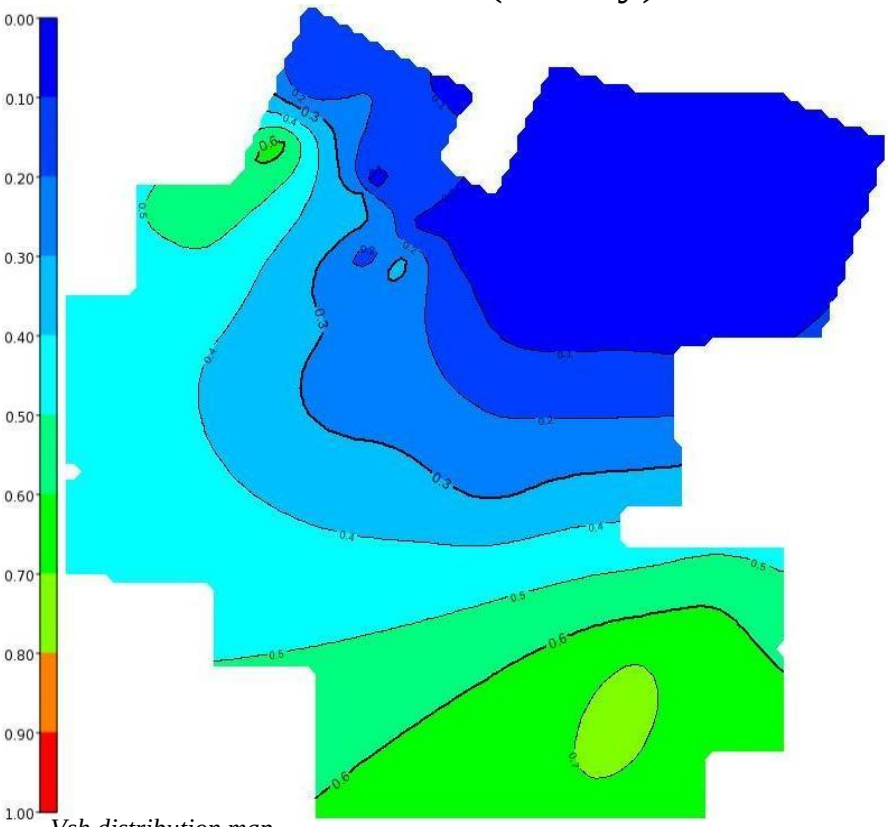

Vsh distribution map

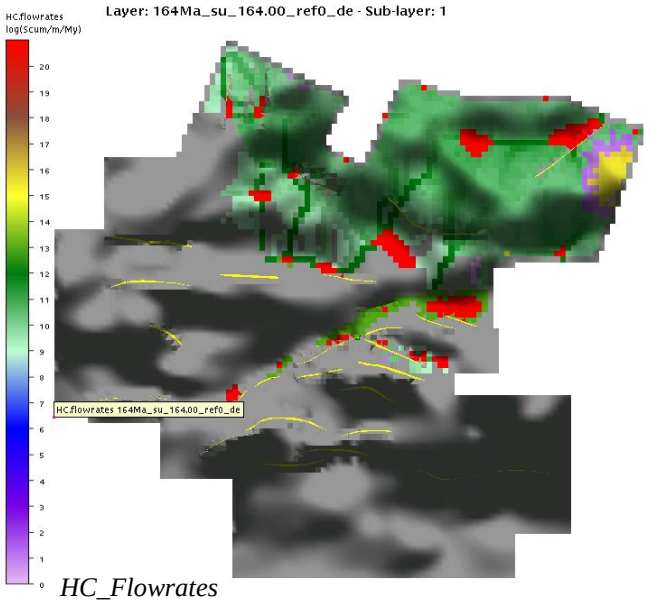

HC_Flowrates

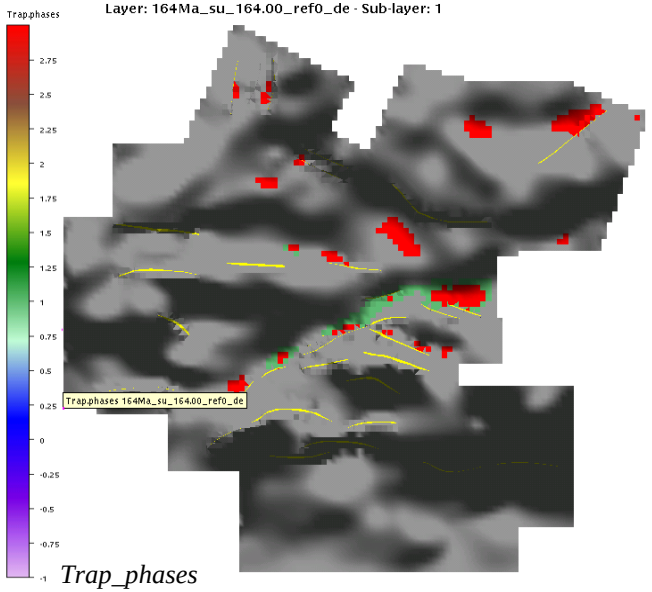

Trap_phases

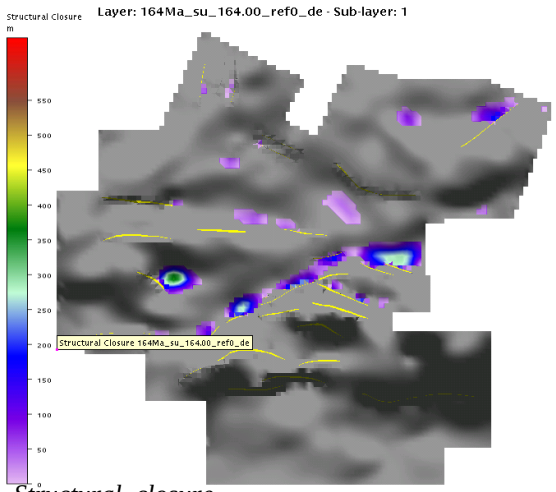

Structural_closure

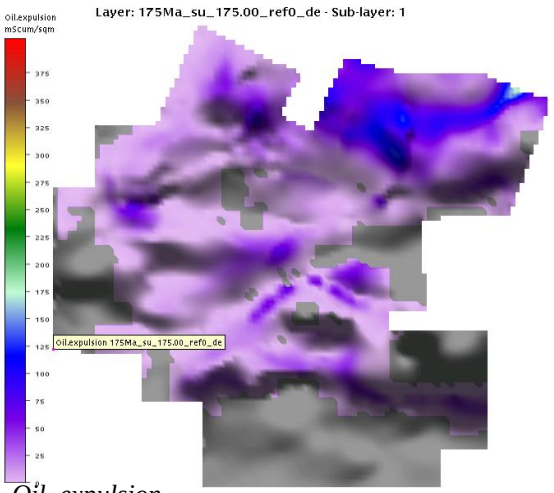

Oil_expulsion

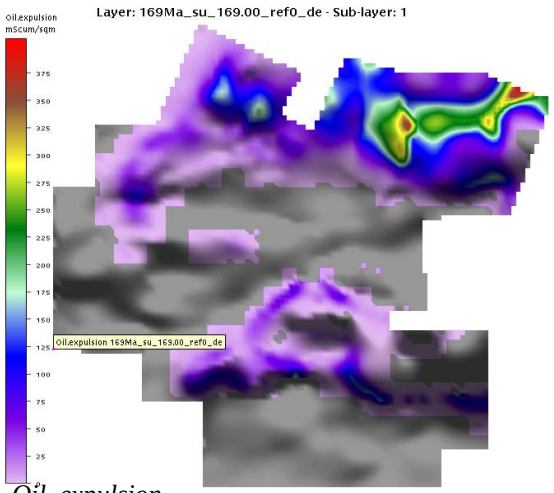

Oil_expulsion

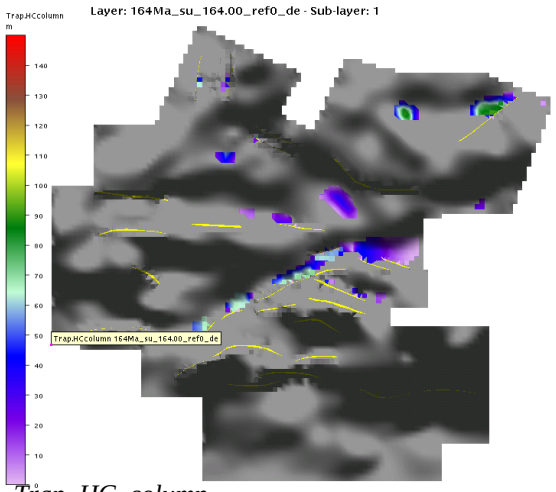

Trap_HC_column

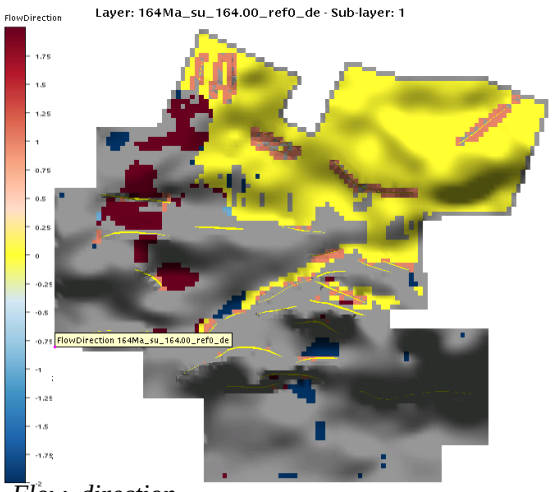

Flow_direction

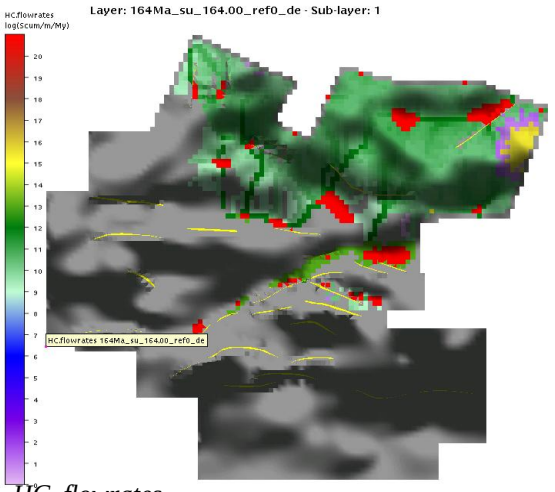

HC_flowrates

ATTACHMENT 8

SCENARIO “C”
LAYER 7_Alam el Bueib (120 My)

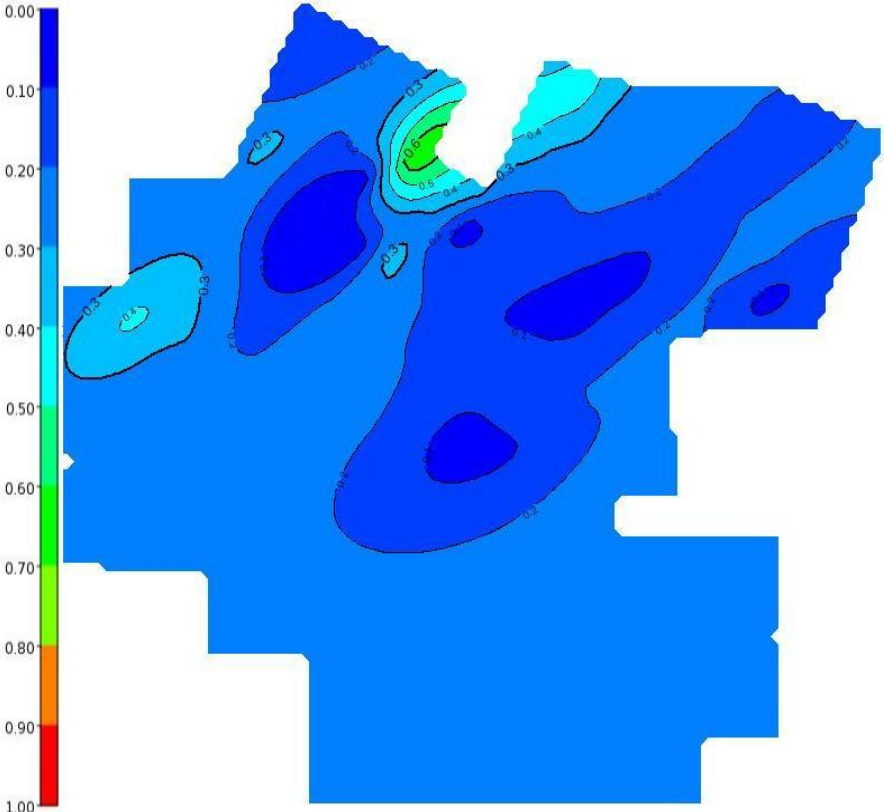

Vsh distribution map

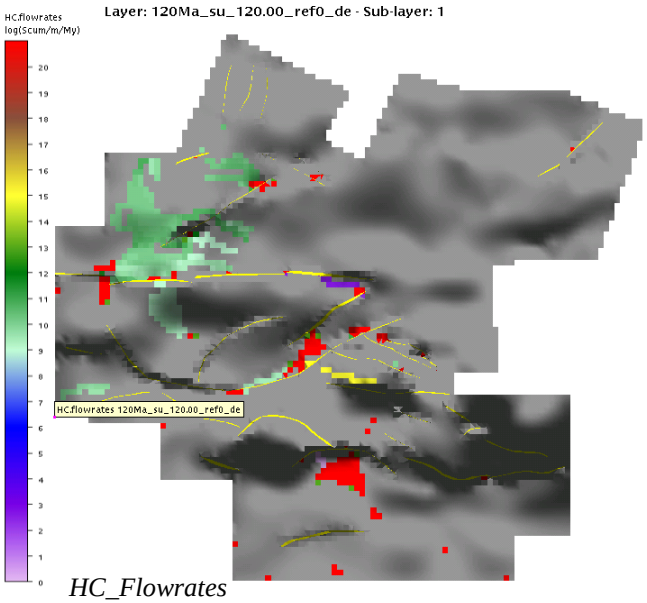

HC_Flowrates

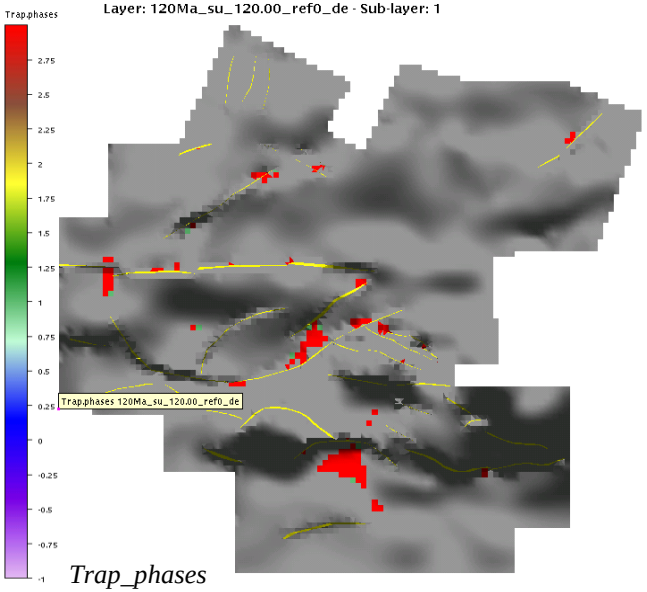

Trap_phases

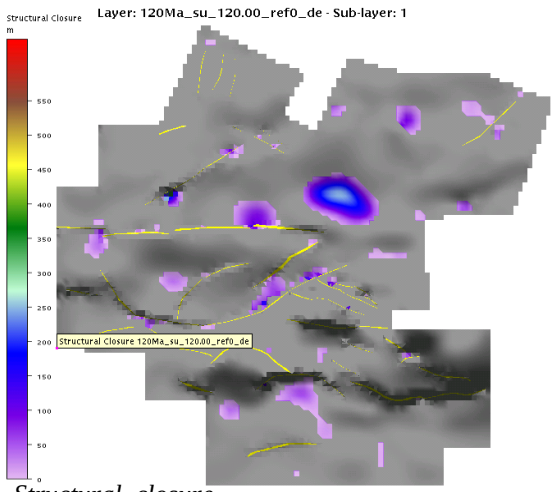

Structural_closure

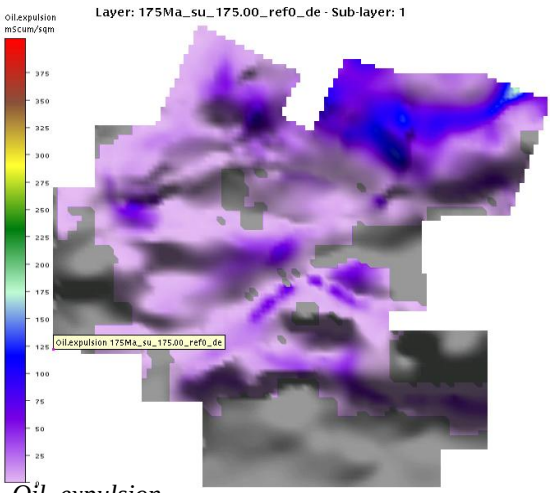

Oil_expulsion

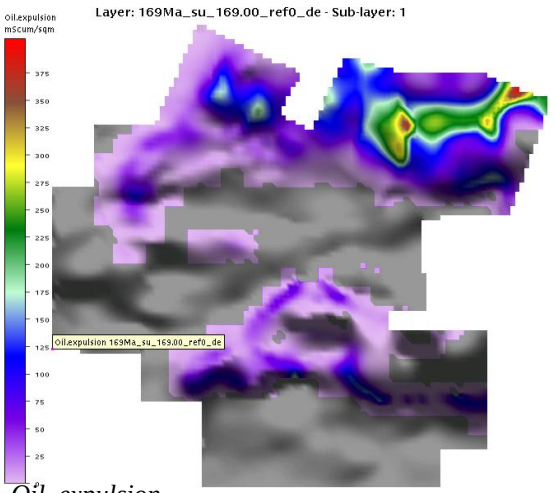

Oil_expulsion

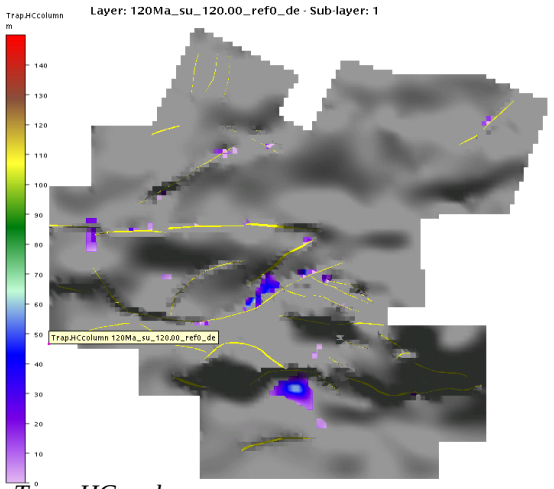

Trap_HC_column

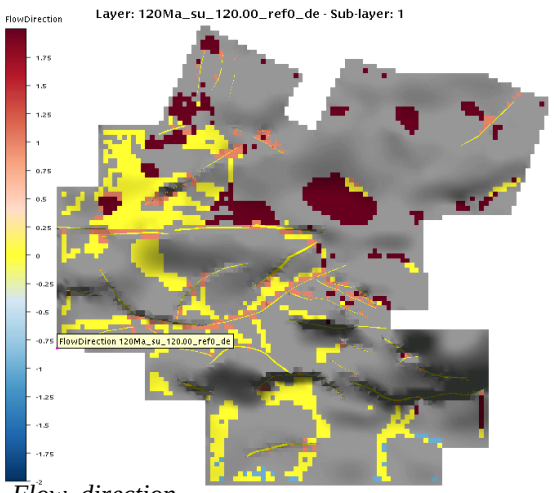

Flow_direction

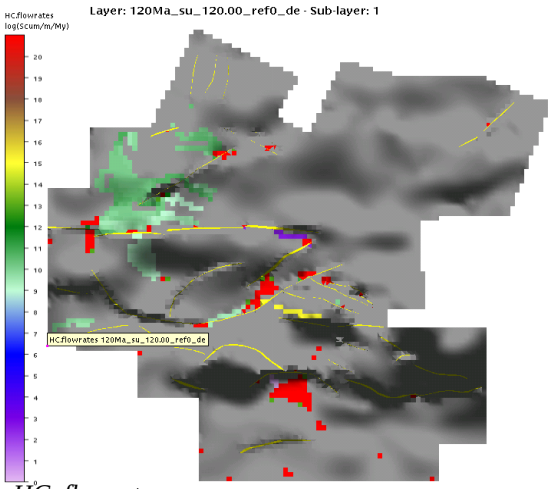

HC_flowrates

ATTACHMENT 9

SCENARIO “C”
LAYER 8_Bahariya (94 My)

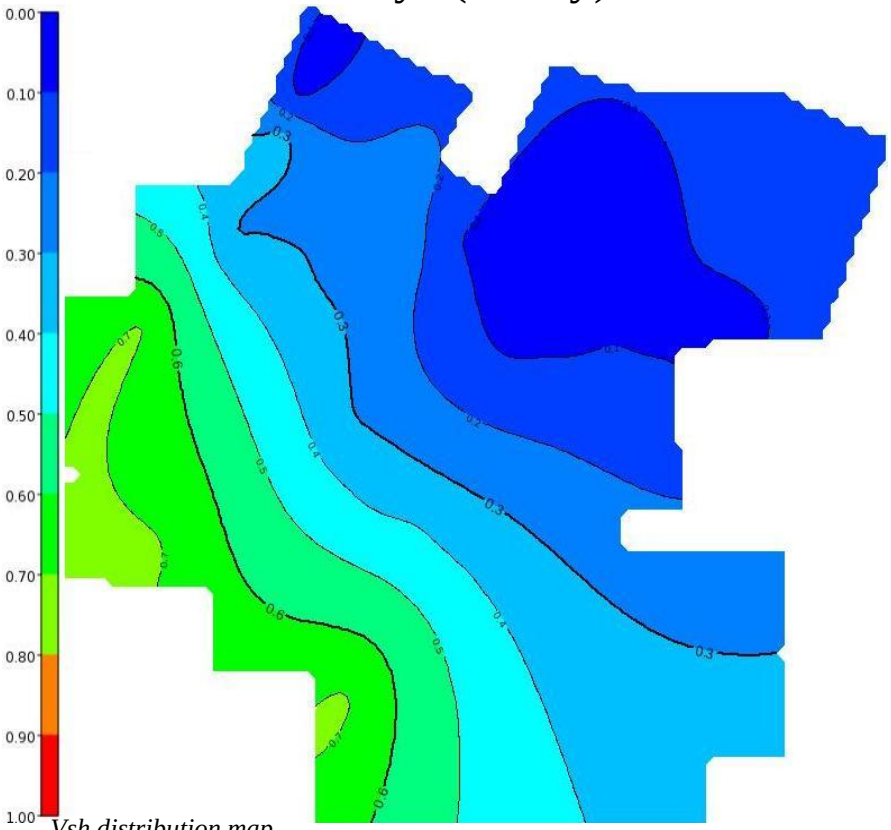

Vsh distribution map

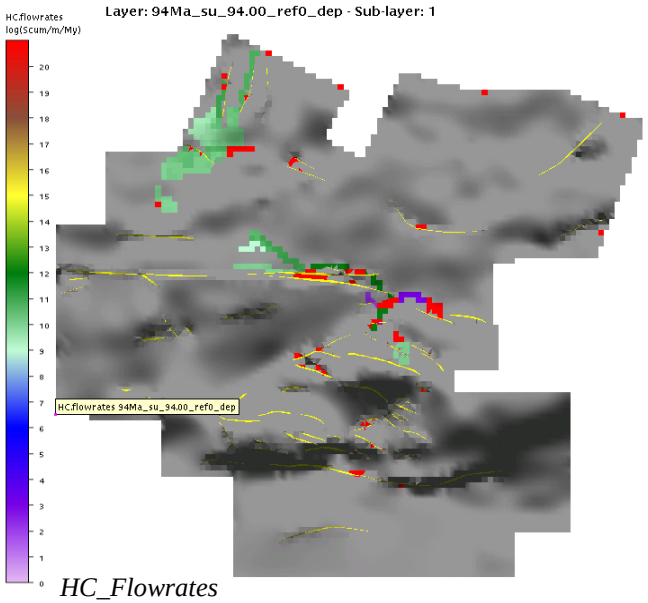

HC_Flowrates

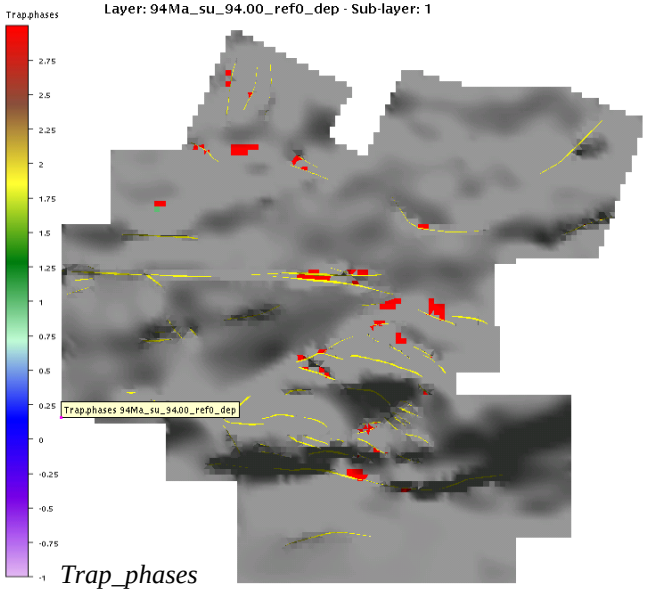

Trap_phases

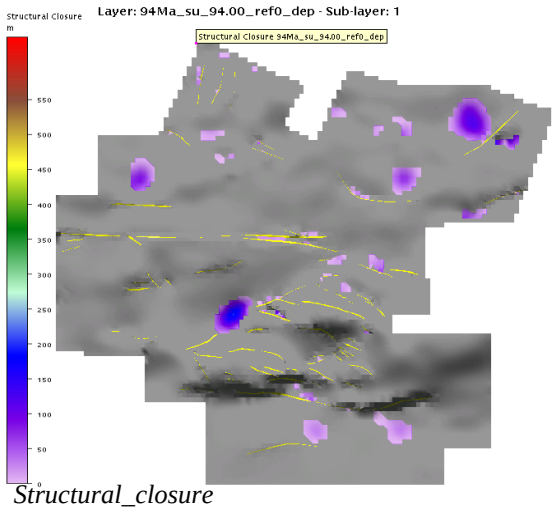

Structural_closure

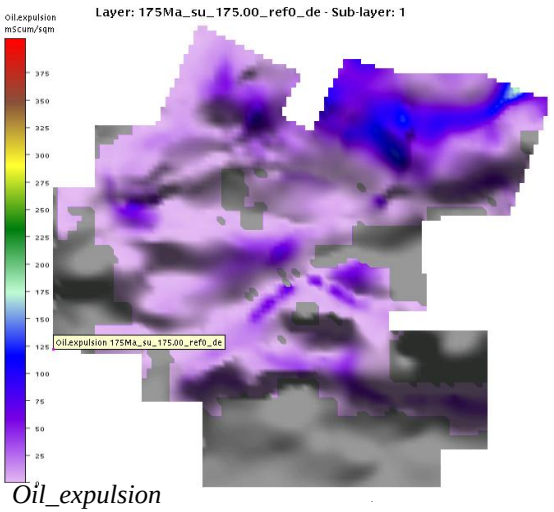

Oil_expulsion

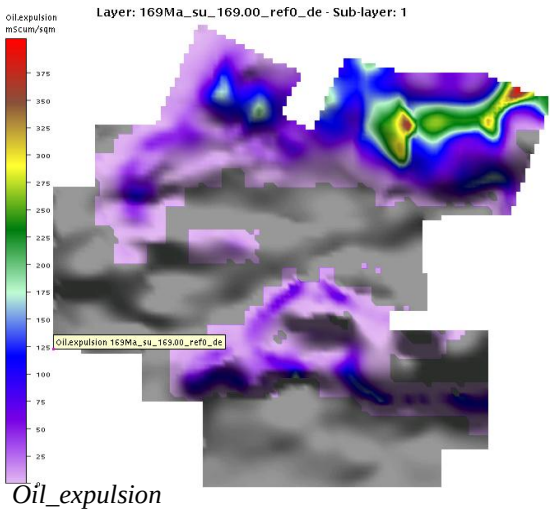

Oil_expulsion

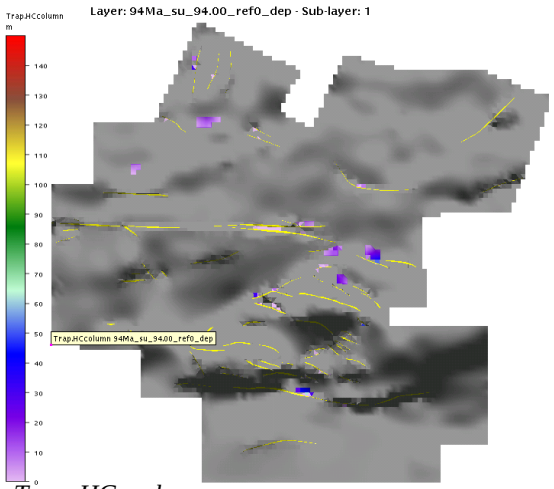

Trap_HC_column

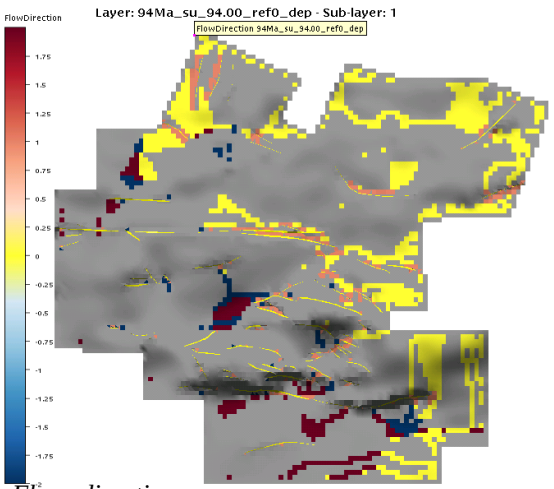

Flow_direction

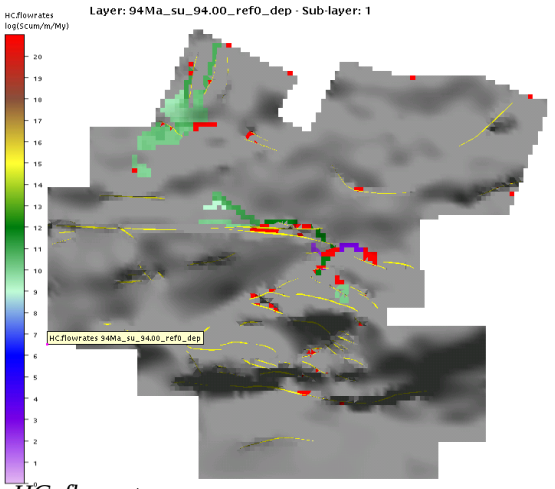

HC_flowrates

ATTACHMENT 10

SCENARIO “D”
LAYER 5_Khatatba 1 (164 My)

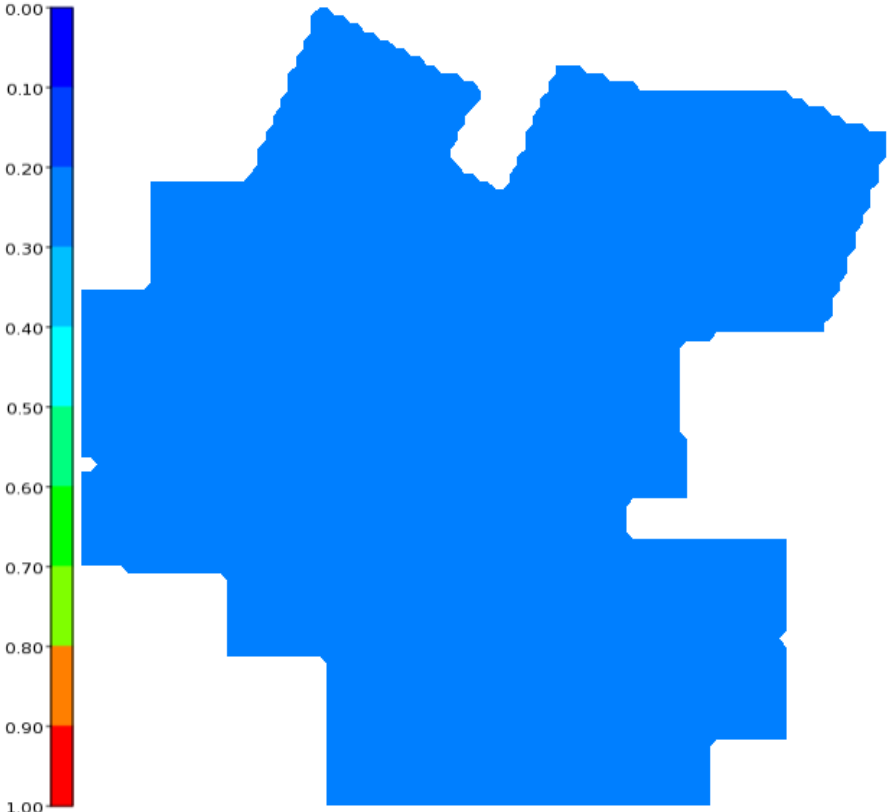

Vsh distribution map

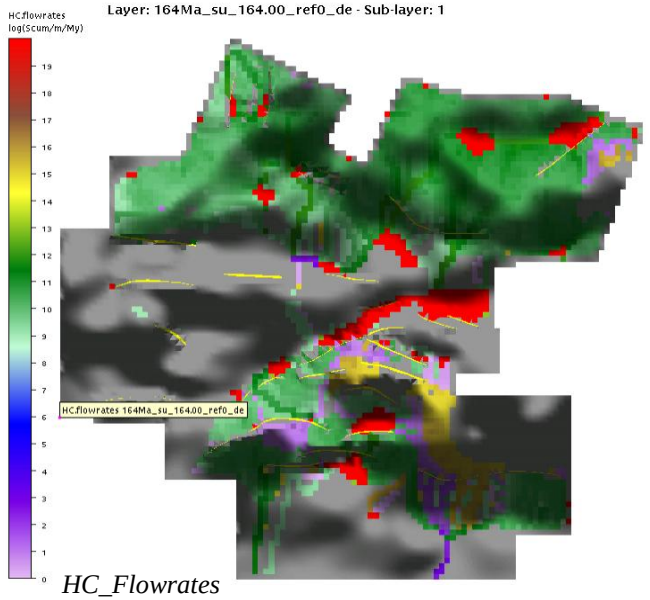

HC_Flowrates

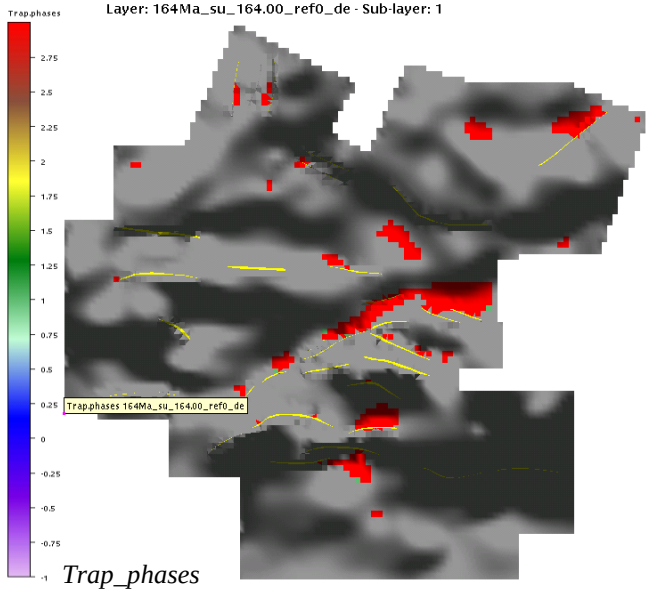

Trap_phases

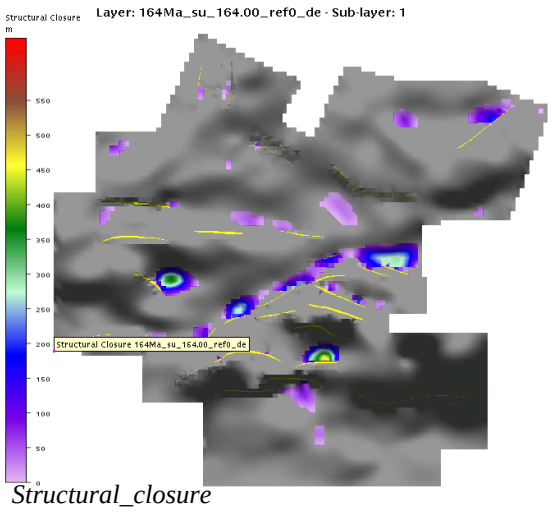

Structural_closure

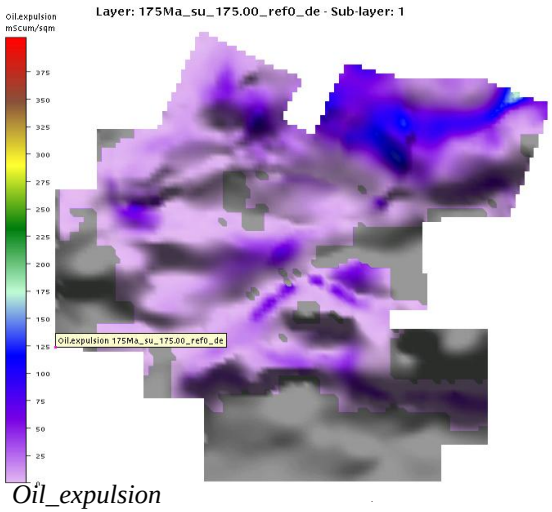

Oil_expulsion

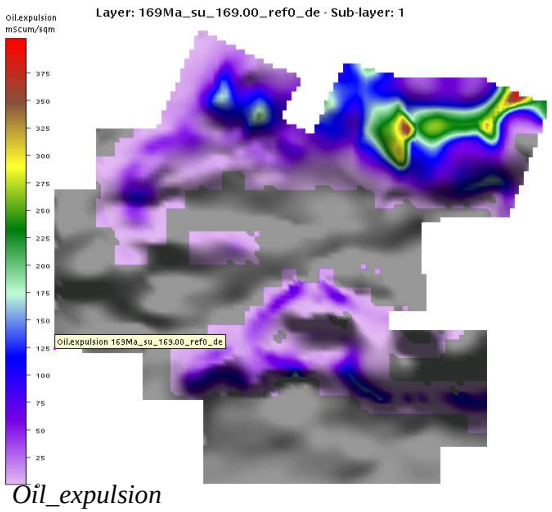

Oil_expulsion

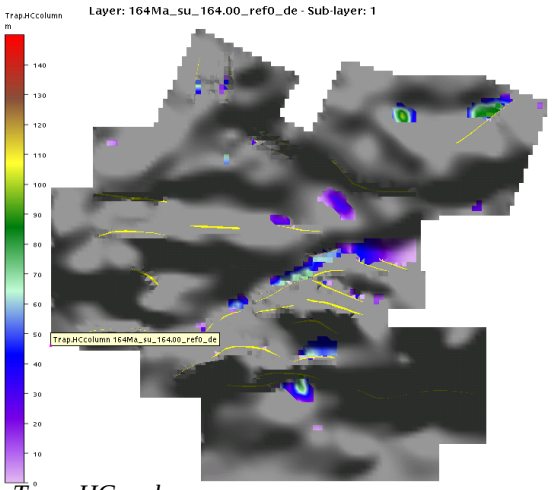

Trap_HC_column

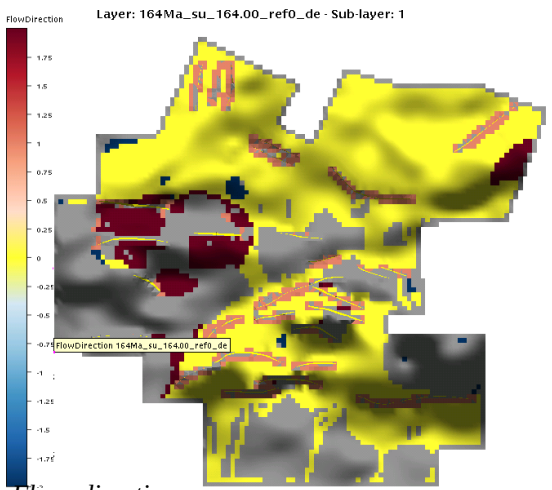

Flow_direction

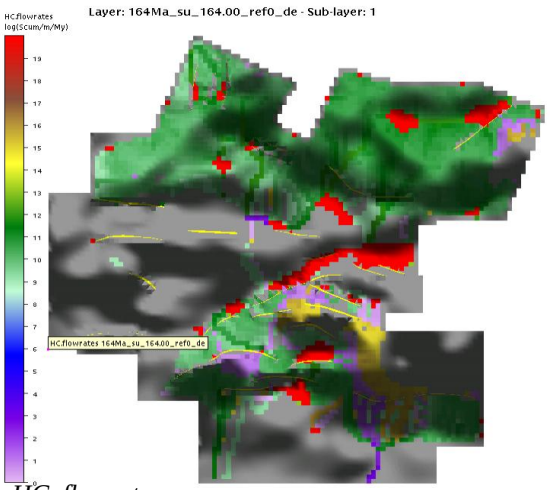

HC_flowrates

ATTACHMENT 11

SCENARIO “D”
LAYER 7_Alam el Bueib (120 My)

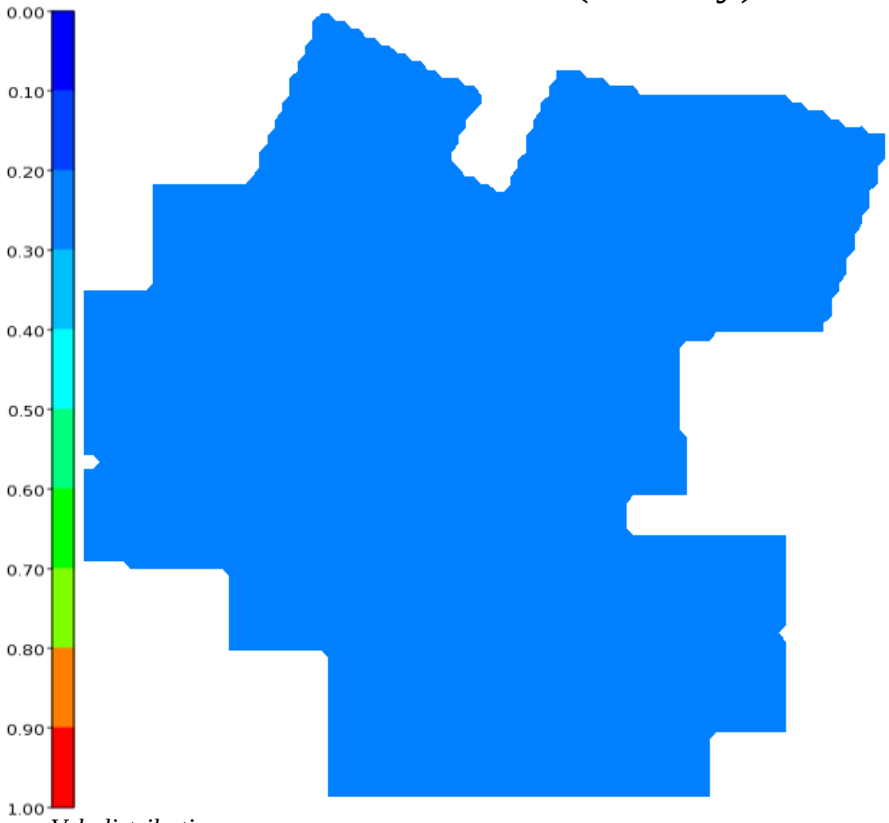

Vsh distribution map

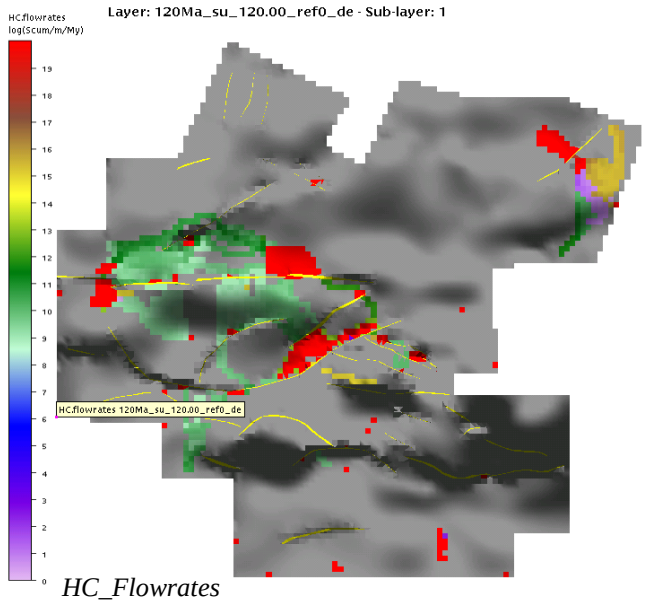

HC_Flowrates

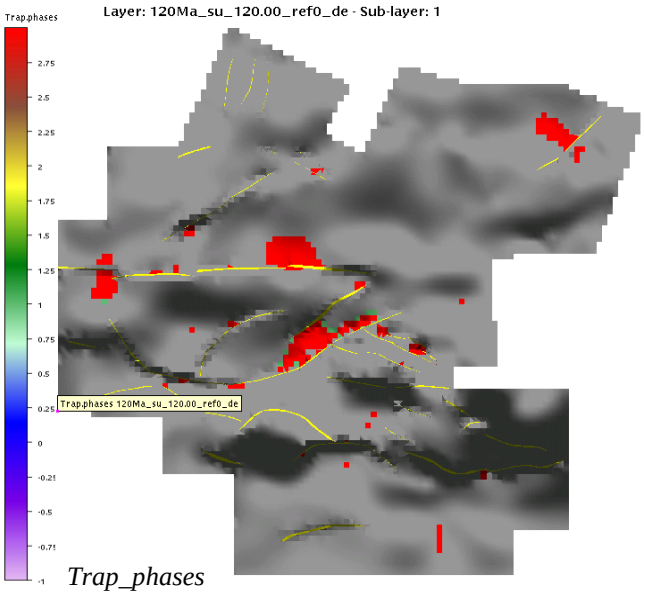

Trap_phases

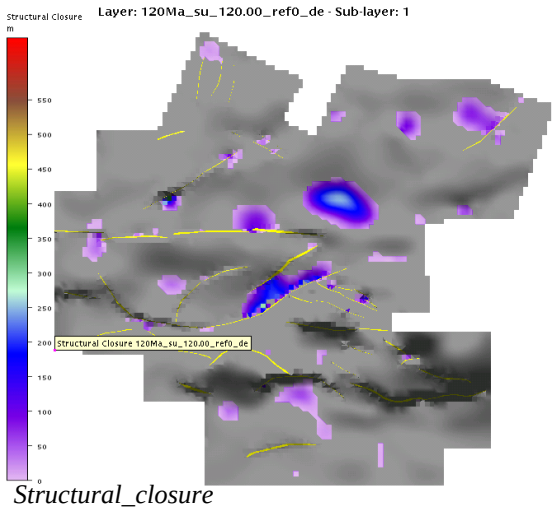

Structural_closure

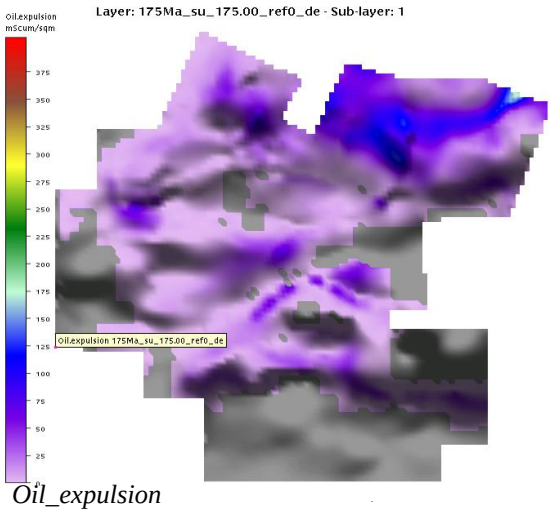

Oil_expulsion

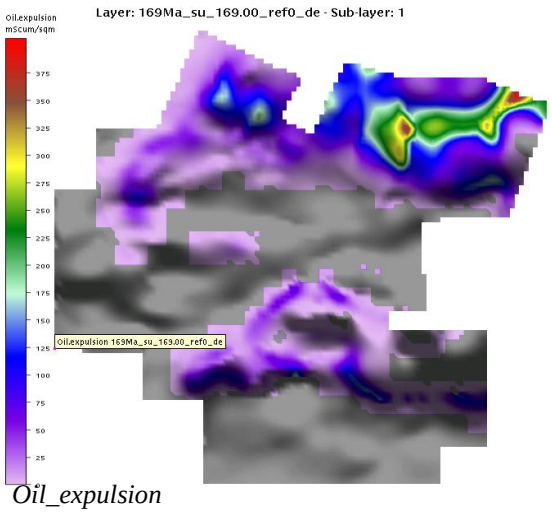

Oil_expulsion

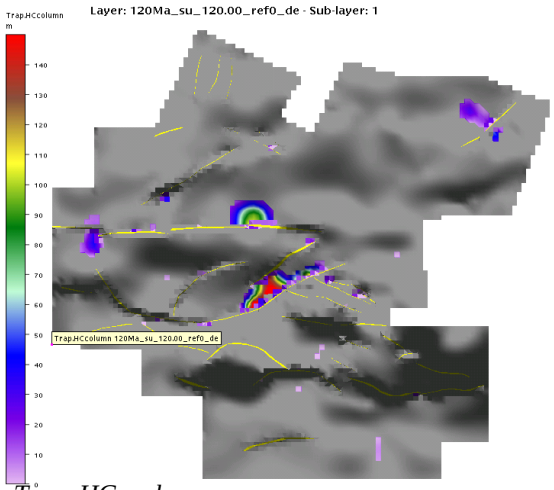

Trap_HC_column

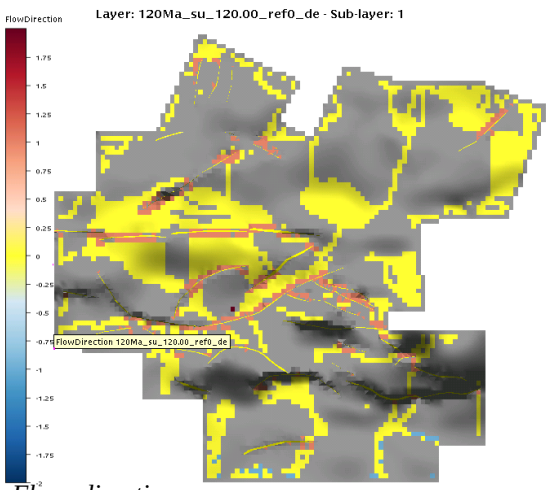

Flow_direction

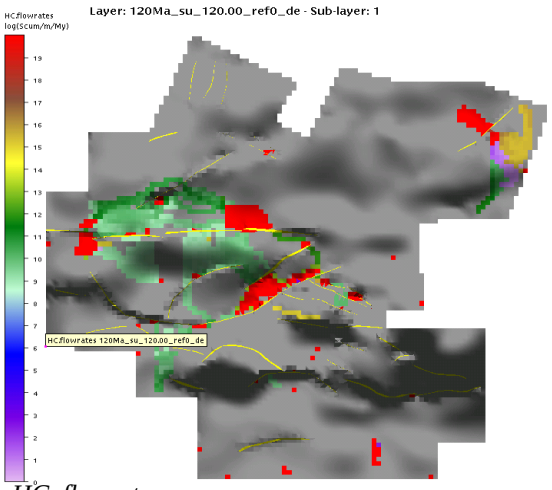

HC_flowrates

ATTACHMENT 12

SCENARIO “D”
LAYER 8_Bahariya (94 My)

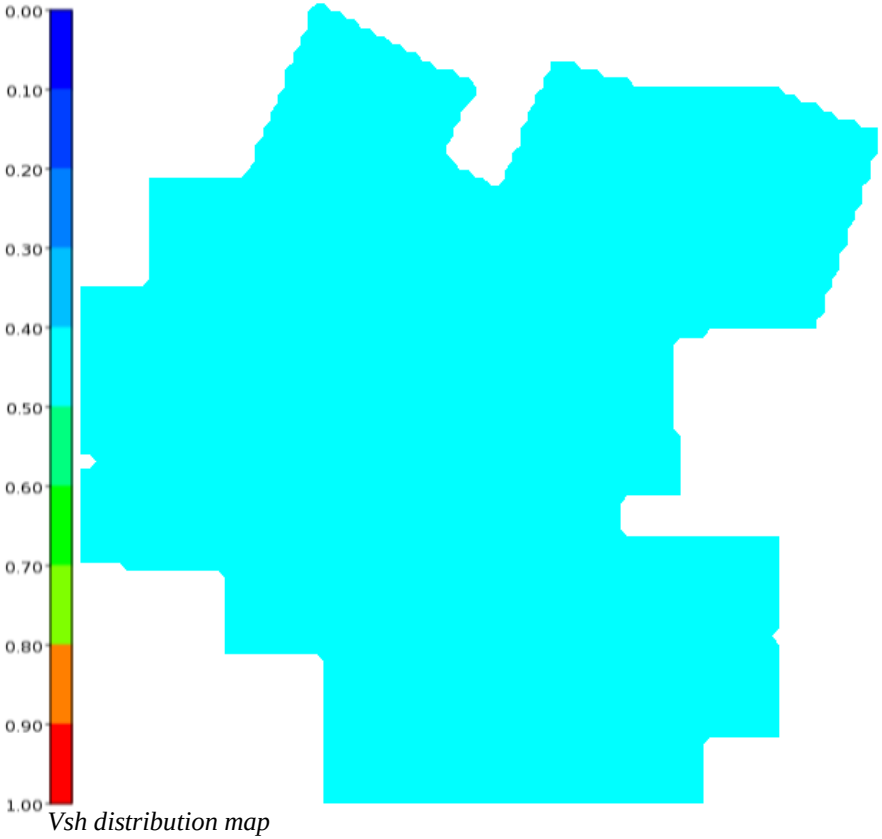

Vsh distribution map

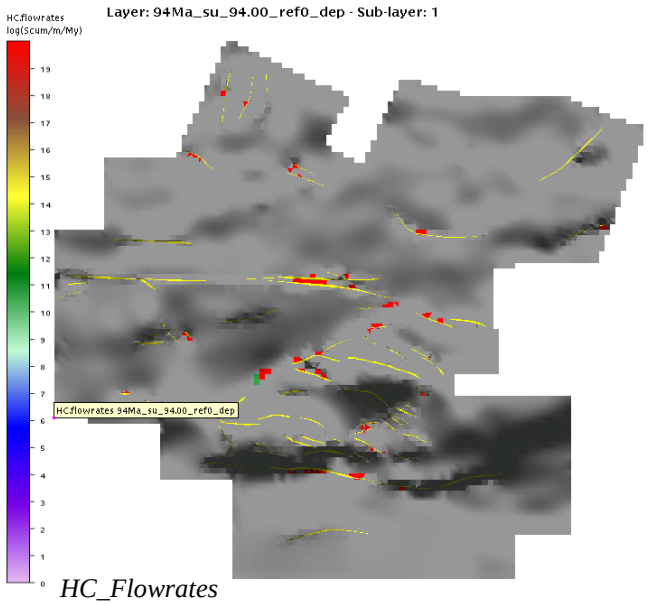

HC_Flowrates

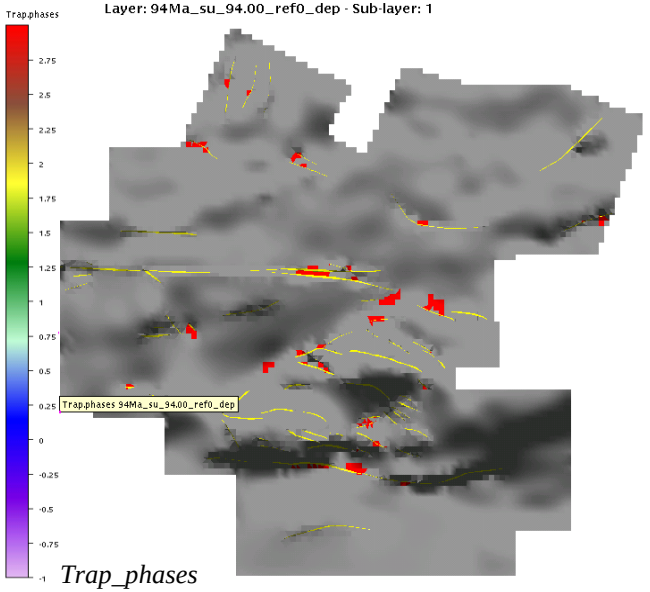

Trap_phases

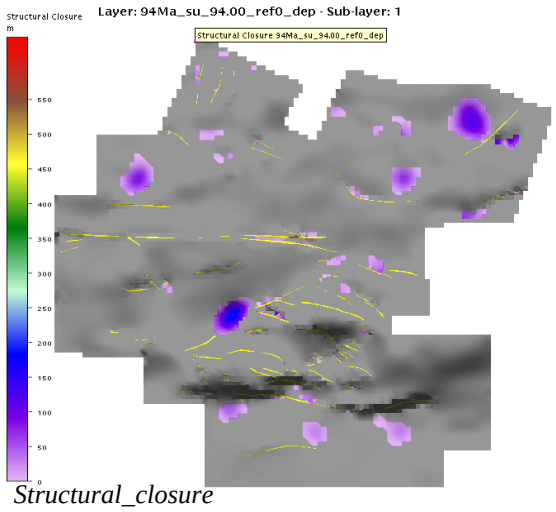

Structural_closure

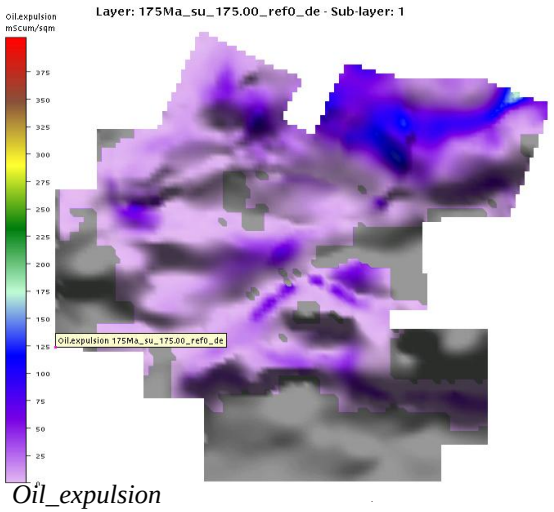

Oil_expulsion

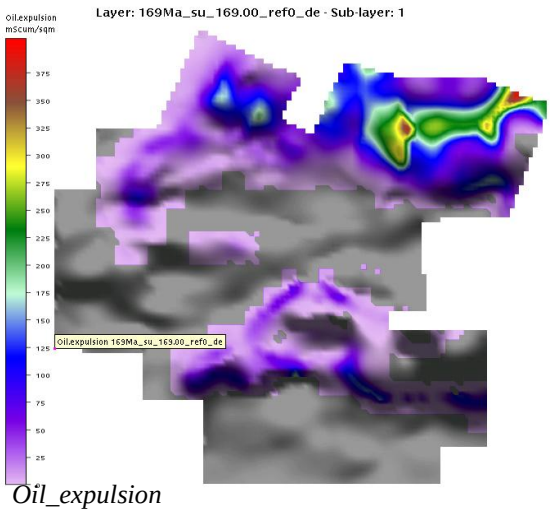

Oil_expulsion

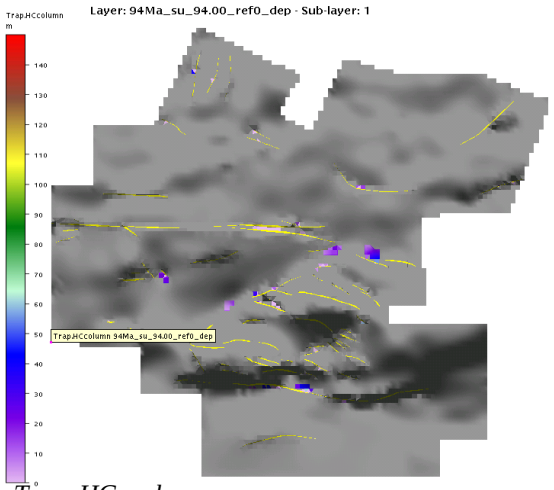

Trap_HC_column

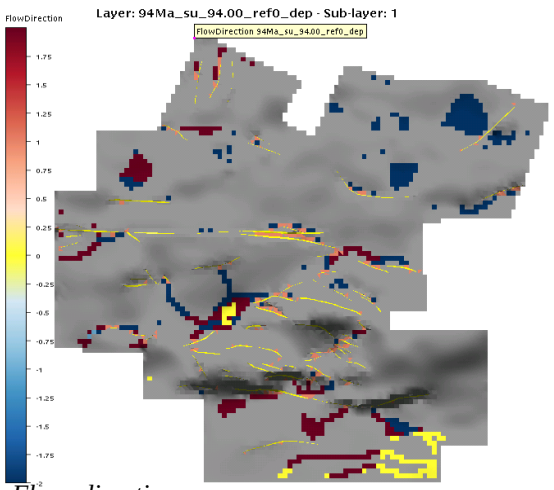

Flow_direction

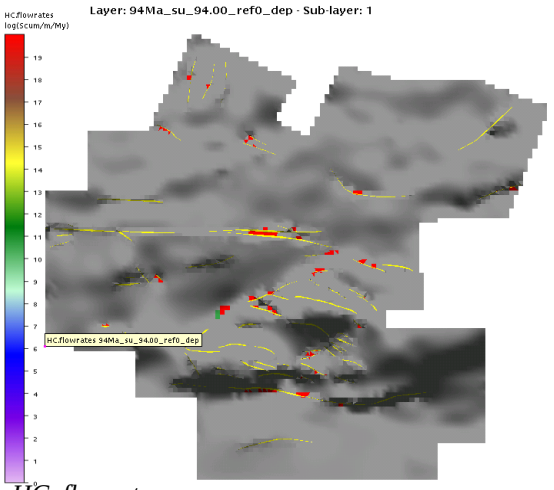

HC_flowrates

Dati

da studio sedimentologico

estratti dalla PSM WESTERN_DESERT_2009

mappe distribuzione di **facies**

logs di 33 pozzi

analizzati per estrarre misure di Vshale

METODO
calcolo Vshale puntuale

per i **layer** (*)
per ogni **pozzo**
ho un valore di **Vshale**

raggruppamenti dati
basato su intervalli di Z
si ottengono valori di Vshale.....

riferiti ai tagli formazionali da log

i tagli Simba sono stati riportati ai log
(senza tenere conto delle formazioni desumibili da log)

OBIETTIVO:
calcolo mappa Vsh
da inserire nel modello
MIGRI

uso sw FLOWMAP

2 scenari/modi
di calcolo

vettori assegnati utilizzando le mappe sedimentologiche dell'area

la differenza è
in alcuni dettagli
dove la mappa sedim.
offre maggiore modalità
di cambio dei vettori

MAPPATURA della Vshale
per ogni layer

vettori assegnati utilizzando le informazioni da bibliografia dell'area

scenario C

scenario A

scenario B

scenario D

tutte le mappe **depth**

gli **espulsi** dalle due sources
profonde 175My e 169My

faglie per i layers
164
156
120
94
come FAGLIE APERTE

importate in....

dal modello SIMBA a litologie costanti
=> Vshale =costante ÷litologie

modello MIGRI
per la migrazione

ognuno
caratterizza un

SCENARI
relativi all'associazione
di **Vshale** nei layers

LEGENDA

dato usato

scenario

sw e/o calcolo applicato

criticità

QC modello
caricato e dati inseriti

estratte le mappe depth
del modello caricato
confrontate numericamente
con quelle caricate
differenze

esito?

OK

QC migrazione precedente
confrontato con la migrazione fatta da SEMI

controllare che il modello
sia 'consistente' rispetto alle scoperte
al 2009
e che lo scema di migrazione sia almeno verificato
(= sono caricati gli stessi carriers)

si assomigliano q.b.

QC modello
&
pozzi (tagli Z)

back-interpolations alle mappe
e confronto con i tagli formazionali

esito?

le mappe della PSM
che sono in Migri
andrebbero ASSESTATE!!!

non previsto

QC MODELLO MIGRI

inserite una Vshale alla volta
il confronto è stato
fatto tra i modelli con tutte le Vshale
map caricate nei layers di interesse

Runs dei modelli MIGRI

controllo e confronto
mappe

flow direction

Trap phases

structural closure

HC Column

HCflowrate

per tutti i run

individuate
trappole da monitorare
per tutti gli scenari

RISULTATI

si osserva un effetto SOGLIA per i valori di Vsh
che vanno acambiare gli accumuli

0,3-0,4

per layer 164My

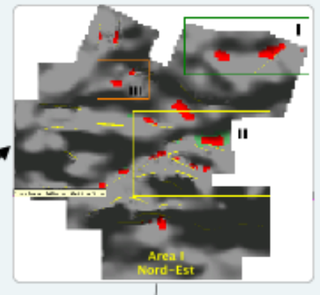

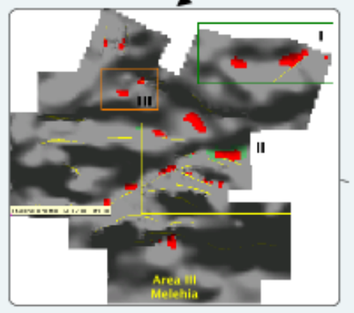

... tutti gli scenari

si trovano accumuli esagerati
con Vsh <0,1
da tutte le mappe
ma sono bassi perchè
siamo in zone carbonatiche

usare anche la Vca!!!!

confronto accumuli
della migrazione
regionale con quella
a scala locale

per lo scenario C

problema della
risoluzione dei grids

gli accumuli sono COMUNQUE
nelle zone corrispondenti